EXPERIMENTAL INVESTIGATION OF NOVEL PROTON EXCHANGE MEMBRANE FUEL CELL AND BATTERY INTEGRATED SYSTEM

by

GUVEN ACIKALIN

A thesis submitted the
School of Graduate and Postdoctoral Studies in partial
fulfillment of the requirements for the degree of

Master of Applied Science in Mechanical Engineering

Faculty of Engineering and Applied Science
University of Ontario Institute of Technology (Ontario Tech University)
Oshawa, Ontario, Canada
August 2023

THESIS EXAMINATION INFORMATION

Submitted by: **Guven Acikalin**

Master of Applied Science in **Mechanical Engineering**

Thesis title: EXPERIMENTAL INVESTIGATION OF NOVEL PROTON EXCHANGE MEMBRANE FUEL CELL AND BATTERY INTEGRATED SYSTEM

An oral defense of this thesis took place on August 10, 2023 in front of the following examining committee:

Examining Committee:

Chair of Examining Committee	Dr. Amirkianoosh Kiani
Research Supervisor	Prof. Ibrahim Dincer
Examining Committee Member	Prof. Martin Agelin-Chaab
Thesis Examiner	Dr. Meaghen Charest-Finn, Ontario Tech University

The above committee determined that the thesis is acceptable in form and content and that a satisfactory knowledge of the field covered by the thesis was demonstrated by the candidate during an oral examination. A signed copy of the Certificate of Approval is available from the School of Graduate and Postdoctoral Studies.

ABSTRACT

In this thesis study, a PEM fuel cell and battery integrated system is developed. The performance assessments of the PEM fuel cell stack are performed through the polarization curve, energy efficiency, exergy efficiency, and open circuit voltage. Furthermore, the performance evaluation of the fuel cell and battery integrated system is performed. The performance assessments of the system are performed through the energy and exergy efficiencies. Moreover, the effect of varying humidifier temperatures on the PEM fuel cell stack is studied. The energy and exergy efficiencies of the PEM fuel cell stack are increased with increasing the humidifier temperature. The highest energy and exergy efficiencies of the developed integrated system are calculated as 6.18% and 6.28%, respectively, while the highest energy and exergy efficiencies of the PEM fuel cell stack are obtained as 14.7% and 14.9%, respectively.

Keywords: Fuel cell; battery; energy; exergy; efficiency

AUTHOR'S DECLARATION

I hereby declare that this thesis consists of original work of which I have authored. This is a true copy of the thesis, including any required final revisions, as accepted by my examiners.

I authorize the University of Ontario Institute of Technology (Ontario Tech University) to lend this thesis to other institutions or individuals for the purpose of scholarly research. I further authorize University of Ontario Institute of Technology (Ontario Tech University) to reproduce this thesis by photocopying or by other means, in total or in part, at the request of other institutions or individuals for the purpose of scholarly research. I understand that my thesis will be made electronically available to the public.

GUVEN ACIKALIN

STATEMENT OF CONTRIBUTIONS

I hereby certify that I am the sole author of this thesis and that no part of this thesis has been published or submitted for publication. I have used standard referencing practices to acknowledge ideas, research techniques, or other materials that belong to others. Furthermore, I hereby certify that I am the sole source of the creative works and/or inventive knowledge described in this thesis.

ACKNOWLEDGEMENTS

First of all, I would like to thank Professor Ibrahim Dincer for his supervision and guidance throughout my master's study and for providing this opportunity.

Also, I would like to thank Muratcan Kenez, Mert Temiz, Dr. Dogan Erdemir and every single person in the lab for their assistance and support.

Finally, I would like to thank my family for their encouragement and endless support.

TABLE OF CONTENTS

LIST OF TABLES

LIST OF FIGURES

LIST OF ABBREVIATIONS AND SYMBOLS

A	area (cm^2)
C	concentration (M)
$\dot{E}$	energy rate (J/s)
ex	specific exergy (kJ/kg)
$\dot{E}x$	exergy rate (J/s)
F	Faraday constant (96500 C/mol)
G	Gibbs free energy (J)
h	specific enthalpy (kJ/kg)
i	current (A)
i_L	limiting current density (A/m^2)
J	current density (A/m^2)
J_L	limiting current density (A/m^2)
J_0	exchange current density (A/m^2)
k	thermal conductivity (W/m-K)
LHV	lower heating value (kJ)
m	mass (kg)
$\dot{m}$	mass flow rate (kg/s)
n	(number of electrons)
$\dot{N}$	molar flow rate (mol/s)
P	pressure (kPa)
R	resistance (ohm)
R_i	internal resistance (ohm)
R	universal gas constant (8.314 kJ/kmol K)
Sh	Sherwood number
t	time (seconds)
T	temperature (°C)
V	voltage (V)
W	power (W)

Greek letters

α	transfer coefficient
δ	Nernst diffusion layer thickness
Δ	change
η	efficiency
ρ	density (kg/m^3)

Subscripts

bg	borosilicate glass
ex	exergy
en	energy
FC	fuel cell
in	inlet
ohm	Ohmic
out	outlet

R	resistance

Acronyms

MPPT	Maximum power point tracking
OCV	Open circuit voltage (V)
PAFC	Phosphoric acid fuel cell
PEM	Proton exchange membrane
PTC	Positive thermal coefficent
PTFE	Polytetrafluoroethylene
Pt	Platinum
Ru	Ruthenium

Chapter 1. Introduction

In the introduction chapter, the importance of renewable energy sources, the significance of hydrogen, hydrogen production methods, hydrogen utilization and fuel cells, and energy storage methodologies are explained. In this study, the PEM (proton exchange membrane) fuel cell is utilized. PEM fuel cell is the device that produces power from the utilization of hydrogen. During the operation of PEM fuel cell, hydrogen is oxidized in the anode of the fuel cell and protons (H^+ ions) are produced. The proton exchange membrane allows the proton to pass. Electrons flow from the external circuit and electricity is produced. In the importance of renewable energy sources part, the increase in CO_2 emissions, Paris Agreement, and the advantages of renewable energy sources are mentioned. In the significance of the hydrogen part, the properties of the hydrogen are explained. In the hydrogen production part, sources of the hydrogen and hydrogen production methods are mentioned. In the hydrogen utilization part, methods for hydrogen utilization techniques, types, and properties of the fuel cells are elaborated. Finally, the aim of the present study is explained.

1.1 Importance of Renewable Energy Sources

Fast increase in CO_2 emissions have an important effect on climate change and global warming [1]. In 1950, CO_2 emissions were 6 billion, in 1990, they were more than 22 billion. Currently, CO_2 emissions overrun 34 billion tons per year, as seen in Figure 1.1. Moreover, coal-fired thermal power plants, engine-powered vehicles and industrial facilities cause most of the CO_2 emissions, as represented in Figure 1.2.

There are lots of arrangements and protocols to reduce CO_2 emissions, and one of the most significant protocols and arrangements is the Paris Agreement. The Paris Agreement is signed by 150 countries. According to the Paris Agreement, limiting the increase in global temperature to 2 degrees Celsius is a reasonable goal. To achieve this goal, regulations are designed to decrease CO_2 emissions by 40% compared to 1990 [4].

To decrease CO_2 emissions and provide clean energy, renewable energy sources are considered essential [5]. Because of the utilization of fossil fuels, high amounts of greenhouse gases are released into the environment continuously. Renewable energy sources like solar power, geothermal power, and wind power are environmentally clean

and safe. Moreover, energy resources based on fossil fuels are threatened by depletion. Renewable energy technologies offer a viable solution for sustainable society and economy. Investments in renewable energy improve growth in the economy and job creation. According to the International Renewable Energy Agency, in 2020, 12 million people are employed worldwide and that will be 42 million people by 2050 [6]. Moreover, because of price volatility in the fossil fuel market, there is instability in the energy prices. Renewable energy sources can provide stability in energy prices because it has less price volatility. So, the transition to renewable energy from fossil fuels is a necessary for energy security, protecting the environment, providing growth in economy, and improving life quality.

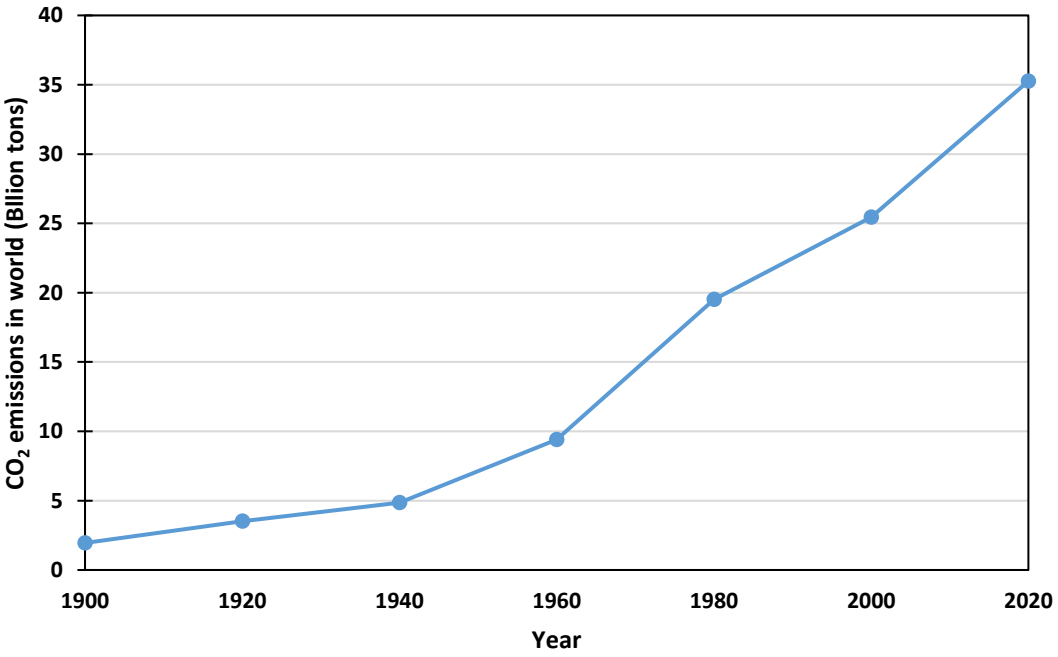

Figure 1.1 Annual CO_2 emissions in world (data from [2])

1.2 Significance of Hydrogen

In energy sources of the future, hydrogen is considered as a potential alternative to fossil fuels. In addition to this, the utilization of the hydrogen can solve the significant environmental problems which are related to the usage of fossil fuels such as climate change and pollution in the air. Because the usage of hydrogen doesn't lead to CO_2 emissions [7].

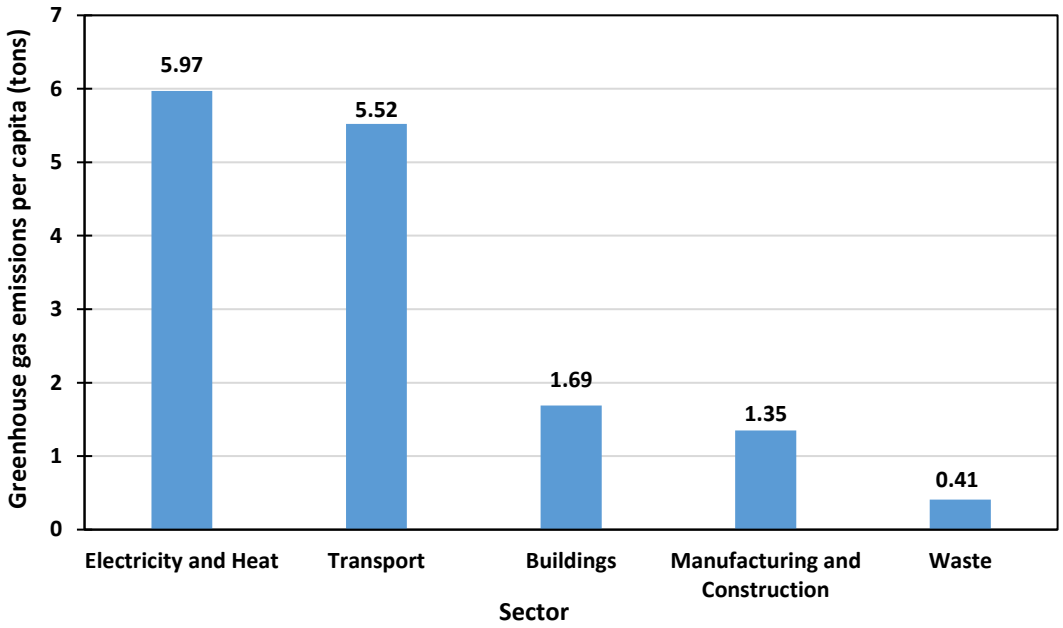

Figure 1.2 Greenhouse gas emissions per capita by sector in USA, 2019 (data from [3])

Long-distance transportation and high efficiency of energy conversion are some of the advantages of hydrogen [7]. In addition to this, higher lower heating value (LHV) and higher heating value (HHV) compared to many of fossil fuels is another advantage of hydrogen as seen in Table 1.1. HHV is the total energy content that also contains the energy of condensing water. HHV is the maximum energy content. LHV is the energy when the vapor is not condensed. LHV is the more realistic value for the actual energy.

The combustion reaction product of the hydrogen is water vapor. Hydrogen can be utilized to store energy for lengthy periods. Moreover, in the situation of intermittent forms of energy like wind and solar energy, hydrogen can be produced when there is more energy than needed and stored. Furthermore, stored hydrogen can be utilized when the energy demand is high. For instance, to produce hydrogen, excess energy can be transferred to the electrolysis which is the production of hydrogen from water. Gasification and thermochemical cycles are the other methods to produce hydrogen. Both physical and chemical methods can be utilized to accomplish the storage of hydrogen. Liquefaction of hydrogen and compressed hydrogen are some of the hydrogen storage methods, and compressed hydrogen is the most commonly used one [8]. Combustion or the fuel cells are the two ways that hydrogen can be used to produce energy

Table 1.1 Higher heating values and lower heating values of fuels at 25°C and 1 atm (data from [8])

Fuel	LHV (kJ/g)	HHV (kJ/g)
Diesel	42.5	44.8
Methanol	18.1	20
Gasoline	44.5	47.5
Methane	50	55.5
Hydrogen	119.9	141.9

1.3 Hydrogen Production Methods

Due to high energy density and environmental sustainability, hydrogen is a promising candidate for the future energy production systems. However, in contrast to fossil fuels, hydrogen is not naturally abundant, but the production of hydrogen can be done from any source of primary hydrogen, such as water. Furthermore, hydrogen can be utilized in a fuel cell or internal combustion engine as a fuel, and it emits water rather than CO_2 as a by-product [9].

Although a high amount of hydrogen is produced from fossil fuels as seen in Figure 1.3, utilization of renewable energy sources will increase as presented in Figure 1.4. Electrolysis of water is one of the most promising methods to produce hydrogen.

In electrolysis, hydrogen and oxygen are produced by splitting water with utilization of an electric current, and it is a highly endothermic process [10]. Alkaline cells, PEM cells, and solid oxide electrolysis cells are the technologies that are often used for electrolysis [9].

The other way of producing hydrogen is using photo electrolysis, also known as photolysis. The photo electrolysis process can be seen in Figure 1.3. Photolysis occurs when the light energy is absorbed in the photo-catalyst. Then, that energy is used to decompose water to oxygen and hydrogen [11]. Similar to electrolysis, the splitting of water occurs when the sunlight is absorbed in semiconducting materials [12]. In particular, the electron-hole pair is made and separated by the electric field between the semiconductor and the liquid when a proton with energy greater than or equal to the

bandgap of the semiconductor hits the semiconducting surface of the anode. In anode, water is split into H^+ and O_2. Then, produced H^+ ions move through the electrolyte to the cathode. The electrons move through an external circuit to the cathode, and they interact with the proton to form H_2 [12].

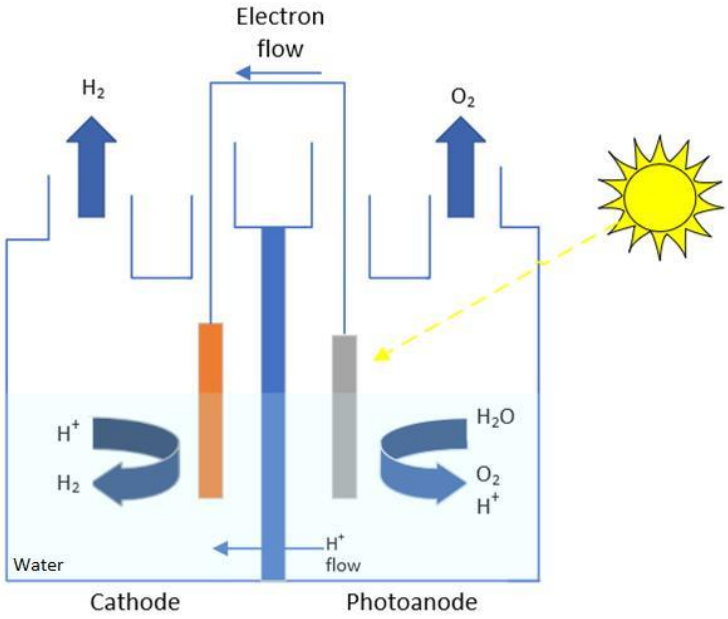

Figure 1.3 Schematic of photo electrolysis process

The other hydrogen production method from renewable energy is biomass gasification. During biomass gasification, biomass is converted to syngas thermochemically in a gasification medium like steam, air and oxygen. The operating temperature is between 500 °C and 1400 °C, and the operating pressure is between the atmospheric pressure to 33 bar [13]. Operating temperature and pressure depend on the application of generated syngas, the scale of the plant and reactor types. The three main reactors for biomass gasification are the indirect gasifiers, fixed bed gasifiers and fluidized bed gasifiers [13]. The significant parameters that affect the yield of the produced hydrogen are the type of biomass, type of catalyst, the ratio of steam to biomass and operating temperature [14].

Another way to produce hydrogen is the biological processes. Over the past few years, biological hydrogen production research has enhanced significantly because of a greater focus on waste reduction and sustainable development. Most of the biological

processes are performed at ambient pressure and temperature, so less energy is required. Furthermore, renewable energy resources are used, and that contributes to waste recycling by using several wastes as feed [15]. Dark fermentations and photo fermentations are the main biological processes used for producing hydrogen gas. Dark fermentation is a biological process that doesn't require light. Suitable substrate, like organic waste, is chosen and placed in a bioreactor that contains specific anaerobic bacteria. Then, those bacteria decompose organic waste and produce hydrogen in dark and anaerobic conditions. Photo fermentation is mainly similar to dark fermentation; however, photo fermentation requires light [16].

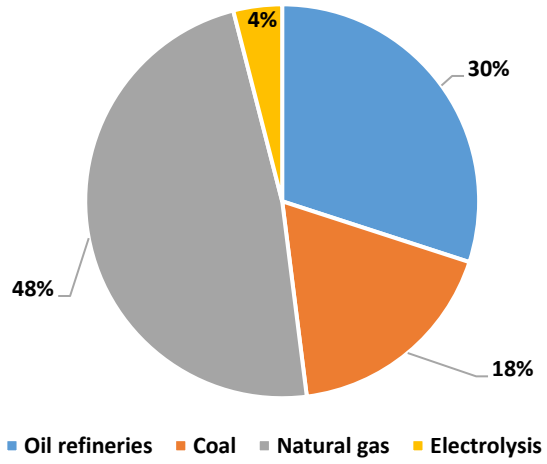

Figure 1.4 Hydrogen production technologies and sources in 2013 (data from [17])

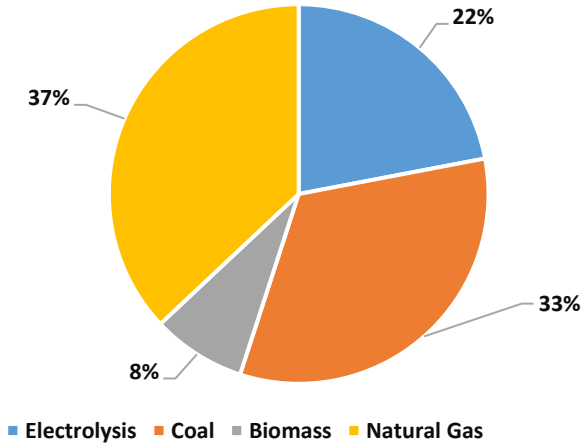

Figure 1.5 Hydrogen production technologies and sources prediction year 2050 (data from [17])

1.4 Hydrogen Utilization and Fuel cells

Currently, mixed and pure forms of hydrogen are utilized in the production of ammonia (27%), steel (3%), methanol (11%) and oil refining (33%). Moreover, hydrogen can be utilized in hydrogenation processes as a reactant, fuel in rocket engines, and in a cryogenic process as a coolant [18]. In addition to this, H_2 can be utilized in cookers, gas boilers, turbines, internal combustion engines and fuel cells [19].

As an energy carrier, hydrogen provides many benefits and improvements in fuel cells that use hydrogen to produce electricity. An interesting and potential application is the utilization of hydrogen as a fuel in passenger automobiles which Toyota demonstrated with the Mirai model in 2014 [18]. Fuel cells have tremendous significance in heating, power generation and transportation because of their modularity and simplicity.

Phosphoric acid fuel cells, polymer electrolyte membrane fuel cells, alkaline fuel cells and solid oxide fuel cells are the major types of fuel cells. Polymer electrolyte membrane fuel cells can produce power from a few kW to hundreds of kW for industrial applications. The capacity of solid oxide fuel cells is available up to tens of MW. Furthermore, the capacity of molten carbonate fuel cells is available from up to tens of MW for industrial co-generation and distributed energy production systems [9].

Another way of producing electricity from hydrogen is microbial fuel cells. That contains anode and cathode electrodes. The growth of bacteria is performed in the anode of the fuel cell under anaerobic conditions, and the bacteria produce electrons there. The transfer of the electron is performed in external circuit of the microbial fuel cell [20].

Another hydrogen utilization method is a hydrogen fueling engine. Hydrogen fueling engine utilizes liquid hydrogen and it operates very efficiently in terms of emissions and fuel economy. Hydrogen can be utilized in traditional motors as an additional fuel. The utilization of hydrogen as an additional fuel enhances the performance of the engine [20]. In Table 1.2, operating temperature, type of the electrolyte, reactions and power output of the alkaline fuel cells, solid oxide fuel cells, phosphoric acid fuel cells, proton exchange membrane fuel cells, molten carbonate fuel cells and solid acid fuel cells are given. In addition to this, there will be an increase in fuel cell market size as seen in Figure 1.6.

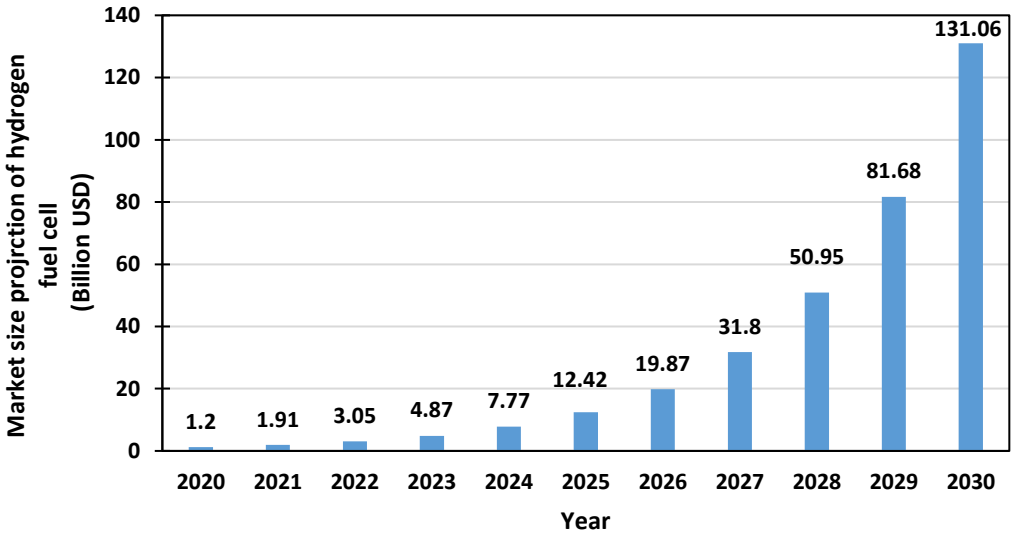

Figure 1.6 Market size projection of hydrogen fuel cells, 2020 to 2030 (data from [21])

1.5 Energy Storage

Renewable energy sources have some problems. One of them is fluctuations observed in solar and wind energy sources. The best way to manage those fluctuations is the energy storage systems. In addition to this, energy storage is very significant for decentralized energy systems [23]. Furthermore, energy storage systems provide a fast response to the demand and the enhancement in the leveling of the load. There are three main forms of energy storage: thermal storage, chemical storage, and mechanical storage [23].

Chemical storage is performed by the utilization of accumulators. The chemical storage systems are able to store and release electrical energy which is known as the charge and discharge of the unit. Chemical storage systems produce electricity from electrochemical reactions and store electricity by chemical reactions. Nickel-iron, lithium-ion, lead-acid, and sodium sulfur are some of examples of chemical storage systems [24].

The other way of storing energy is thermal energy storage. The thermal energy storage systems are divided into two; latent heat thermal energy storage and sensible heat storage. In latent heat thermal energy storage systems, for storing and releasing energy, the latent heat of phase change materials is utilized. The latent heat thermal energy storage systems store energy from the phase change between solid and liquid phases [25].

Table 1.2 Features of fuel cells that utilizes H_2 as a fuel (data from [22])

Type of Fuel Cell	Operating Temperature (°C)	Electrolyte	Reaction at the Anode/Cathode	Power Output
Alkaline Fuel Cell	65-90	Potassium hydroxide	$H_2 + 2OH^- \rightarrow 2H_2O + 2e^-$	1 kW-100 kW
Solid Oxide Fuel Cell	740-1000	Ceramic (ZrO_2/Y_2O3)	$H_2 + O^{2-} \rightarrow H_2O + 2e^-$ $\frac{1}{2}O_2 + 2e^- \rightarrow O^{2-}$	1 kW-10 MW
Phosphoric Acid Fuel Cell	150-220	Phosphoric acid	$H_2 \rightarrow 2H^+ + 2e^-$ $\frac{1}{2}O_2 + 2H^+ + 2e^- \rightarrow H_2O$	200 kW-10 MW
PEM Fuel Cell	60-90	SO_3H-Polymer	$H_2 \rightarrow 2H^+ + 2e^-$ $\frac{1}{2}O_2 + 2H^+ + 2e^- \rightarrow H_2O$	100 mW-1 MW
Molten Carbonate Fuel Cell	610-650	Molten salt	$H_2 + {CO_3}^{2-} \rightarrow H_2O + CO_2 + 2e^-$ $\frac{1}{2}O_2 + CO_2 + 2e^- \rightarrow {CO_3}^{2-}$	500 kW -10 MW
Solid Acid Fuel Cell	65-90	NR_3^+-Polymer	$H_2 + 2OH^- \rightarrow 2H_2O + 2e^-$ $\frac{1}{2}O_2 + H_2O + 2e^- \rightarrow 2OH^-$	100 mW-100 kW

In latent heat thermal energy storage systems, paraffin, non-paraffin, alcohols, and salts are utilized [25]. Latent heat systems are generally utilized in solar power plants, district heating systems, and buildings that require high energy.

In sensible heat storage systems, heat is stored with materials-specific heat capacity. During sensible heat storage, the phase change is not observed while there is an increase in the temperature of the thermal energy storage material. In general, the phase of the storage materials is solid or liquid, and those materials generally have high specific heat capacity. Water, thermal oil and molten salts are the common materials that are utilized in sensible heat storage systems.

The other energy storage method is pumped hydro storage. In this storage system, the power of the water is utilized. That system is utilized for high-capacity power production. During the demand for electric load is low, pumps are utilized for transferring the water from the lower reservoir to the upper reservoir. When the demand is increased, water flows from the upper reservoir to lower reservoir and electricity is produced by generators.

1.6 Hydrogen Storage

The utilization of fuel cells and hydrogen devices in residential usage may potentially prove to be beneficial. Fuel cells that utilize hydrogen offer a way to generate electricity for houses. In addition to this, for heating and producing hot water, combustion of hydrogen can be performed. Furthermore, it is a significant improvement for delocalized energy production. Delocalization production of the energy is the centralized energy production and distribution of this energy to distant places. Decentralization production of the energy is the producing and distributing the energy locally. Decentralized production improves energy security and enhances the use of renewable energy sources. The utilization of hydrogen is also improved in vehicles and transportation, such as in boats, drones, fuel-cell vehicles, and trains. Globally, a significant number of stations for hydrogen fuel are planned to be established to support the utilization of vehicles that utilize hydrogen fuel cells [26]. Furthermore, the storage of the hydrogen is very significant and hydrogen storage methods are listed as follows:

- Utilization of solid-state materials
- Hydrogen compression
- Hydrogen liquefaction
- Utilization of metal-organic frameworks
- Underground compression

The utilization of solid-state materials is one of the significant methods for hydrogen storage. The temperature and pressure of the system affect the capacity of hydrogen storage. Ammonia borane is one of the materials that store hydrogen. Ammonia borane possesses important benefits due to its high hydrogen content of 19.6%, which enables effective control over dehydrogenation processes. Consequently, it is considered as a promising candidate for the storage of hydrogen [27].

Alternatively, compression of the hydrogen gas is considered. Hydrogen gas can be stored between 300-700 bars [28]. Currently, that is common for vehicles, such as Toyota Mirai, that utilizes fuel cell [29]. According to research, at 800 bars, hydrogen tubes provide 13 wt% gravimetric density [30]. However, at 700 bars, the hydrogen tube utilized in Toyota Mirai provides 5.7 wt% gravimetric density [29]. So, the properties of

compressed hydrogen tubes change according to application. The materials that are utilized for compressed hydrogen tubes are nylon-6 or carbon fiber, which provide safety for the tubes [31].

Also, hydrogen can be stored in liquid form at -253 °C, which is a cryogenic condition [32]. A liquid hydrogen tank doesn't pressurize the hydrogen but holds it as a cryogenic liquid [33]. To minimize the heat transfer rate, insulation of the tank must be performed appropriately. The heat transfer rate can be decreased by increasing the ratio of volume/surface [33]. Liquified hydrogen has higher energy density compared to compressed hydrogen; however, it requires much more energy to maintain.

Hydrogen also can be stored by using metal-organic frameworks. They generally perform efficiently at lower temperatures. Metal-organic frameworks are utilized in supercapacitors and batteries [34]. Metal-organic frameworks are porous materials that contains crystalline structures. In order to achieve hydrogen storage, the diffusion of hydrogen molecules is required within these crystalline structures [35]. The crystal size and hydrogen diffusivity in a metal-organic framework have an impact on the adsorption rate [35]. The hydrogen storage capacity of metal-organic frameworks can be enhanced by adding precious metals like palladium and platinum [36].

The other way of hydrogen storage is underground storage. Hydrogen storage can be performed in salt caverns and aquifers [37]. For the storage of the large amounts of hydrogen, salt caverns are ideal. Because of the impermeable structure of the salt, salt caverns provide stability and prevent the escape of the hydrogen [38]. Aquifers are porous media that contain water in their pores. That water can be salty or fresh. The most significant advantage of the aquifers is the great level of storage capacity. But, in aquifers, undetected faults and leakage can be observed [38].

1.7 Battery-Fuel Cell Integrated System

The fuel cell is a device that produces energy from electrochemical processes. Fuel cell produces electricity as long as fuel is supplied to the fuel cell. Generally, hydrogen and oxygen are used as fuel in fuel cell systems.

A hybrid power supply contains two or more different components that act as a single power production to produce or store power. One of the advantages of hybrid power supplies compared to regular ones is excess energy can be stored in one of the hybrid power supply's components, such as ultracapacitor or a battery [39].

Batteries and fuel cells are similar; however, chemical fuel is not injected into batteries continuously for producing electric power [40]. Producing power when the fuel is supplied, silence and zero emissions are advantages of the PEM fuel cells. However, slow dynamics and long start-up time are the disadvantages of the PEM fuel cells. On the other hand, batteries have better dynamic response time compared to fuel cells; however, batteries have long recharge time and lower specific energy [41]. So, the battery system is required to integrate with the fuel cell system for improving the performance of the system and better dynamic response to load change. Furthermore, PEM fuel cells operate more efficiently during steady state operation. So, the integration of the energy storage system to the PEM fuel cell is very significant for increasing the efficiency of the system. When the electric load is lower than the amount of produced power in the fuel cell, excess power produced from the fuel cell can be utilized for charging a battery. However, when the electric load is higher than the amount of power produced in the fuel cell, the battery can be discharged. In addition to this, an instant increase in electric load can be handled by the battery system.

1.8 Motivation

Through the past decades, the global production and consumption of energy have increased significantly. In the future, they are expected to increase steadily. The environment has been affected negatively because of the increased fossil fuel utilization. Throughout the world, the utilization of fossil fuels has seriously damaged the ecosystem because it leads to an increase in CO_2 emissions.

Hydrogen is an energy carrier with a lot of potential and a source of energy that doesn't threaten to the environment. Also, the utilization method of hydrogen is very significant for producing power from hydrogen efficiently. Fuel cells have significant potential for power production by utilizing hydrogen. Fuel cells operate with high efficiency at constant load, and it can be improved by integration of battery by handling

peak loads. Moreover, the integration of fuel cells into battery systems provides flexible power solutions.

The fuel cell can produce power steadily, and when the demand is high, the battery provides peak power. In addition to this, the lifetime of the fuel cells is higher than the battery systems, so integration of the fuel cell to the battery system provides high performance for longer periods. For a battery-fuel cell integrated system, the type of the fuel cell is determined as a proton exchange membrane fuel cell because it has the highest power density compared to the other fuel cells and the low operating temperature of PEM fuel cells makes them convenient for mobile applications.

The battery type is determined as a lithium-ion battery because they have high energy density, so they can store a significant amount of energy with a low volume of space, and they can be charged quickly compared to the other types of batteries. In this thesis, the integration of PEM fuel cell with lithium-ion battery systems is investigated.

1.9 Objectives

This study investigates PEM fuel cell and Li-ion battery integrated systems for providing flexible energy solutions and reaching higher efficiencies. The specific objectives of this thesis study are listed as follows:

- To build a fuel cell stack and battery pack based integrated system.
- To investigate the proton exchange membrane fuel cell experimentally and integrate this to the battery pack.
- To perform analysis and performance assessment of the experimental setup through the energy and exergy efficiencies.
- To develop a scale-up system for a selected location and evaluate the system through the energy and exergy efficiencies.

1.10 Novelties

Fuel cell and battery integrated systems are commonly used in several applications like transportation, marine applications, and portable power generation. There are several studies on PEM fuel cell and Li-ion battery integrated systems with different kinds of control methods and configurations. However, there are a few experimental studies on

PEM fuel cell and battery integrated system with maximum power point tracking control method, and those systems are not connected to the electric load. In this study, a novel PEM fuel cell and Li-ion battery integrated system with an MPPT controller is built, and this system is connected to an electric load. Performance evaluation of the system is performed. Moreover, a case study is performed for PEM fuel cell and battery integrated system.

Chapter 2. Literature Review

In this chapter, a review of the studies related to battery-fuel cell integrated systems is included. Research and comparison for the different types of fuel cells and batteries are performed. The impact of electrode materials, operating temperatures, and the type of batteries are elaborated.

2.1 Proton Exchange Membrane Fuel Cells

In the PEM fuel cell, a proton-conducting polymer electrolyte membrane is used. The main components of the PEM fuel cells are a polymer electrolyte membrane, catalyst layer, gas diffusion layer, bipolar plates and gaskets.

The gas diffusion layers are placed outside of the catalyst layers, and they are used for removing produced water and transporting reactants through the catalyst layer. Gases diffuse through the gas diffusion layer [42].

Usually, the material of the membrane is perfluorinated sulfonic acid polymer [43]. The half-reactions allow protons to pass through to complete the overall reactions separated by the membrane. The current is produced when an electron on the anode side is forced to pass through an external circuit [44]. Furthermore, PEM fuel cells utilize porous carbon electrodes that include platinum catalysts, and that is one of the disadvantages of PEM fuel cells because of the high cost of platinum.

Generally, graphite with a gas flow channel is used as bipolar plates in PEM fuel cells. They have high electrical conductivity and corrosion resistance; however, they are fragile and that cause difficulty in long-term usage. Many bipolar plate materials are utilized in PEM fuel cells, such as titanium, carbon composites, stainless steel and aluminum [45]. Carbon composite bipolar plates contain carbon fillers that provide impermeability and strength [46]. These materials provide lower electrical conductivity if the amount of carbon fillers is low [47]. Increasing the number of fillers and combining different types of them like graphite particles, carbon black and carbon fibers improves the conductivity of the composite [48]. However, a high amount of filler utilization decreases the strength of the material and causes the failure of the material. The advantages of metals are high conductivity, lower permeability, simple machining, and

better strength. So, they are candidates for bipolar plate materials in PEM fuel cells [46]. The significant challenge of metals is corrosion caused by an acidic environment. That causes the formation of metal ions and oxidants [46]. Corrosion on metallic bipolar plates is prevented with a coating technique. Composite coating, metallic coating and carbon-based coating are coating categories that are utilized for aluminum bipolar plates. In pure metallic coating, noble metals that have weak interaction with aluminum are utilized [49].

The desired membrane materials of PEM fuel cells have good ionic conductivity. However, those materials prevent the transport of the electron. In addition to this, they must provide chemical and thermal stability. A thick Nafion-117 membrane provides mechanical strength and separation of reactants. PFSA (perfluoro sulfonic acid) membranes are utilized below 100 °C. Chemical stability and mechanical strength are provided by its hydrophobic part, and the hydrophilic part provides absorption of the water [50]. Dupont's Nafion is a commonly utilized PFSA membrane. PEM fuel cells provide higher power density, although they have lower volume and weight compared to the other fuel cells [51].

Generally, catalyst materials used in PEM fuel cells are carbon-black and platinum. The catalytic activity of platinum is very high, but it is very expensive and affected easily by CO poisoning. As a result, many researchers are focusing on different catalyst materials. Mainly, alloys of platinum such as Pt-Cr, Pt-Co, Pt-Mn show good kinetics [46]. In addition to this, the utilization of non-precious metals, such as cobalt or iron, demonstrates high performance [52].

Another problem is the CO poisoning of the platinum catalyst. To prevent effect of CO on the platinum catalyst, the Pt-Ru catalyst can be utilized. PEM fuel cells utilize oxygen obtained from the air, water, and hydrogen. PEM fuel cells operate at approximately 80°C, which is a lower operating temperature compared to the other type of fuel cells, and that makes them convenient for portable applications [53]. The effects of operating temperature and type of membrane on the performance of the PEM fuel cell can be seen in Table 2.1 below.

According to research, thermal and water management results in significant increase in electric current and operating time of PEM fuel cells [54]. According to White

and Nguyen [55], the downstream flow field had decreased water holding in the membrane, ionic conduction and osmosis coefficient that leads to a decrease in the performance of the fuel cell. In addition to this, at higher current densities, humidification conditions of gas fuel have an important effect on the output voltage, however; the high amount of humidification leads to an increase in the content of water in the flow field, and that causes a decrease in reactive area in flow field which decreases the performance of the PEM fuel cell.

According to Dohle [56], the performance of the PEM fuel cell is affected by the layer shape of the diffuser, distribution of gas flow, oxygen consumption and transport of the gas. Results showed that a long channel leads to a decrease in the effective work area and limited current density. An increase in the number of flow channels and the ratio of flow channel width led to homogenous oxygen distribution and an increase in fuel consumption. As a result of that, the performance of the fuel cell can be increased.

Research done by Li et al [57]. demonstrates the effect of concentration of the oxygen on PEM fuel cells. During high load operation, supplying excess oxygen to fuel cell can improve the reduction reaction by preventing the reduction reaction limitation in the cathode. However, providing excess oxygen may cause waste of oxygen gas, so optimization must be performed for the oxygen feed. Experiments demonstrated that forced convection and natural convection had the same effects on the performance of the fuel cell at low current density. When the current density is increased, for natural convection, the performance of the cell is decreased; however, forced convection provides high voltage.

Research done by the Liu et al. [58] showed that utilization of baffle-blocked flow channels improves the transport of reactant and the performance of PEM fuel cells. Because of the blockage effects caused by baffles, more fuel gas is transported through the gas diffusion layer, improving the chemical reactions in PEM fuel cell system.

Although PEM fuel cells have lots of advantages, utilization of them may be dangerous. Hydrogen leakage is a significant danger of the PEM fuel cell. If there is a leak in the hydrogen storage system or PEM fuel cell, hydrogen may leak, and that may cause an explosion. Because hydrogen gas is highly flammable. For preventing this,

overheating of the PEM fuel cell must be prevented. Excess heating of the PEM fuel cell leads to degradation of the material and leakage of the hydrogen. To prevent excess heating of the PEM fuel cells, cooling system must be used [59].

The working principle of PEM fuel cell can be seen in Figure 2.1. Furthermore, components of PEM fuel cell can be seen in Figure 2.2. Hydrogen is supplied to the anode of the fuel cell. The platinum catalyst in the anode of the fuel cell separates hydrogen gas into electrons and proton (H^+). Then, protons are carried through a proton exchange membrane. Only protons can pass through the proton exchange membrane, while electrons are blocked. That charge separation leads to electrical potential generation. Oxygen is supplied to the cathode of the fuel cell. The oxygen molecules react with protons and water is produced as a result of this exothermic reaction.

Chemical reactions for the PEM fuel cells are:

Anode: $H_2 \rightarrow 2H^+ + 2e^-$ (2.1)

Cathode: $\frac{1}{2}O_2 + 2H^+ + 2e^- \rightarrow H_2O$ (2.2)

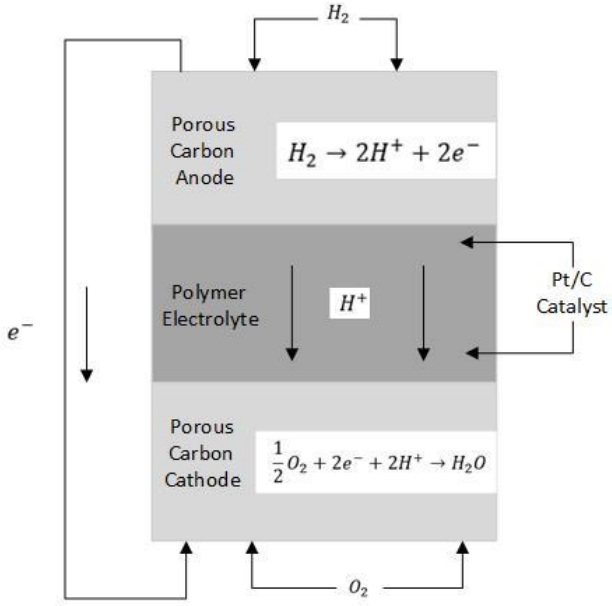

Figure 2.1 Schematic of PEM fuel cell

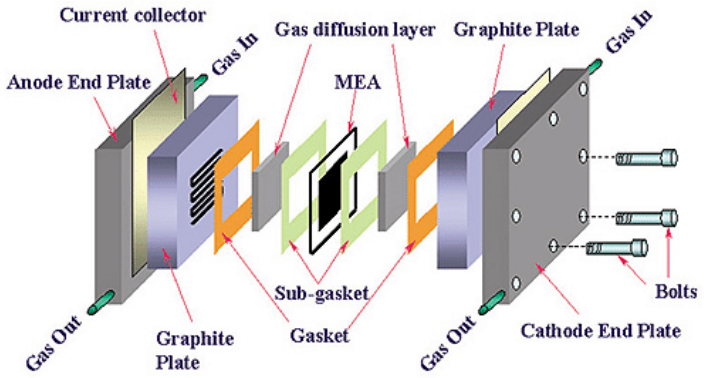

Figure 2.2 Components of PEM fuel cell [66]

Table 2.1 Effect of temperature and relative humidity on power density of fuel cell

Membrane	Active area (cm^2)	Anode-Cathode Relative Humidity (%)	Operating Temperature (°C)	Power Density at 0.5 V (W/cm^2)	References
Nafion 112	5	100	25	0.31	
			45	0.32	
			65	0.33	[60]
SPES/SPEEK	5	100	60	0.19	
			70	0.23	
			80	0.27	
			90	0.23	[61]
Nafion 1135	5	0	35	0.184	
			65	0.34	[62]
Nafion	5	0	60	0.19	
			65	0.2	
			70	0.24	
			75	0.31	
			80	0.26	[63]
Nafion 115	51.84	100	50	0.66	
			60	0.7	
			70	0.74	
			80	0.77	[64]
SPEEK	100	100	20	0.14	
			40	0.25	
			60	0.4	
			80	0.7	[65]

2.2 Solid Oxide Fuel Cells

Solid oxide fuel cells utilize electrolyte that is made of a dense, non-porous ceramic compound. Solid oxide fuel cells have 60% energy efficiency [53].

The solid oxide fuel cell's working temperature is between 600 °C and 1000 °C, and that provides the ability to operate with cogeneration systems by utilizing produced waste heat [43]. However, high operating temperatures require high temperature resistant materials. In addition to this, noble metals that have resource availability problems are not present for solid oxide fuel cells [67]. Moreover, solid oxide fuel cells can operate by utilizing lots of fuels like carbon monoxide, hydrocarbons, and hydrogen [68].

A schematic of the solid oxide fuel cell can be seen in Figure 2.3. Solid oxide fuel cells contain two electrodes that are layered around a hard ceramic electrolyte like zirconia. The anode of the fuel cell is fed with hydrogen, and the cathode of the fuel cell is fed with oxygen from the air. In high operating temperatures, hydrogen oxidizes with oxygen ions, then, water and free electrons are produced. The electrons produced in the oxidation process through the anode produce an electric current. At the cathode, oxygen accepts those electrons and produces oxygen ions. Then, the produced oxygen ions move through the solid electrolyte [67].

Because oxidation of fuel is performed at the anode side, electrocatalytic activity of it must be enhanced. Another significant point in the anode is porosity in the structure of it for improving the gas flow through the reaction site. Generally, they have a porosity between 20% and 40% [69].

The chemical stability of the anode is another important point. That shouldn't give a reaction at higher temperatures with electrolytes and interconnects [70]. Because of that, generally, nickel-yttria-stabilized zirconia is utilized as anode material. The main reason for that is good catalytic performance and high conductivity of the nickel [71].

There is also a lot of research on gadolinium-doped ceria that provides lower operating temperatures. Solid oxide fuel cells that utilize gadolinium-doped ceria perform high-efficiency operations at lower temperatures [72]. In addition to this, there are developments in metal-ceramics materials for the anode of solid oxide fuel cells that

utilize hydrocarbon as a fuel [73]. At the cathode of the solid oxide fuel cell, oxygen gas is reduced to oxygen ions. For the reduction of the oxygen gas, the cathode must perform good catalytic performance [70]. Because of its high conductivity, generally, strontium-doped lanthanum manganite is used as a cathode of the solid oxide fuel cell [74]. One of the most significant parts of the fuel cells is an electrolyte. In solid oxide fuel cells, the most important function of the electrolyte is preventing electron diffusion. Furthermore, electrolytes must provide good ionic conductivity because, for the redox reaction of fuel, protons are transported through electrolytes [75]. Generally, Yttria-stabilized is utilized as an electrolyte because, at high temperatures, it provides good ionic conductivity and stability [76]. Chemical reactions for the solid oxide fuel cells are:

Anode: $H_2 + O^{2-} \rightarrow H_2O + 2e^-$ (2.3)

Cathode: $\frac{1}{2}O_2 + 2e^- \rightarrow O^{2-}$ (2.4)

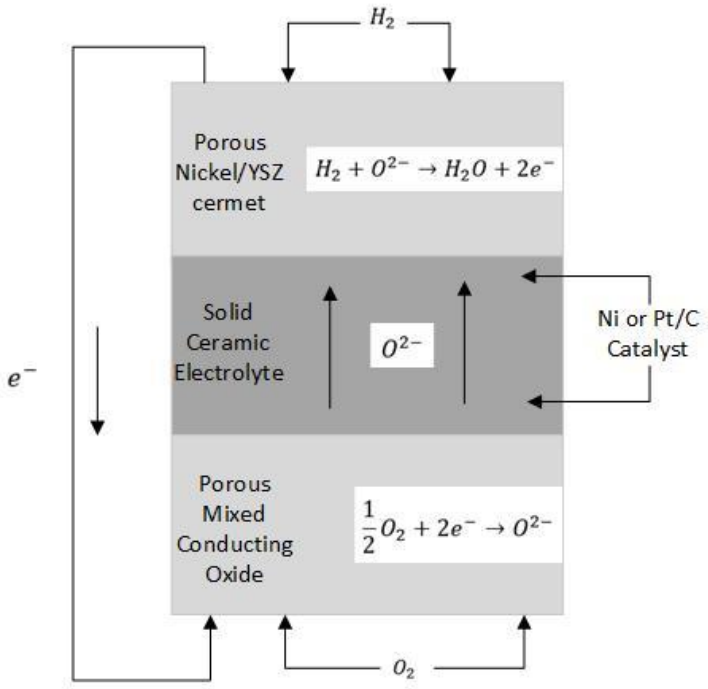

Figure 2.3 Schematic of solid oxide fuel cell

2.3 Alkaline Fuel Cells

Alkaline fuel cells are among the first developed fuel cell technologies, and they were utilized in the United States space program for producing water and electricity in spacecraft [53]. Their efficiencies are close to 70% [77].

Alkaline fuel cells utilize a potassium hydroxide electrolyte which is in aqueous form. In alkaline fuel cells, OH^- is conducted from the cathode to the anode. Consumption of water occurs at the cathode of an alkaline fuel cell while production of it occurs at the anode. Excess water in the system causes dilution of the KOH electrolyte and that affects the performance of the fuel cell negatively [43].

The most significant advantages of alkaline fuel cells are low-cost electrolytes, low material cost, and it provides potential for nonprecious catalysts [77]. The electrodes contain a hydrophobic layer and an active electrocatalyst layer. The active layer contains a mixture of PTFE, catalyst, and carbon black. The hydrophobic layer provides gas diffusion through the reaction site [78].

There is a lot of research on improvement in electrode materials of alkaline cells. In alkaline fuel cells, generally, nickel electrode is utilized, and that can be improved with copper impregnation. The copper inside the nickel reduces the contact resistance of the electrode [79].

Like other fuel cells, alkaline fuel cells have limits on the number of contaminants that they can tolerate in the input gas streams that are utilized. Different gases can cause impurities, and that leads to poisoning of the fuel cell. According to most of the research, carbon dioxide poisoning in oxidant stream is observed, and that prevents the utilization of terrestrial Alkaline Fuel Cells that operates with air [78].

There are strategies for preventing carbon dioxide poisoning. One of them is carbon dioxide removal by chemical absorption. According to Simader and Kordesch [78], 0.03% of carbon dioxide is removed with a soda lime filled tower. The concentration of OH^- in the electrolyte decreases over time, and precipitation of K_2CO_3 occurs at the surface of the electrolyte. That problem can be solved by the utilization of CO_2 scrubbers.

The schematic of the alkaline fuel cell can be seen in Figure 2.4. Chemical reactions for the alkaline fuel cells are:

Anode: $H_2 + 2OH^- \rightarrow 2H_2O + 2e^-$ (2.5)

Cathode: $\frac{1}{2}O_2 + 2e^- + H_2O \rightarrow O^{2-}$ (2.6)

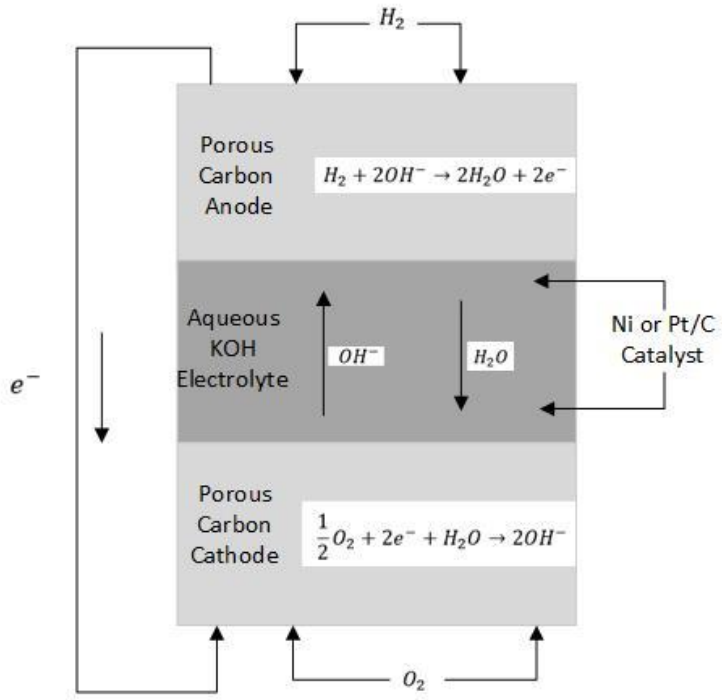

Figure 2.4 Schematic of alkaline fuel cell

2.4 Phosphoric Acid Fuel Cell

In phosphoric acid fuel cells, phosphoric acid is utilized as an electrolyte. It is placed between graphite electrodes that contain platinum catalyst [43]. Phosphoric acid fuel cells provide long-term performance and well reliability. However, utilization of platinum catalysts is a significant disadvantage of PAFC because of its high cost. In addition to this, the utilization of phosphoric acid as an electrolyte is another disadvantage because it is corrosive [43]. The utilization of platinum with graphite reduces the load of Pt significantly. However, the utilization of platinum with carbon reduces the active surface area and causes agglomerations.

The operating temperature of a phosphoric acid fuel cell is approximately 150-200 °C [80]. The phosphoric acid fuel cell operates with high efficiency. For instance, in combined power systems, total efficiency is 87%, and electrical efficiency is 37% [81].

The schematic of the phosphoric acid fuel cell is demonstrated in Figure 2.5. In PAFC, electrolyte conducts proton, so protons are transported through the anode to the cathode. In addition to this, electrons flow from an external circuit. Air is fed through the cathode side of the cell and oxygen gives a reaction with electrons and electrons and proton [81].

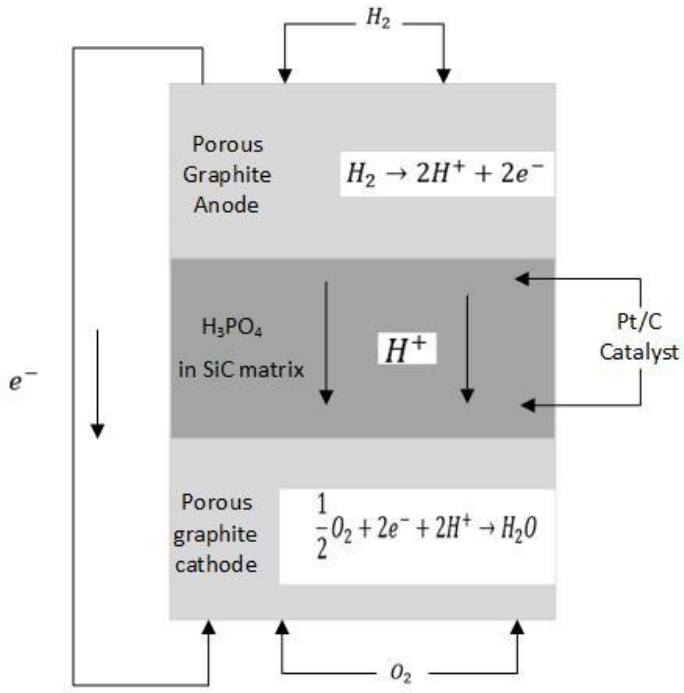

Figure 2.5 Schematic of phosphoric acid fuel cell

Like in other fuel cells, the anode and cathode provide diffusion of gas through the gas channel. Because the electrolyte is in the liquid phase, electrodes must be hydrophobic. That can be achieved by the utilization of polytetrafluoroethylene placed as a backing layer. In addition to this, PTFE is utilized for preventing flooding in pores. The phosphoric acid electrolyte provides chemical and thermal stability. Furthermore, it's not affected by CO_2. In previous phosphoric acid fuel cells, because of the corrosion in materials, dilute phosphoric acid was utilized, but now, 100% H_3PO_4 is utilized [82]. Phosphoric acid is placed in a SiC matrix that has 0.1-0.2 mm thickness. Because of the

small thickness, the matrix provides a small thickness with limited mechanical properties [81]. Moreover, electrodes must provide good conductivity for electricity, so electrons are able to flow with low resistance [80]. The cathode and anode reactions are:

Cathode: $H_2 \rightarrow 2H^+ + 2e^-$ (2.7)

Anode: $\frac{1}{2}O_2 + 2H^+ + 2e^- \rightarrow H_2O$ (2.8)

2.5 Lithium Ion Battery

In rechargeable lithium-ion batteries, transportation of lithium ions occurs between the cathode and anode while discharging and charging. The aluminum foil is simple to process and utilized as a cathode for collecting current.

For separators, polypropylene or polyethylene are utilized. At 25 °C temperature, the ionic conductivity of the electrolyte is 10^{-2} S/cm, which is significantly low compared to the conductivity of other electrolytes. The separator films are utilized for minimizing the internal resistance, securing the energy capacity, and providing enough current.

The materials of lithium-ion batteries provide good thermal stability. When there is an increase in the temperature of the battery, electrolyte decomposition and external short circuits can be observed. For providing safety, gas discharge vents and PTC devices are used [83]. In lithium-ion batteries, the anode material is carbon. There are also researches on anodes for improving lithium absorption capacity.

For high-rate batteries, $Li_4Ti_5O_{12}$ nanocomposite material is tested. In addition to this, for improving overcharge safety, carbon fiber anodes are used rather than carbon powder to improve the safety of charge [84].

The suitable operating temperature of lithium-ion batteries is up to 60 °C. However, the operating temperature of lithium-ion batteries that contain $LiPF_6$ in electrolytes is 100 °C. In addition to this, Lewis's base additives utilization slows down the decomposition of electrolyte [84]. For the cathode material, lithium aluminum/nickel/cobalt is utilized in lithium-ion batteries.

Another development for the cathode material of lithium-ion batteries is the use of lithium iron phosphate instead of lithium cobalt oxide. The advantage of this material is

improving safety and decreasing the cost [84]. However, the disadvantage of lithium iron phosphate is low conductivity, but conductivity can be improved by coating with Fe_2P or carbon [84], [85].

In the industry of lithium-ion batteries, battery safety is a key design requirement. Because of the oxidation of solvents or lithium deposition, charging lithium-ion batteries higher than 4.6 $Vcell^{-1}$ may cause dangerous events like explosion or fire. For high-capacity lithium-ion batteries, electrolyte $LiB(C_2O_4)_2$ (LiBOB) is utilized as a safe electrolyte. In addition to this, for preventing short circuits and overcharges, internal and external devices can be utilized [84].

Details related to nominal voltage, cathode, anode, electrolyte, and reaction of batteries can be seen in Table 2.2 and Table 2.3. Both lithium-ion batteries and nickel batteries perform efficiently. However, the weight energy density of a lithium-ion battery is 1.5 times higher compared to the nickel metal hydride battery. As demonstrated in Table 2.2, nickel battery nominal voltage is 1.2 V; however, it is 3.7 volts for lithium-ion batteries.

Table 2.2 Properties of battery system (data from [83])

Battery System	Anode	Cathode	Electrolyte	Nominal Voltage
Ni-Cd	Cd	NiOOH	NiOOH	1.2
Lead acid	Pb	PbO2	H2SO4 aq solution	2
Lithium Ion	Li+C	CoO2	Organic electrolyte +Li salt	3.7
Ni-MH	Hydrogen adsorbed alloy	NiOOH	KOH aqueous solution	1.2

Table 2.3 Battery system and reaction (data from [83])

Battery System	Reaction
Ni-Cd	$Cd + 2OH^- \leftrightarrow Cd(OH)_2 + 2e^-\ (anode)$ $2NiOOH + 2H_2O + 2e^- \leftrightarrow 2NiOH_2 + 2OH^-$(cathode)
Lead acid	$Pb + SO_4^{2-} \leftrightarrow PbSO_4 + 2e^-\ (anode)$ $PbO_2 + 4H^+ + SO_4^{2-} + 2e^- \leftrightarrow\ PbSO_4 + 2H_2O\ (cathode)$
Lithium Ion	$Li(C) \leftrightarrow Li^+ + e^-\ (anode)$ $Li^+ + e^- + CoO_2 \leftrightarrow LiCoO_2\ (cathode)$
Ni-MH	$H_2 + 2OH^- \leftrightarrow 2H_2O + 2e^-\ (anode)$ $2NiOOH + 2H_2O + 2e^- \leftrightarrow\ 2Ni(OH)_2 + 2OH^-$

2.6 Fuel cell and Battery Integrated System

PEM fuel cells have a significant advantage compared to the lithium-ion battery systems. PEM fuel cells provide higher energy density compared to the lithium-ion battery systems, so fuel cells can provide more energy for a given volume. Furthermore, the refueling of the fuel cell system is faster than the refueling of the lithium-ion battery system. In addition to this, PEM fuel cells have a longer operating life. Lithium-ion batteries can degrade during the charge and discharge cycle, and that causes the disposable of the battery; however, PEM fuel cells can provide consistent operation for longer time. Disposal of batteries causes heavy metal pollution, and that affects the environment negatively [86].

PEM fuel cells provide high efficiencies at low operating temperatures. However, PEM fuel cells cannot handle quick changes in power demand. Batteries provide quick response to variations in energy demand, and integration of fuel cell and battery improves the efficiency of the overall system by providing load balance between fuel cell and battery. Furthermore, excess energy can be stored in the battery during low power demand operations, and that stored energy can be utilized during peak load operations [87].

Farsi and Rosen [88] studied PEM fuel cells and lithium-ion battery electric vehicles integrated with thermal management systems. The performance of the PEM fuel cell is improved with preheating of the feed air. At a 0.4 A/cm^2 current density operation, the energy efficiency of the PEM fuel cell is calculated as 45% for 10 °C feed air temperature and it is 48% for 40 °C feed air temperature. In addition to this, the removal of the heat produced in lithium-ion batteries is very significant for efficient operation. During the operation, 3.5 W per unit area of the lithium ion battery is removed and operation of the lithium ion battery is performed at 25 °C.

Choi and Yu [89] undertook a study on the development of PEM fuel cell and battery hybrid system for the propulsion of boat. PEM fuel cell generates 50kW power, and 47 kWh energy is stored in battery. The boat was designed for generating 86 kW for achieving 14 km/hour. Fuel cells supply energy alone until 40 kW power production. After reaching 40 kW power production, both battery and fuel cell produce power.

Folkesson and Anderson [90] studied on hybrid PEM fuel cell bus. Results are obtained from the Scania PEM fuel cell bus. The overall efficiency of the fuel cell system is 40% and fuel consumption of the fuel cell bus is approximately 48% lower than the normal Scania bus. In this system, 50 kW capacity fuel cell that contains 210 number of cells is utilized. When speed of the bus increases, both fuel cell and battery provide power. Furthermore, battery is charged by electric motors when the bus brakes.

MPPT (maximum power point tracking controller) finds and provides the optimal operating point, which is a maximum power point. That provides maximum power and improves overall efficiency. Prekumar and Vishnupriya [91] studied on analysis of the MPPT controller for charging battery with PEM fuel cell. The analysis of the system is performed in the MATLAB Simulink software. Test have been performed at different operating conditions like different operating temperatures and pressures. Charging efficiency is calculated between 83% and 96%. Results show that the MPPT controller is suitable for the fuel cell systems for maximizing the output power.

2.7 Research Gaps

There are several studies on PEM fuel cell and battery integrated systems. That system has a wide application area such as transportation, aerospace, or residential applications. For the fuel cell and battery integrated system, several control methods are utilized; however, there are research gaps in the literature. MPPT controller has not been used for battery and Li-ion battery integrated system experimentally, and this system has not been connected to the electric load. Moreover, performance assessments of a MPPT controlled PEM fuel cell and battery integrated system has not been performed through the energy and exergy efficiencies. In this study, these research gaps are addressed by building MPPT controlled fuel cell and battery integrated system and performing performance assessments of this integrated system through the energy and exergy efficiencies.

Chapter 3. Experimental Setup and Procedure

In Chapter 3, information related to the experimental procedure, electrochemical modelling of fuel cell, experimental setup and equipment is presented. Each piece of equipment is described in detail. Also, the methodologies of the experiments are mentioned.

3.1 Experimental Procedure

In Figure 3.1, a flow chart for fuel cell performance experiments is demonstrated. Firstly, a PEM fuel cell is built. After that, experiments are performed to determine the fuel cell's flow rate and inlet pressure. At different pressures and flow rates, measurement of open circuit voltage is performed by using a multimeter. The operating pressure and flow rate of the hydrogen are determined experimentally. The capacity of the assembled PEM fuel cell is determined by increasing the inlet flow rate of the fuel cell and measuring the open circuit voltage at different flow rates by using a multimeter. After a certain flow rate, the open circuit voltage of the PEM fuel cell does not change, and that point is determined as the capacity of the PEM fuel cell. Then, the fuel cell is connected to the electric load. Firstly, the humidifier temperature is arranged to 20 °C, and voltage values are obtained at different operating currents. Afterward, polarization curves and power density graphs are prepared, and the performance of the fuel cell system is analyzed through an energy and exergy efficiencies. Then, the same procedure is repeated for 50 °C, 65 °C and 80 °C humidifier temperatures. The highest efficiency and power density is obtained at 80 °C.

In Figure 3.2, the flow chart for fuel cell-battery integrated system experiments is demonstrated. Firstly, a PEM fuel cell is built, and experiments are performed for determining the optimum operating humidifier temperature, pressure and flow rate. Then, the capacity of the Li-ion battery is determined according to controller operating parameters and PEM fuel cell capacity. Later on, the working mode of the controller is arranged, and an integrated system is built by connecting the PEM fuel cell, electric load, and lithium-ion battery to the controller. Then, optimization between the controller, boost converter of the fuel cell and electric load is done. Optimization is performed according to electric load limitations. The electric load doesn't operate below 5.4 V. The outlet

voltage of the boost converter and operating current of the electric load are optimized by trial and error. After that, the effect of the electric load on the system is observed by changing the current of the electric load, and experimental data is obtained. Then, by using obtained experimental data, calculations for the energy and exergy efficiencies are performed. Furthermore, performance assessment of the integrated system was performed through energy and exergy efficiencies.

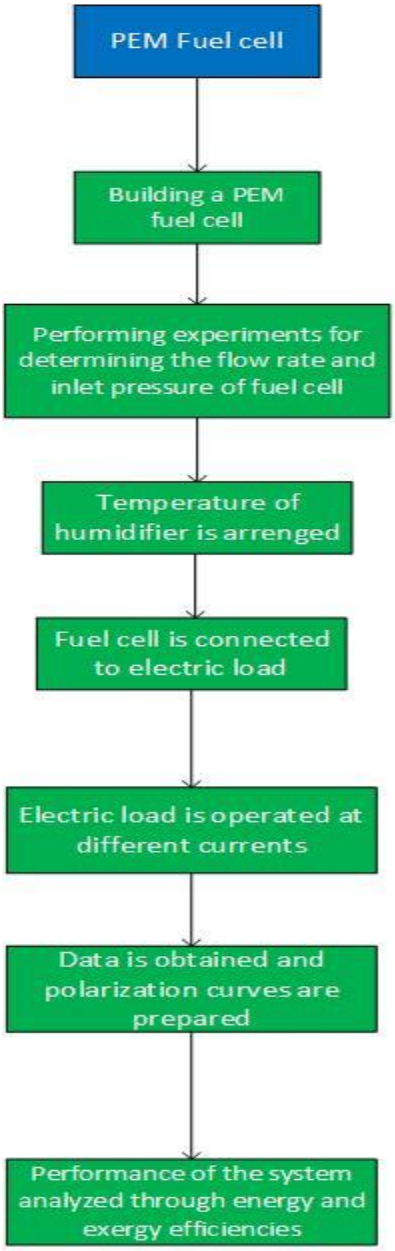

Figure 3.1 Flow chart for fuel cell performance experiments

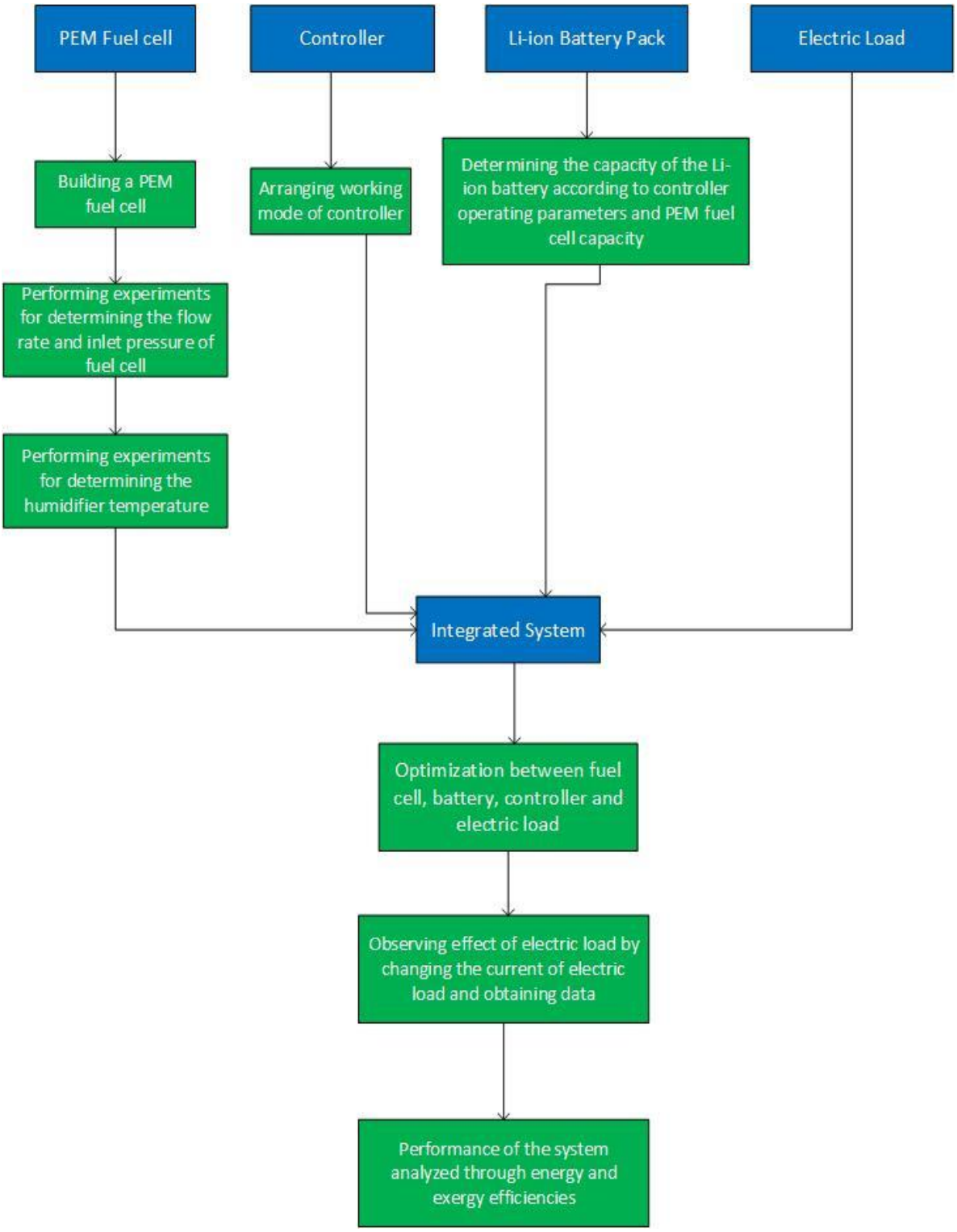

Figure 3.2 Flow chart for fuel cell-battery integrated system experiments

3.2 Electrochemical Modelling of Fuel Cell

In this chapter, electrochemical analysis of PEM fuel cells is demonstrated. Hydrogen is fed through the anode side of the PEM fuel cell. The reaction that occurred in the anode side of the fuel cell is demonstrated in equation 3.1 and the electrochemical reaction that occurred in the cathode side of the fuel cell is demonstrated in equation 3.2.

The Gibbs equation for the reaction in a fuel cell system is:

$$\Delta G = \Delta H - T\Delta S \tag{3.1}$$

In equation 3.1, ΔG is the change in Gibbs energy and ΔS is the change in the entropy of the system. In fuel cells, electrical energy is produced from the chemical energy of reactants. The current output of the fuel cell and the potential of the electrical cell show the produced electricity. The highest cell potential is observed during reversible operation. That reversible cell potential at 25 °C temperature and atmospheric pressure can be demonstrated as:

$$E_r^0 = \frac{\Delta G(T_0,P_0)}{nF} \tag{3.2}$$

Where G is the Gibbs at standard temperature (T_0) and standard pressure condition (P_0), F is the Faraday's constant and n is the number of transferred electrons. The fuel cell potential calculation is performed by the Nernst equation:

$$E_{\text{Fuel Cell}} = E_r^0 - \frac{RT}{nF}\ln(K) \tag{3.3}$$

In the Nernst equation, K indicates the equilibrium constant which is the molar fraction ratio of reactants and products. At low temperatures, the inert gases have an impact on the reversible potential. $E_{fuelcell}$ denotes the cell voltage. When current is produced, several voltage losses are observed. In this case, the expression for the voltage of the fuel cell is:

$$V_{\text{Fuel Cell}} = E_{\text{Fuel Cell}} - V_{ohm} - V_{act} - V_{conc} \tag{3.4}$$

In this expression, V_{act} denotes the activation overpotential caused from the resistance of the electrochemical reaction. During electrochemical reactions, on the surface of the electrode, adsorption of molecules and reactant atoms is observed. That has an impact on

activation overpotential. The Butler-Volmer equation demonstrated the relation between current density and overpotential:

$$J = J_0(e^{\frac{\alpha * n * V_{act}}{RT}} - e^{\frac{(1-\alpha) * n * V_{act}}{RT}}) \quad (3.5)$$

In Butler-Volmer equation, J_0 represents the exchange current density. Exchange current density is obtained in equilibrium. So, the number of reduced products and oxidized reactants are equal to each other. Moreover, the exchange current density illustrates how simply an electrochemical process can be carried out. The α represents the transfer connection which depends on the reaction at the electrodes. The T represents the temperature and R represents the gas constant. In addition to this, Faraday's constant and the number of transferred electrons are represented by F and n respectively. V_{act} denotes the overpotential of activation. Arrangement for Butler-Volmer is performed and Tafel equation is obtained for the calculation of the activation overpotential in high electrode overpotentials:

$$V_{Activation} = \frac{RT}{anF} \ln\left(\frac{J}{J_0}\right) \quad (3.6)$$

Furthermore, the calculation for the fuel cell total activation overpotential is calculated from the equation 3.7;

$$V_{act} = V_{act,C} + V_{act,A} \quad (3.7)$$

In equation 3.7, $V_{act,C}$ and $V_{act,A}$ denote the actual voltage of cathodic activation over potential and anodic activation over potential which can be calculated from equation 3.6. The variation of cathodic and anodic exchange current densities depends on the reactions occurred on the anode and cathode. When there is a rise in the current density of the fuel cell, for supplying the necessary quantity of electron transfer, electrochemical reactions with higher kinetics are observed. As a result of an increase in the rate of the reaction, although the limited rate of mass transfer, the consumption rate of the reactants is increased. Because of the mass transfer limitation, although the products of the reaction are generated, excess accumulation of products can be observed in the cell. That accumulation may prevent the transfer of the reactants in the fuel cell. The maximum limit of produced current is determined according to mass transfer limitation. When the

current density is closer to the limiting current density, mass transfer rate limitation in the cell prevents current density increase. Limiting current density for half-cell reaction can be calculated from equation 3.8:

$$J_L(x) = \frac{(nFC_{i,avg})}{L/D_{a-b}^{eff}} \quad (3.8)$$

In equation 3.8, n represents the number of electrons, $C_{i,avg}$ indicates the average concentration of species, Faraday's constant is denoted by F, L represents the porous layer thickness, and the diffusion coefficient of species is denoted by D_{ab}^{eff}. In addition to this, the average concentration of species can be calculated by equation 3.9.

$$C_{i,avarage} = C_{i,avarage\ inlet} e^{\frac{h_m x}{bv_{avg}}} \quad (3.9)$$

In equation 3.9, $C_{i,avarage}$ represents the average concentration of a reactant at the fuel cell inlet, b denotes the flow channel width, $V_{average}$ represents the inlet flow velocity, x denotes the distance of the flow and h_m is the coefficient of the mass transfer. The mass transfer coefficient can be calculated equation 3.10.

$$Sh = \frac{D_h h_m}{D} \quad (3.10)$$

where the Sherwood number is denoted as Sh, D_h is the hydraulic diameter and the diffusion coefficient is represented as D. Moreover, concentration polarization is calculated from equation 3.11.

$$V_{con} = \frac{RT}{nF} \ln\left(\frac{J_L}{J_L - J}\right) \quad (3.11)$$

In equation 3.11, V_{conc} is concentration polarization in the anode or cathode, and the sum of the concentration overpotential of the anode and cathode gives the total concentration overpotential.

$$V_{con,total} = V_{con,cathode} + V_{con,anode} \quad (3.12)$$

Moreover, when the current is supplied by the fuel cell, because of the electrical resistances of the fuel cell, losses in voltage are observed. The equation 3.13 can be used for the calculation of the ohmic overpotential:

$$V_{ohmic} = JR \tag{3.13}$$

where J represents the current density and R is the electrical resistance of the fuel cell. The polarization curve is a very significant demonstration of fuel cells at different currents. It is a graph of voltage output vs current density. The polarization curve calculations are performed by using equation 3.14:

$$E_{cell} = E_{r,T,P} - \frac{RT}{\alpha F}\ln\left(\frac{i+i_{loss}}{i_0}\right) - \frac{RT}{nF}\ln\left(\frac{i_L}{i_L - i}\right) - iR_i \tag{3.14}$$

where i_{loss} represents the current loss, α represents the transfer coefficient, i_0 represents the reference exchange current density, R_i is the internal resistance, i_L is the limiting current density, i_0 is the reference exchange current density, F is the Faraday's constant, n is the number of electrons involved and R is the gas constant.

3.3 Experimental Set up for Performance Assessment of Fuel Cell Stack

The hydrogen gas is fed at 13 psi pressure through the anode side of the PEM fuel cell. At the anode side of the cell, the reaction in equation 2.1 occurs. The working principle of the PEM fuel cell can be seen in Figure 2.1. For analyzing the performance of the PEM fuel cell, the experimental setup demonstrated in Figure 3.3 is used. For measurement of the temperature and flow, thermometers and flow meters are used, respectively. To analyze the performance of the fuel cell, polarization curve, and open circuit voltage tests are performed. For the measurement of the open circuit voltage of the fuel cell, a multimeter is used, and for the polarization curve, a discharger is utilized. For obtaining the polarization curve, the current is drawn in different values and voltage is measured at that current. The schematic of the fuel cell stack performance assessment setup can be seen in Figure 3.4. The air is fed through the cathode side of the fuel cell after the humidification process. At the cathode side of the cell, the reaction in equation 2.2 occurs. The type of utilized humidifier is the bubbler humidifier. Air is supplied into a water-filled flask that has an inlet-outlet, and humidified. The heater is used for the temperature arrangement of the humidifier. The humidifier temperature and flow rate of the hydrogen are varied for analyzing the fuel cell performance at different operating conditions. The schematic of the fuel cell performance assessment setup can be seen in Figure 3.4.

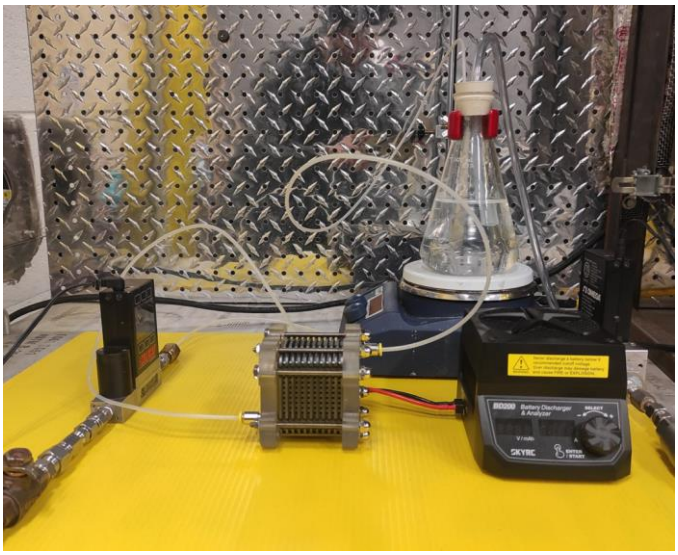

Figure 3.3 Photo of experimental set up for performance assessment of fuel cell

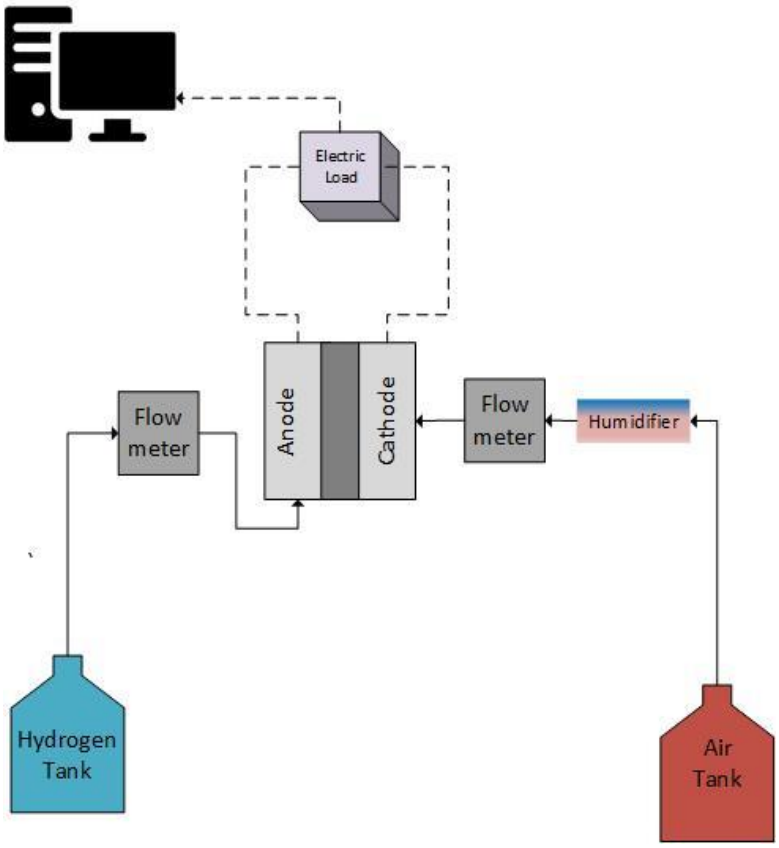

Figure 3.4 Schematic of Fuel Cell Performance Assessment Set-Up

3.4 Components of the Fuel Cell

In this part, components of the proton exchange membrane fuel cell are described in detail. Moreover, the component properties and specifications are provided. Components of fuel cell stack was bought from the fuel cell store website [92].

3.4.1 Proton Exchange Membrane

The most significant component of the PEM fuel cell is the proton exchange membrane. It is a permeable and selective membrane that provides proton transfer from the anode to the cathode. Mostly, the raw material of the PEM fuel cell is perfluoro sulfonic-acid polymer like Nafion. The formula of Nafion is demonstrated in Figure 3.5. Nafion provides perfect chemical stability and proton transfer while preventing the transfer of electrons. This phenomenon is very significant for the electrochemical reactions in PEM fuel cells. Moreover, the chemical and thermal stabilities are one of the important advantages of the proton exchange membrane. It is able to operate in oxidizing or acidic conditions, and its operating temperature range is very high. At the anode side of the proton exchange membrane, H^+ ions and electrons are produced from the dissociation of the hydrogen through the platinum catalyst surface. The produced H^+ ions are transferred to proton exchange membrane, and electron transfer is prevented. The electrons flow in an external surface of the fuel cell to produce electricity. At the cathode side of the proton exchange membrane, water is produced as a result of a reduction reaction by the reaction between transferred protons and supplied oxygen gas. Membrane assembly is demonstrated in Figure 3.6. In this experiment, a membrane assembly that contains a Nafion membrane, platinum catalyst and gas diffusion layer is utilized. There are gas diffusion layers and gas diffusion layers at both faces.

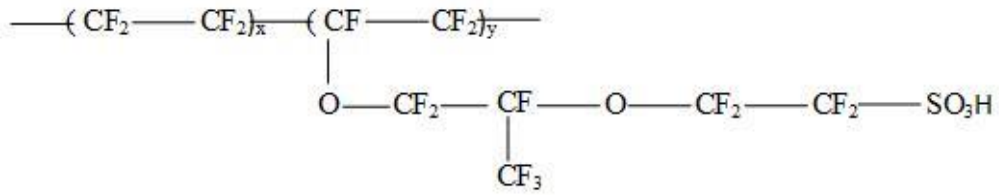

Figure 3.5 Formula of the Nafion

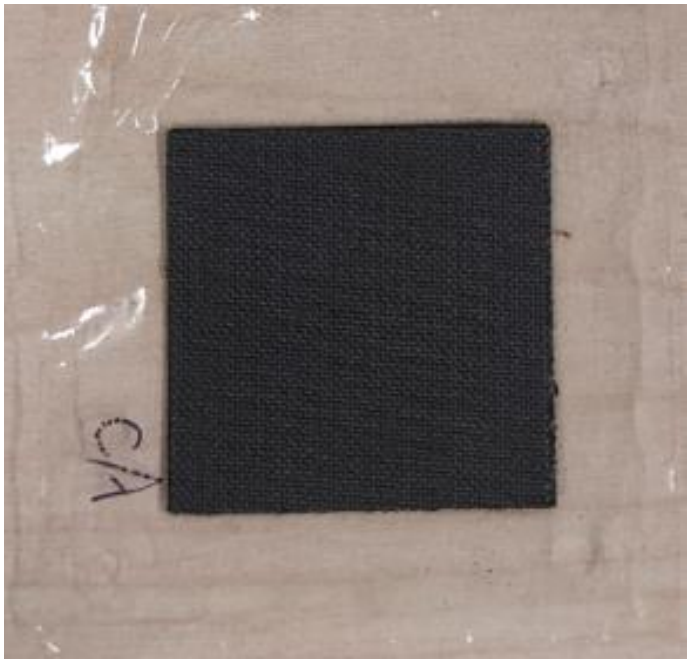

Figure 3.6 Photo of membrane-catalyst-gas diffusion layer assembly

In Table 3.1, the technical specification of the proton exchange membrane can be seen. The proton exchange membrane material Nafion contains polytetrafluoroethylene with sulfonic acid and ether ketone groups. The membrane thickness is 0.002 inches. In addition to this, the membrane assembly contains 0.5 mg/cm^2 60(wt)% platinum on Vulcan.

Table 3.1 Technical data of proton exchange membrane (data was taken from [93])

Platinum Loading mg/cm^2	0.5
Type of Gas Diffusion Layer	Carbon Fiber Cloth
Thickness of the Gas Diffusion Layer (microns)	410
Active Membrane Area (cm^2)	10
Membrane Area (cm^2)	28.09
Thickness of the membrane (inches)	0.002
Type of Membrane	Nafion 212
Anode &Cathode Catalyst	60% (wt) Platinum on Vulcan

3.4.2 Bipolar Plates

One of the main and significant components of the PEM fuel cell is the bipolar plate. Bipolar plates separate the cells of the stack and provide an area for the flow of the fluid. On both surfaces of the membrane, there are gas diffusion layers, catalyst layers, and those are placed between the gas diffusion layers. Bipolar plates operate as an anode and cathode for each cell. The hydrogen fed from the anode of the fuel cell is transferred through the channels from the anode of one cell to the anode of the next cell. At the cathode of the fuel cell stack, fed oxygen and produced water is transferred to the cathode of the next stacks by flow channel plates. Removal of water is significant for preventing flooding and providing efficient process. The anode and cathode sides of the bipolar plate used in the PEM fuel cell system are demonstrated in Figures 3.7 and 3.8. There are flow channels on bipolar plates. Those flow channels distribute fuel gases and enhance the active reaction area. Furthermore, the pressure drop is a significant parameter for the fuel cell system. Those flow channels are designed by considering minimizing pressure drop. Generally, raw materials of the bipolar plates are composites, metals or graphite. In the utilized PEM fuel cell system, the raw material of the bipolar plate is graphite. Graphite bipolar plates provide long-life operation, stability, and improvement in thermal and electrical conductivity.

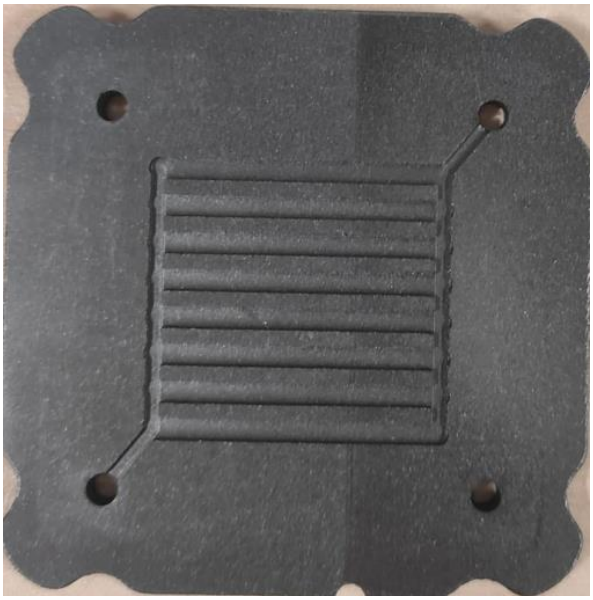

Figure 3.7 Photo of anode Side of the Bipolar Plate

Figure 3.8 Photo of cathode side of the bipolar plate

The total flow length of the anode side and cathode side of the bipolar plate are 240 mm and 432 mm respectively. Specifications of bipolar plates can be seen in Table 3.2.

Table 3.2 Technical specification of utilized bipolar plate (Data from [94])

Technical Specification	
Material of the Bipolar Plate	Graphite
Active Area (cm^2)	10
Total Area (cm^2)	25
Flow Length of Anode Side (mm)	240
Flow Length of Cathode Side (mm)	432

3.4.3 Gaskets

In the PEM fuel cell, between each bipolar plate, gaskets are placed for preventing leakage from the fuel cell stack. Moreover, gaskets provide compression for the stack. The material of the utilized gasket is PTFE. The used gasket in the PEM fuel cell stack can be seen in Figure 3.9. In addition to this, the fuel cell stack is compressed with high pressure for preventing leakages. So, the fuel cell efficiency is enhanced by the utilization of a gasket and prevention of the leakage.

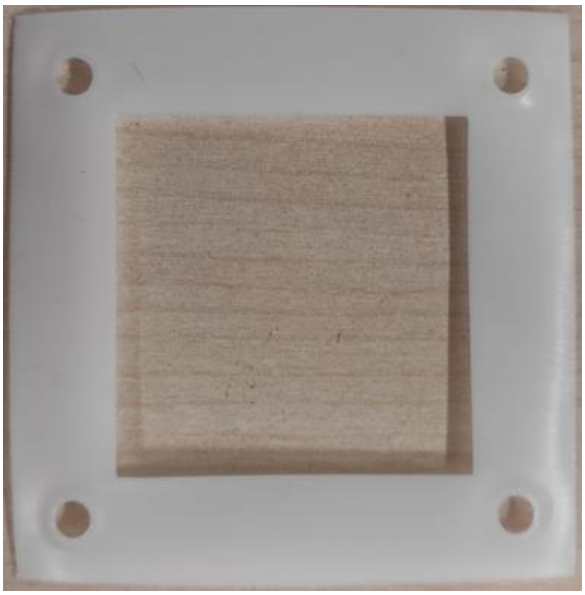

Figure 3.9 Photo of utilized gasket in fuel cell

3.4.4. End Plates and Current Collectors

For pressurizing the membrane assembly, bipolar plates and electrodes are used Furthermore, to provide the perfect contact between the layers, end plates are utilized. In the PEM fuel cell stack, plastic end plates are utilized. The produced current is collected by the current collector in the PEM fuel cell. Generally, it is made of conductive material with a high surface area for increasing the collection of the current. The utilized current collector and side plates can be seen in Figure 3.10.

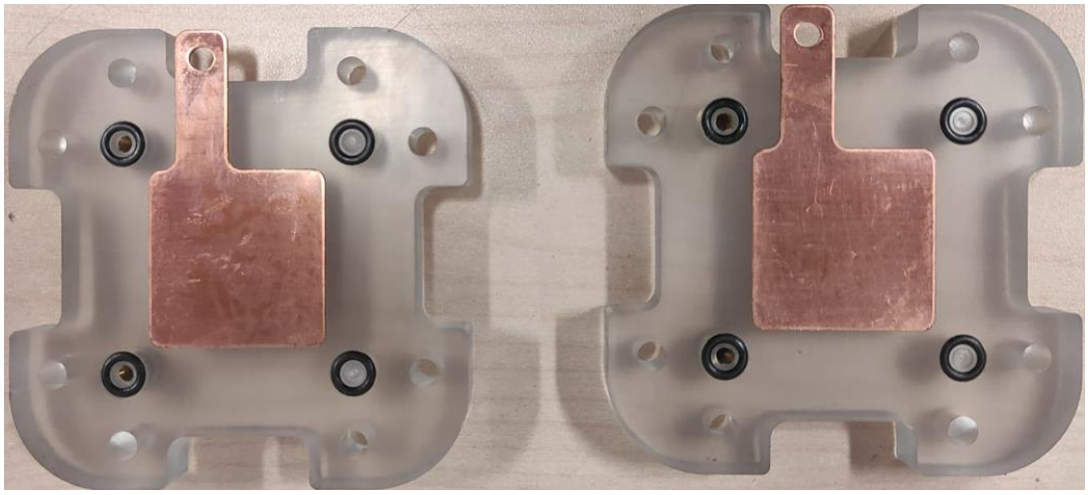

Figure 3.10 Photo of end plates and current collectors

3.4.5 Fuel Cell Stack

The PEM fuel cell stack is demonstrated in Figures 3.11 and 3.12. Firstly, the anode current collector is placed on a plastic end plate. Then, the graphite anode end plate is placed on the current collector. After that, the gasket and catalyst-membrane assembly are placed on the anode end plate. Then, the bipolar plate is placed on the catalyst-membrane assembly. The catalyst membrane assembly is sandwiched between channel plates which provide transfer of reactants fed from the anode side of the fuel cell through the anode side of the cell and reactants fed from the cathode side of the fuel cell through the cathode side of the cell. Ten cells are placed in that way and compressed with the other end plate. On both sides of the flow channel, PTFE gaskets are installed for prevention of leakage. Then, washers, threaded rods, and acorn nuts are placed, and the stack is pressurized to prevent gas leakage during the process. Because hydrogen has high reactivity, any leaks that occur in proton exchange membrane fuel cells have the potential to be explosive. The PEM fuel cell stack is demonstrated in Figures 3.11 and 3.12.

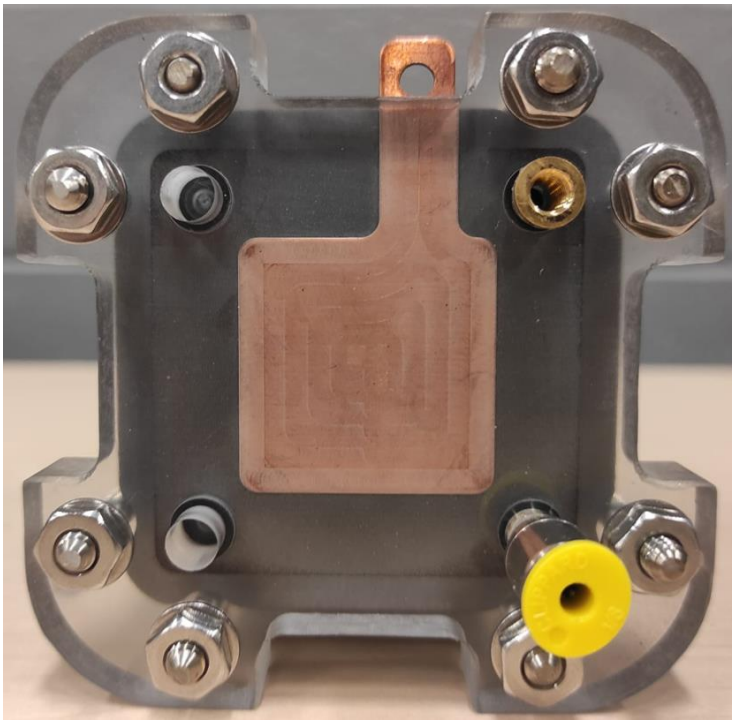

Figure 3.11 Photo of front view of the PEM fuel cell

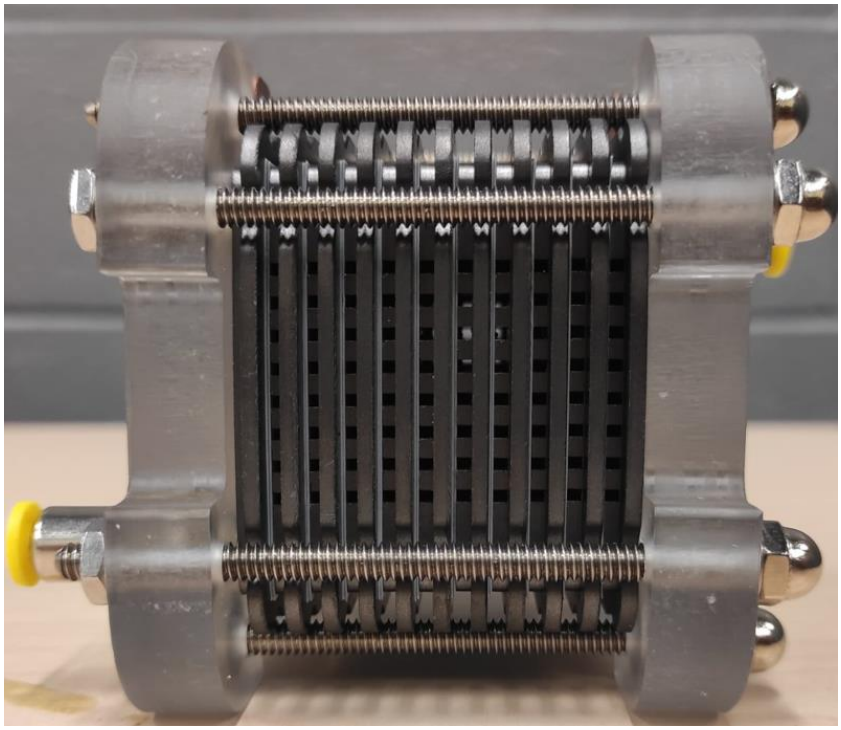

Figure 3.12 Photo of Side view of the PEM fuel cell

3.5 Lithium-Ion Battery Pack

For the fuel cell-battery integrated system, the type of the utilized battery is determined as a lithium-ion battery. The utilized battery management system is 2 PCS PCB Protection board and the model of the Li-ion battery is LFP 18650-1500. Battery packs were prepared in laboratory. Battery pack is shown in Figures 3.13 and 3.14. The lithium-ion battery is utilized because it provides high energy density. Low discharge rate is another advantage of lithium-ion batteries. In addition to this, they are lighter compared to other type of batteries. Six number of 3.2 V batteries and a battery management system are combined into a battery pack. One battery pack contains 3 series – 2 parallel connected lithium-ion batteries. 2 battery packs are connected. The total voltage provided by the battery pack is 19.2 V. In the battery pack, a battery management system is used to provide safe charge and discharge, short circuit protection, and prevention from over charge-discharge. Technical properties of the battery are given in Table 3.3.

Table 3.3 Properties of utilized lithium-ion battery (data from [95])

Model	LFP 18650-1500
Nominal voltage (V)	3.2
Nominal capacity (mAh)	1500
Operating temperature for the charge (°C)	0-60
Weight (g)	38

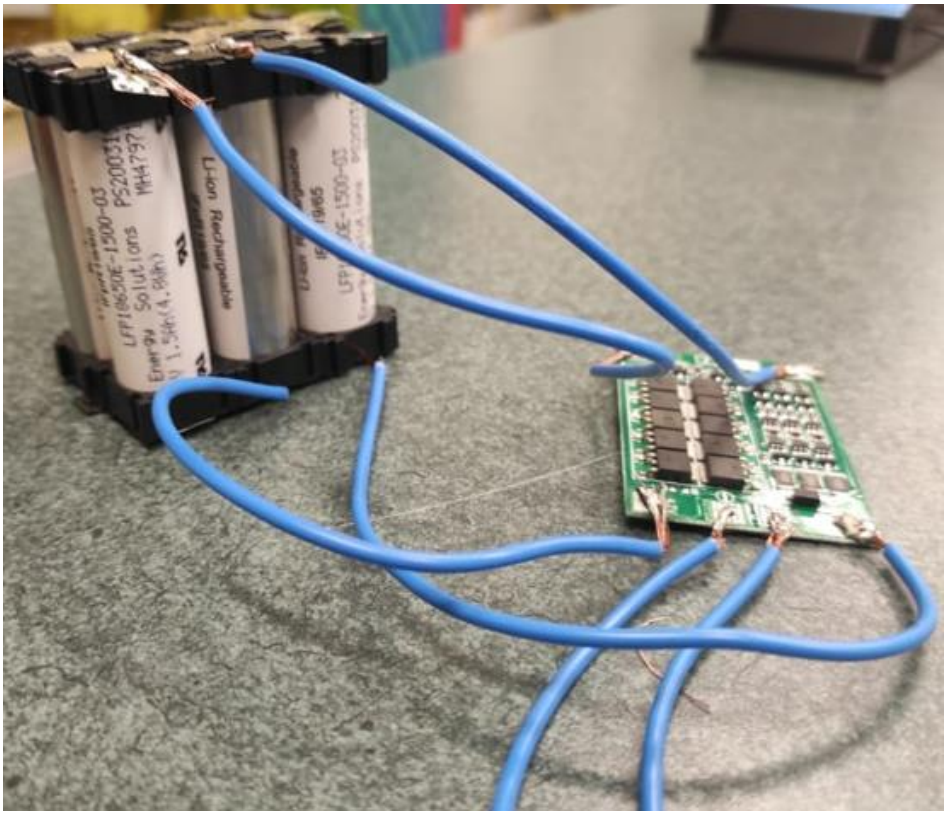

Figure 3.13 Photo of battery pack

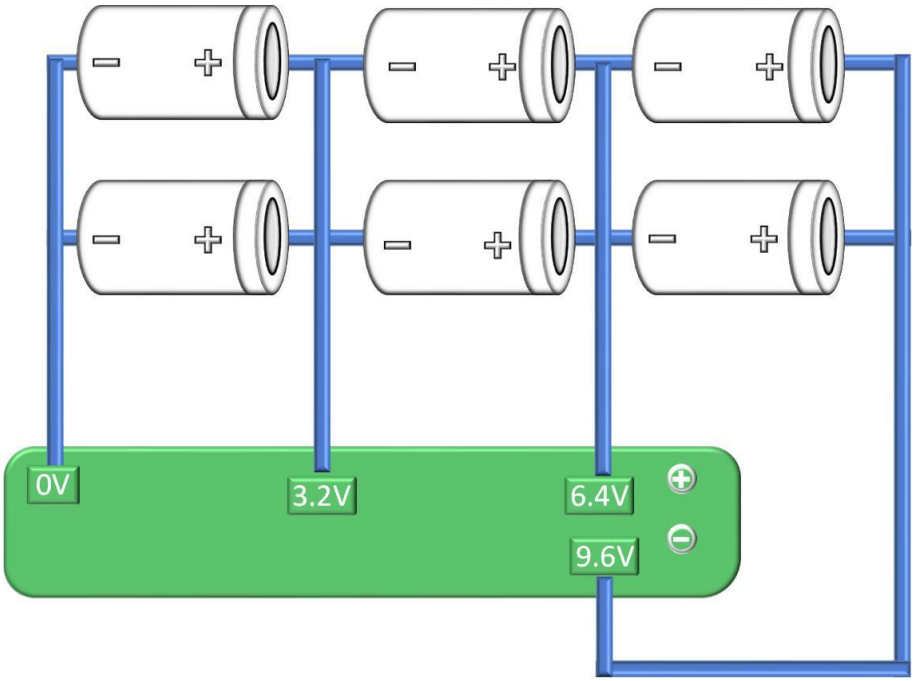

Figure 3.14 Configuration of battery pack

3.6 Humidification

The usage of humidifiers has an important role in the operation of polymer electrolyte membrane fuel cells. Firstly, for the transfer of the H^+ ion, the membrane must be humidified sufficiently. In addition to this, lack of humidity causes internal resistance to increase, and that decreases the efficiency. In addition to this, humidification of PEM fuel cells decreases the stresses on the membrane, and that improves stability. In this system, a humidifier is utilized for humidifying inlet air to the cathode of the fuel cell. The type of utilized humidifier is the bubbler humidifier. Air is supplied into a water-filled flask that has an inlet and outlet.

3.7 Voltage Enhancement of Fuel Cell

In a fuel cell system, the maximum produced voltage is around 9 volts; however, the controller works with 12/24 volts. So, for increasing the voltage of the fuel cell system, a DC-DC boost converter is used. The boost converter is also known as the set-up converter. Boost converters contain semiconductors like diodes, and energy storage components such as inductors or capacitors. Boost converters increase the voltage while decreasing the current of the system. Boost converter increases the output voltage of the

system by storing energy in an inductor and transferring it to an output capacitor. On phase and off phase are the two significant phases of the operation. During on phase, the transistor is turned on and current flow to capacitor through inductor. Storage of energy is performed in magnetic field and that increases the voltage. During off phase, transistor is turned off and voltage is produced through the opposite direction and that provides conduction of the diode. Output voltage is increased because of the energy transfer from the inductor to the capacitor output. In the fuel cell battery integrated system, DC programmable variable voltage ZK-4KX boost converter is used which is shown in Figure 3.15. The technical specifications of the boost converter can be seen in Table 3.4.

Table 3.4 Properties of the utilized boost converter (data from [96])

Model	ZK-4KX
Input Voltage (V)	5.0-30
Output Voltage (V)	0.5-30
Voltage Display Resolution (V)	0.01
Conversion Efficiency (%)	88
Power Protection (W)	50
Working Frequency (KHZ)	180

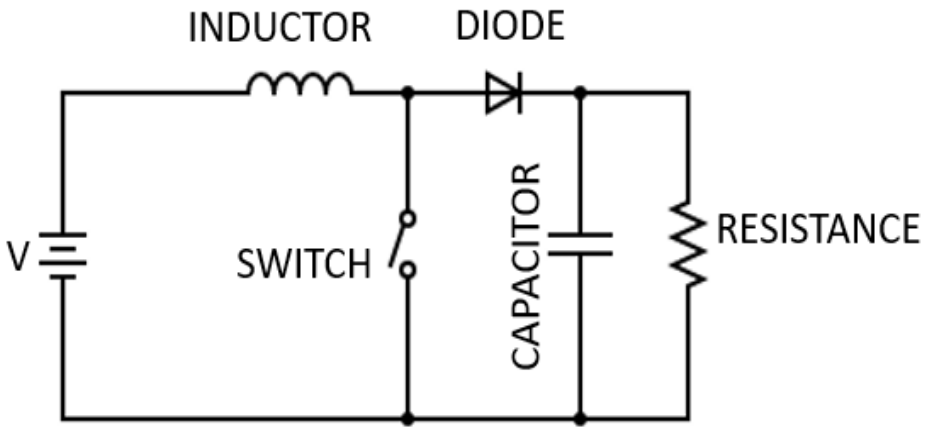

Figure 3.15 Boost converter diagram

3.8 Control of Fuel cell and Battery Integrated System

In this study, MPPT (maximum power tacking) charge controller is used for integrating the battery, fuel cell and electric load. The MPPT solar controller (xw-lcd001-a) was

bought from the Sywan [97]. Firstly, the battery is connected to the charge controller, then, the fuel cell system and finally, the electric load is connected. The DC electricity is produced from the fuel cell system. Voltage depends on the amount of consumed hydrogen. The produced DC electricity is directed to batteries and electric load. The MPPT controller maximizes the produced voltage. The MPPT controller uses an algorithm that tracks the current and voltage of the fuel cell, and it determines the highest power output point. MPPT controller arrange the drawn current for the process. Also, the controller checks the demand from the load. Furthermore, controller controls the charge and discharge of the battery. When the produced energy in fuel cell is higher than the electric load, excess energy is directed into the battery system. However, if the power produced from the fuel cell is lower than the electric load, the battery is discharged.

Table 3.5 Properties of MPPT controller [98]

Model	xw-lcd001-a (BL912A)
Charge current	20 A
Battery voltage	12 V/ 24 V (auto)
Charge current	20 A
Discharge current	10 A
Equalization	14.4 V
Discharge stop	10.7 V
Discharge reconnect	12.6 V
Charge reconnect	13 V

3.9 Voltage Measurement

For analyzing the performance of the proton exchange membrane fuel cell, a discharger is utilized. Furthermore, discharger is the electric load for the system. The performance of the fuel cell is analyzed through a polarization test. In addition to this, an open voltage circuit test is performed by utilization of the multimeter. The open voltage circuit test is a measurement of anode-cathode voltage without electric load. That is the voltage of the stack without ohmic and activation losses. Moreover, the polarization curve demonstrates the relation between current and voltage which is utilized for analyzing the performance of the fuel cell. The polarization curve demonstrates the ohmic losses, concentration losses, and activation losses with the variation of current density. For obtaining the

polarization curve, the current is drawn in different values and voltage is measured at that current. As an electric load, BD 200 battery discharger is utilized. The discharger is connected to a computer and data has been collected with DisCharger software [99]. The technical sheet of the BD 200 discharger can be seen in Table 3.6.

Table 3.6 Technical sheet of BD 200 battery discharger (data from [100])

Voltage Range (V)	5.4-35
Maximum Discharge Power (W)	200
Current Range (A)	0.01-30
Low Voltage Alert (V)	<5.2
High Voltage Alert (V)	>35

3.10 Flow Measurement

In this study, for the flow of hydrogen, ALICAT MC Series mass flow controller, and for the flow of air, Omega FMA-LP flow meter is used. These flow meters calculate the flow rates based on the theory of differential pressures. Those flow meters utilize pressure sensors for measuring the pressure losses in laminar flow.

Table 3.7 Technical sheet of Omega FMA-LP (data from [101])

Maximum pressure (psig)	50
Operating temperature (°C)	10 - 50
Response time (ms)	10
Supply Voltage (V-dc)	7-30
Supply current (mA)	100

3.11 Experimental Uncertainty Analysis

To better understand the changes in results produced at different conditions, it is necessary to estimate the uncertainties related to experimental studies and results. Random and systematic errors are utilized in the quantification of the uncertainty analysis. Inaccuracies in equipment and problems in the experimental design may cause errors. Those errors are known as systematic errors. Those kinds of errors lead to deviations in actual experimental results. In addition to this, during repeated experiments deviation in the results is observed. Those kinds of errors are known as random errors. Mainly, these deviations in the results of the experiments are caused by the environment

and during the measurements. The uncertainty evaluation can be performed from equation 3.15. In equation 3.15, random errors are represented by R and systematic errors are demonstrated by S.

$$U = \sqrt{R^2 + S^2} \tag{3.15}$$

In this study, the voltage display accuracy of the BD200 discharger is ±60 mV and the accuracy of the current display is ±60 mA. Each of the experiments are performed for 3 times and for specifying the random errors. From equation 3.16, the relative standard deviation caused by the deviation in experimental results can be calculated from equation 3.16. In equation 3.16, Avrg demonstrates the mean values of the results, SD represents the standard deviation and RD is the relative deviation.

$$RD\% = \frac{SD}{Avrg} \times 100 \tag{3.16}$$

Chapter 4. Case Study

In this chapter, the experimental development of a fuel cell and battery integrated system, and the performance assessment of this system are demonstrated. Later on, the fuel cell and battery system is scaled up, and case study is performed for a certain place theoretically.

4.1 Development of Fuel cell and Battery Integrated System

To improve the efficiency of the fuel cell system, the battery pack and controller are integrated to the fuel cell stack. The configuration of the fuel cell and battery integrated system and experimental setup can be seen in Figures 4.1 and 4.2. In this system, the fuel cell provides energy to the battery pack and DC electric load. When the energy produced by the fuel cell is higher than the electric load, the excess energy is stored in the battery. However, when it is lower than the electric load, the battery will be activated, and it provides energy to the electric load. That provides steady-state operation for the fuel cell system. Moreover, the lifespan of the fuel cell improves. For improving the energy and exergy efficiencies of the system, the integration of the battery to the fuel cell is essential.

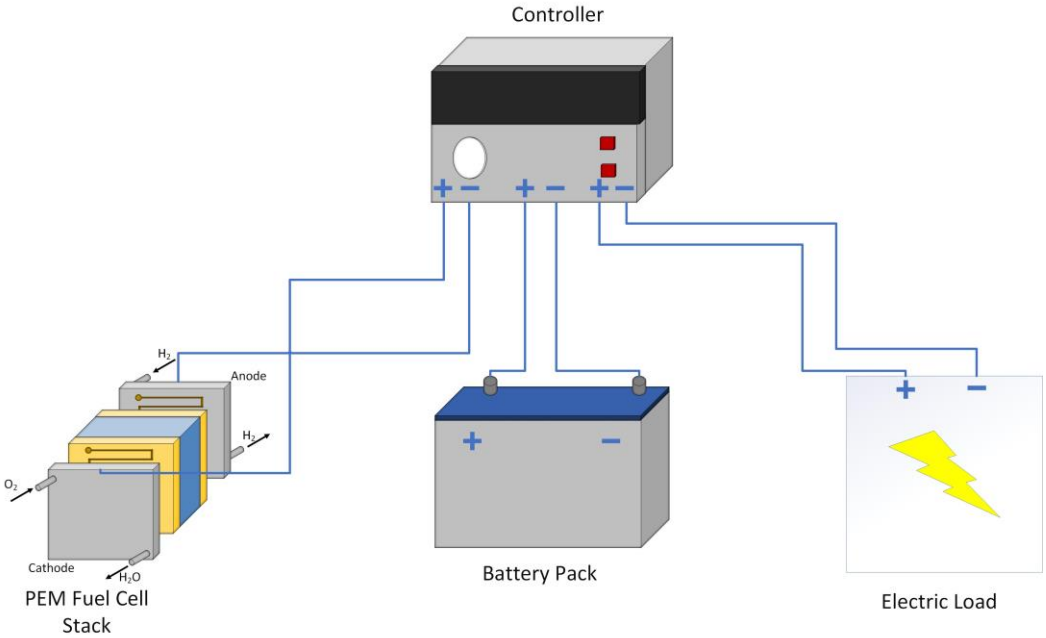

Figure 4.1 Schematic of Fuel cell and Battery integrated system

Figure 4.2 Photo of fuel cell and Battery integrated system experimental setup

4.2 Performance Assessment of Fuel Cell and Battery Integrated System

In this section, an electrochemical analysis of the PEM fuel cell system is demonstrated. For electricity production, hydrogen is fed through the anode of the PEM fuel cell and used as fuel. In equation 2.1, the oxidation reaction of hydrogen at the anode and in equation 2.2, the reduction reaction at the cathode is demonstrated. The overall reaction of the PEM fuel cell is:

$$H_2 + \frac{1}{2}O_2 \rightarrow H_2O \tag{4.1}$$

The Gibbs of the reaction can be calculated from equation 3.1. During the operation of the PEM fuel cell, electricity is produced from the chemical energy of the hydrogen and other reactants. The output of the current and fuel cell potential demonstrates the produced electricity. The upper limit cell potential is obtained during the reversible operation, which is reversible cell potential. The reversible cell potential is demonstrated by equation 4.2 at the pressure of 1 atm and 25 °C temperature. The reactant and product partial pressure or concentration have a significant impact on the reversible cell potential. For the calculation of the cell potential of a PEM fuel cell, The Nernst equation is used:

$$\mathrm{E_{FC}} = \mathrm{E_{FC}^{\circ}} + \left(\frac{\mathrm{RT}}{2\mathrm{F}}\right) \ln\left(\frac{\mathrm{P_{O_2}^{0.5} P_{H_2}}}{\mathrm{P_{H_2O}}}\right) \tag{4.2}$$

where the partial pressure of components is represented by P. The 0.5 is the reaction coefficient of the O_2 in the PEM fuel cell reaction. Furthermore, the coefficient of the H_2 and H_2O are 1. During the operation, water is produced, hydrogen and oxygen are consumed. When the fuel cell supply current, lots of losses in voltage is observed. That is mainly caused by ohmic loss, concentration loss, and activation loss.

The produced power from the fuel cell can be calculated from the equation:

$$\dot{W} = J \times V \tag{4.3}$$

The performance of the PEM fuel cell is evaluated through energy and exergy efficiencies. The energy efficiency calculation is performed from equation 4.4 and the exergy efficiency calculation is performed in equation 4.5:

$$n_{fc,energy} = \frac{\dot{W}_{Fuel\ Cell}}{LHV_{H_2} \times \dot{N}_{H_2}} \tag{4.4}$$

$$n_{fc,exergy} = \frac{\dot{W}_{Fuel\ Cell}}{ex_{H_2} \times \dot{N}_{H_2}} \tag{4.5}$$

Where produced power in a fuel cell is represented by $\dot{W}_{Fuel\ Cell}$, $\dot{N}_{H_2}$ denotes the hydrogen flow rate in moles, LHV_{H_2} and ex_{H_2}represents the specific exergy of hydrogen. In addition to this, energy and exergy efficiencies are calculated by considering consumed energy by the humidifier. Energy consumed for increasing the temperature of water is calculated from equation 4.6:

$$Q_{s,w} = m_w \times c_{p,w} \times \Delta T_w \tag{4.6}$$

where $Q_{s,w}$ is sensible heat for increasing the temperature of water, m_w is the mass of the water, $c_{p,w}$ is the specific heat capacity of the water, and ΔT_W is the temperature change of the water. Mass of the water is 400 g and heat capacity of the waster is 4.18 kJ/kg-K.

Furthermore, exergy supplied by the heater for increasing the temperature of the water is calculated from equation:

$$Ex_{Q_{s,w}} = Q_{s,w} \times (1 - \frac{T_{avg,w}}{T_{heater}}) \tag{4.7}$$

where $T_{avg,w}$ is the average of final temperature and initial temperature of the water and T_{heater} is the final temperature of the heater. Initial temperature of the water is 20 °C.

In equation 4.8, heat required for the keeping temperature of the water constant is calculated:

$$Q_C = \frac{k_{bg} \times A_{Flask} \times (T_w - T_{surrounding}) \times \Delta t}{L_{Flask}} \quad (4.8)$$

This equation is the thermal conduction equation. In this equation, Q_C the amount of heat supplied by the heater for keeping the temperature of the water constant, k glass is the thermal conductivity of the glass, A_{Flask} is the area of the flask, T_w is the temperature of the water, $T_{surrounding}$ is the surrounding temperature, Δt is the duration of the operation, k is the thermal conductivity of the borosilicate glass and it is determined as 1.40 W/m-K [102]. L_{Flask} is the thickness of the flask. The surface area of the flask is 0.03 m^2, and the thickness of the flask is 0.002 m. The duration of the operation is taken as 300 seconds in all analysis. All experiments are performed 25 minutes. In first 20 minutes, setup reaches a steady state, and data is obtained in last 5 minutes [103].

In equation 4.9, exergy supplied by heater for keeping temperature of the water constant is calculated:

$$Ex_{Q_C} = Q_C \times (1 - \frac{T_{surr}}{T_w}) \quad (4.9)$$

where T_w is the water and T_{heater} is the final temperature of the heater, T_{surr} is surrounding temperature and it is 20°C.

Energy and exergy efficiencies are calculated by considering consumed energy by the humidifier from equation 4.10:

$$\mathrm{n_{fc,h,energy}} = \frac{\dot{W}_{\mathrm{Fuel\ Cell}} \times \Delta t}{\mathrm{LHV_{H_2}} \times \dot{N}_{H_2} \times \Delta t + Q_{s,w} + Q_C} \quad (4.10)$$

$$\mathrm{n_{fc,h,exergy}} = \frac{\dot{W}_{\mathrm{Fuel\ Cell}} \times \Delta t}{\mathrm{ex_{H_2}} \times \dot{N}_{H_2} \times \Delta t + Ex_{Q_{s,w}} + Ex_{Q_C}} \quad (4.11)$$

Energy and exergy efficiencies of the fuel cell and battery integrated system is calculated with and without considering humidifier energy. Battery charging and discharging losses

are determined as 5%. Furthermore, there are different energy and exergy efficiency calculations for battery charge and discharge cases.

Energy and exergy efficiencies without considering humidifier energy is as follows:

For the battery charge situation,

$$n_{energy} = \frac{\dot{E}_{\text{Supplied to Electric Load}} + \dot{E}_{\text{Battery charge}} + \dot{E}_{\text{Battery charge losses}}}{LHV_{H_2} \times \dot{m}_{H_2}} \quad (4.12)$$

$$n_{exergy} = \frac{\dot{E}x_{\text{Supplied to Electric Load}} + \dot{E}x_{\text{Battery charge}} + \dot{E}x_{\text{Battery charge losses}}}{ex_{H_2} \times \dot{m}_{H_2}} \quad (4.13)$$

For the battery discharge situation,

$$n_{energy} = \frac{\dot{E}_{\text{Supplied to Electric Load}}}{LHV_{H_2} \times \dot{m}_{H_2} + \dot{E}_{\text{Battery Discharge}} + \dot{E}_{\text{Battery Discharge Loss}}} \quad (4.14)$$

$$n_{exergy} = \frac{\dot{E}x_{\text{Supplied to Electric Load}}}{ex_{H_2} \times \dot{m}_{H_2} + \dot{E}x_{\text{Battery Discharge}} + \dot{E}x_{\text{Battery Discharge Loss}}} \quad (4.15)$$

Energy and exergy efficiencies by considering humidifier energy is as follows:

For the battery charge situation,

$$n_{energy} = \frac{(\dot{E}_{\text{Supplied to Electric Load}} + \dot{E}_{\text{Battery charge}} + \dot{E}_{\text{Battery charge losses}}) \times \Delta t}{(LHV_{H_2} \times \dot{m}_{H_2}) \times \Delta t + Q_{s,w} + Q_C} \quad (4.16)$$

$$n_{exergy} = \frac{(\dot{E}x_{\text{Supplied to Electric Load}} + \dot{E}x_{\text{Battery charge}} + \dot{E}x_{\text{Battery charge losses}}) \times \Delta t}{(ex_{H_2} \times \dot{m}_{H_2}) \times \Delta t + Ex_{Q_{s,w}} + Ex_{Q_C}} \quad (4.17)$$

For the battery discharge situation,

$$n_{energy} = \frac{\dot{E}_{\text{Supplied to Electric Load}} \times \Delta t}{(LHV_{H_2} \times \dot{m}_{H_2} + \dot{E}_{\text{Battery Discharge}} + \dot{E}_{\text{Battery Discharge Loss}}) \times \Delta t + Q_{s,w} + Q_C} \quad (4.18)$$

$$n_{exergy} = \frac{\dot{E}x_{\text{Supplied to Electric Load}} \times \Delta t}{(ex_{H_2} \times \dot{m}_{H_2} + \dot{E}x_{\text{Battery Discharge}} + \dot{E}x_{\text{Battery Discharge Loss}}) \times \Delta t + Ex_{Q_{s,w}} + Ex_{Q_C}} \quad (4.19)$$

4.3 Case Study for Fuel Cell and Battery Integrated System in California State

In this study, a novel simulation and case study for the fuel cell and battery integrated system are performed. The case study is performed for California State and electric load

data is 10^6 times decreased and scaled for this study. Electric load data is for 2018. Electric load data for this study is downloaded from the website of the National Research Energy Laboratory [104]. Data is downloaded as a 15-minute data as excel file.15-minute data is converted into hourly data, then, it is converted into daily data for analysis. For this study, California state is chosen as case study place because of its leadership in renewable energy systems. California state is the pioneer in renewable energy adoption. Regulations and policies have a significant effect on its energy landscape [105]. Furthermore, California state has problems related to fossil fuels like high cost, shortage, and environmental concerns [106]. In this study, two different cases are studied. In the first case (case-1), the PEM fuel cell produces 14 kWh/hour of power and in the second case (case-2), 18 kWh/hour of power is produced constantly.

Fuel cells generate electrical energy from the utilization of chemical energy. On the other hand, energy storage and delivery can be performed efficiently by the utilization of battery systems. So, the integration of these two components enhances the overall efficiency.

Integration of fuel cell and battery systems improves the lifecycle of the system. Batteries are affected negatively by the charging-discharging cycle, and that causes degradation; however, fuel cells are not affected in that way. So, batteries can be used for short-term charging, discharging, and energy storage while fuel cells are utilized constantly. Utilization of fuel cell and battery systems improves the lifecycle of the overall system.

In addition to these, this system reduces CO_2 emissions. Production of hydrogen can be performed by renewable energy sources. Moreover, when hydrogen is utilized in fuel cell, water is produced rather than CO_2, as this approach reduces the CO_2 emissions.

In experimental setup maximum efficiency of fuel cell is calculated as 14.7% which is low compared to the commercial fuel cells used for real life applications such as vehicles, or power systems. The efficiency of the fuel cells used in real life applications is approximately 60%. Because of that, efficiency of the fuel cell is assumed as 60% for this case study. During battery charging and discharging, there is a 5% loss. The hydrogen consumption of the fuel cell is calculated as 0.58 kg per hour. The fuel cell produces

energy constantly to improve the lifetime of the fuel cell and to reduce the slow response effect. In addition to this, batteries are utilized for providing energy for the peak loads. For example, in some hours, the electric load is much higher than the production capacity of the fuel cell. In that case, batteries provide energy with fuel cell and manage the peak electricity load.

Moreover, batteries provide faster response, so it can manage peak loads efficiently. Furthermore, batteries can degrade after charge-discharge cycles. So, the integration o fuel cell and battery system improve the lifecycle of the integrated power system. When the produced energy from the fuel cell is higher than the electric load, excess energy is directed to the battery system and the battery is charged. However, when the produced energy from the fuel cell system is lower than the load, the battery system is discharged.

The schematic of the fuel cell–battery integrated system is demonstrated in Figure 4.3. In this system, DC provides the connection between the fuel cell, battery, power controller and DC to AC power converter. The DC bus controller controls the power flow between fuel cell, battery system and DC/AC power converter. That provides flexibility in power management. The capacity of the battery system is determined as 7500 kWh. In the simulation, firstly, the determination of fuel cell capacity is done according to the hourly electrical load. Then, hourly battery charge and battery level – hours graph is prepared. According to this graph, the capacity of the battery is determined. Moreover, for analyzing the system, battery charge and hydrogen fuel cell for load–day, electrical load and fuel cell energy for load–day, hourly electrical load graphs are prepared.

Moreover, daily energy efficiency and exergy efficiency calculations have been performed and they have been demonstrated with graphs. Energy efficiencies and exergy efficiencies are calculated in two different ways:

When the electrical load is more than the capacity of the utilized fuel cell, the calculation for the energy efficiency is;

$$n_{energy} = \frac{\dot{E}_{\text{Supplied to Electric Load}}}{LHV_{H_2} \times \dot{m}_{H_2} + \dot{E}_{\text{Battery Discharge}} + \dot{E}_{\text{Battery Discharge Loss}}} \quad (4.20)$$

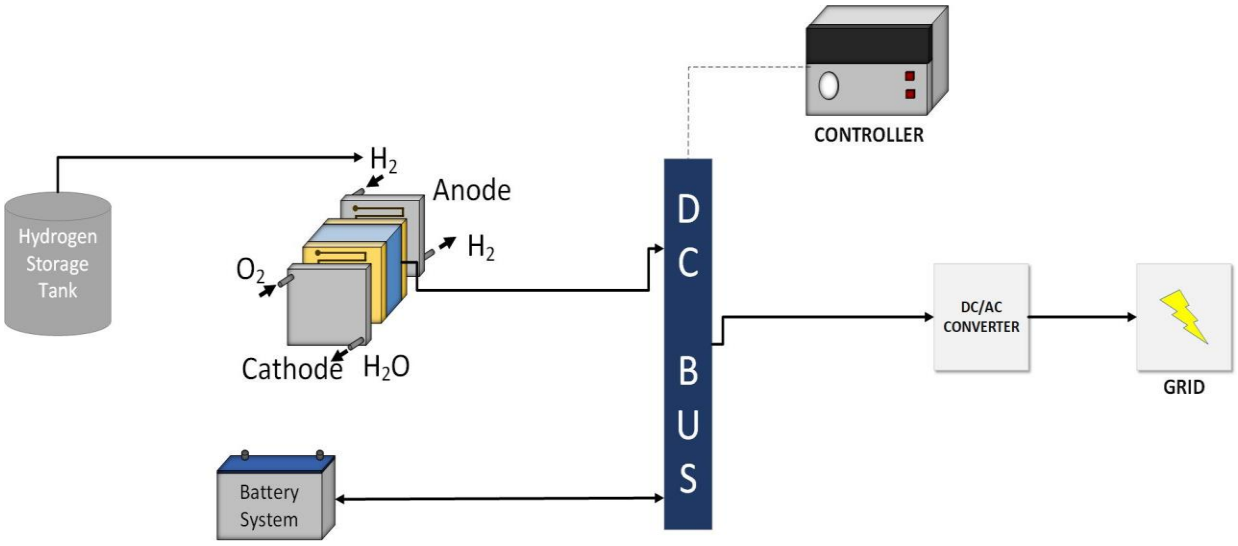

Figure 4.3 Schematic of battery and fuel cell integrated system for grid

When the electrical load is lower than the capacity of the utilized fuel cell, the calculation for the energy efficiency is;

$$n_{energy} = \frac{\dot{E}_{\text{Supplied to Electric Load}} + \dot{E}_{\text{Battery charge}} + \dot{E}_{\text{Battery charge losses}}}{LHV_{H_2} \times \dot{m}_{H_2}} \quad (4.21)$$

When the electrical load is greater than the capacity of the utilized fuel cell, the calculation for the exergy efficiency is;

$$n_{exergy} = \frac{\dot{E}x_{\text{Supplied to Electric Load}}}{ex_{H_2} \times \dot{m}_{H_2} + \dot{E}x_{\text{Battery Discharge}} + \dot{E}x_{\text{Battery Discharge Loss}}} \quad (4.22)$$

When the electrical load is lower than the capacity of the utilized fuel cell, the calculation for the exergy efficiency is;

$$n_{exergy} = \frac{\dot{E}x_{\text{Supplied to Electric Load}} + \dot{E}x_{\text{Battery charge}} + \dot{E}x_{\text{Battery charge losses}}}{ex_{H_2} \times \dot{m}_{H_2}} \quad (4.23)$$

Chapter 5. Results and Discussion

In Chapter 5, analysis, discussion, and demonstration of the experimental and theoretical study are performed. Moreover, the temperature of the humidifier's impact on fuel cell performance is observed. Furthermore, a performance evaluation of the battery and fuel cell experimental setup is performed. In addition to this, the results of the case study for fuel cell and battery integrated system are discussed.

5.1 Performance Results of Fuel Cell

The open circuit voltage of the one PEM cell is calculated as 1.23 V and 12.3 V theoretically using the Nernst equation. The results of the experiments demonstrate the irreversibility occurrence. At 20 °C and 1 atm feed hydrogen conditions, the open circuit voltage of the stack is measured as 8.73 V. The theoretical open circuit voltage of the cell is higher than the experimental one. That may be caused by the crossover of the fuel. The fuel crossover is the leak of the fuel through the membrane from the anode to the cathode. That may cause a short circuit situation, lowering the efficiency of the cell and production of undesired products [107]. There are also other parameters that can decrease the open circuit voltage of the PEM fuel cell. The parameters utilized in theoretical calculations of the PEM fuel cell are given in Table 5.1. In Figures 5.1 and 5.2, a comparison of experimental data and theoretical data is demonstrated in polarization curves and power density graphs. The results of the theoretical calculations and experiments are closer to each other, but the experimental results are less than the theoretical ones. That may be caused by ohmic drops. Resistive losses caused by wiring and connections are not considered in theoretical calculations. The other reason is the heterogeneity of the electrode surface. In theoretical calculations, the surface of the electrode is assumed uniform; however, in experiments, it has impurities and roughness. The highest power density for the theoretical calculations is 0.138 W/cm^2, and the experimental peak power density is 0.093 W/cm^2 at a current density of 0.017 A/cm^2. Experimental tests are performed three times. Three is the minimum number of experiments required for uncertainty analysis and standard deviation calculations, so experiments are performed three times.

Table 5.1 Properties of PEM Fuel Cell for theoretical calculations (data from [108]):

E_R (V)	1.23
Temperature (K)	298
Pressure (bar)	1
i_o (A)	1.00E-04
i_L (A)	1.5
i_{loss} (A)	0.002
R_i $(ohm - cm^2)$	0.03
α	1
F $(\frac{C}{mol})$	96485
n	2
R $(\frac{J}{mol\,K})$	8.314

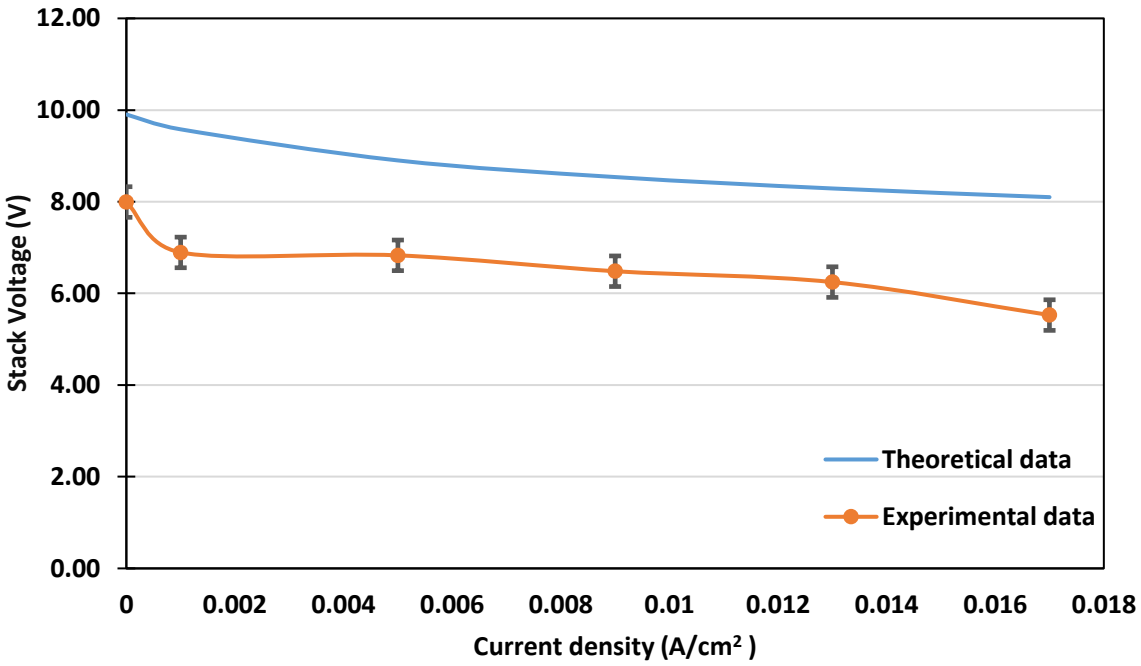

Figure 5.1 Stack voltage vs current density comparison for 20°C operation

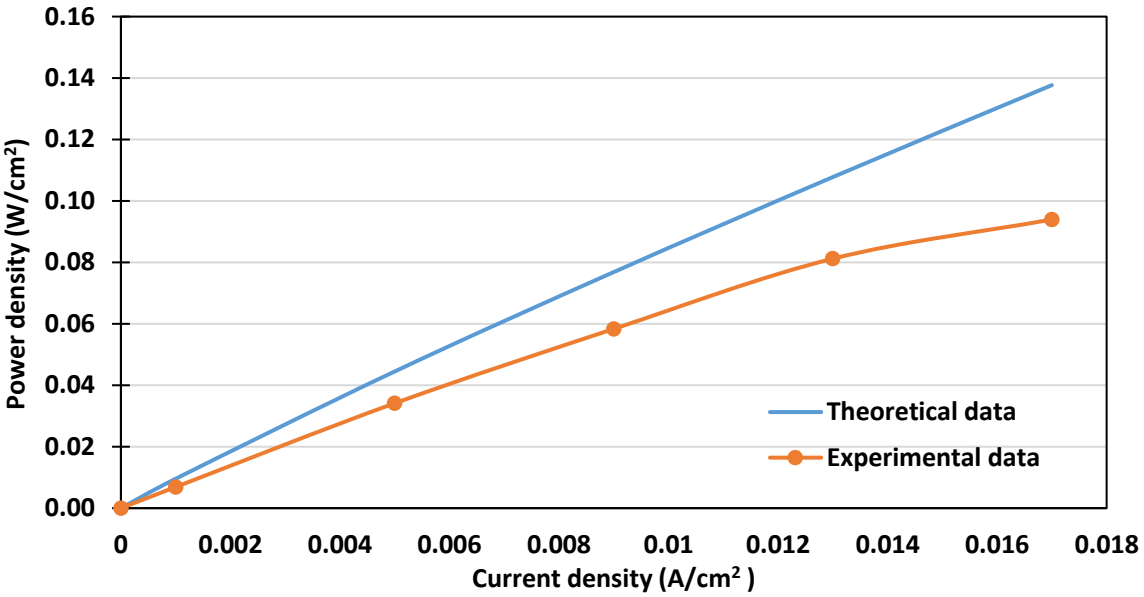

Figure 5.2 Power density vs current comparison

5.2 Results of Humidifier Temperature Effect on Fuel cell

Analysis of the performance of the proton exchange membrane fuel cell under different humidifier temperatures is performed. Especially at the cathode side of the PEM fuel cell, an increase in the temperature of the humidifier improves the reduction of oxygen. In this study, analyses for the performance of the PEM fuel cell at 20 °C, 50 °C, 65 °C and 80 °C humidifier temperatures are performed. The highest humidifier temperature is determined as 80 °C because higher than 80 °C humidifier temperature causes excessive water, and that leads to flooding in the PEM fuel cell which causes a decrease in the proton conductivity of the membrane and reduces the performance of the fuel cell [109]. The stack voltage vs current density graph can be seen in Figure 5.3. Furthermore, power density vs current density graphs for 20 °C can be seen Figure in 5.4. As demonstrated in the polarization curves, the highest open circuit voltage is measured between 7.96 and 8.16 V. The average voltage of the fuel cell is obtained as 6.89 V at 0.001 A/cm^2, 6.83 V at 0.005 A/cm^2, 6.48 V at 0.009 A/cm^2, 6.24 V at 0.013 A/cm^2 and 5.52 V at 0.017 A/cm^2. Furthermore, peak power density is measured between 0.092 W/cm^2 and 0.096 W/cm^2. The average power density is calculated as 0.0068 W/cm^2 at 0.001 A/cm^2, 0.034 W/cm^2 at 0.005 A/cm^2, 0.058 W/cm^2 at 0.009 A/cm^2, 0.081 W/cm^2 at 0.013 A/cm^2 and 0.094 W/cm^2 at 0.017 A/cm^2.

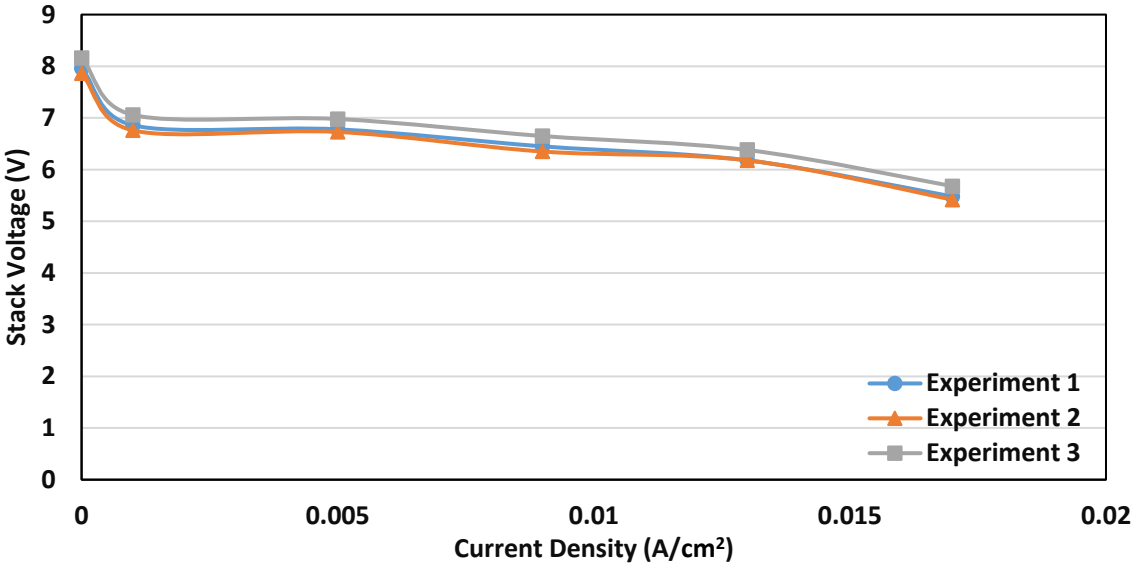

Figure 5.3 Stack Voltage vs current density at 20 °C humidifier temperature

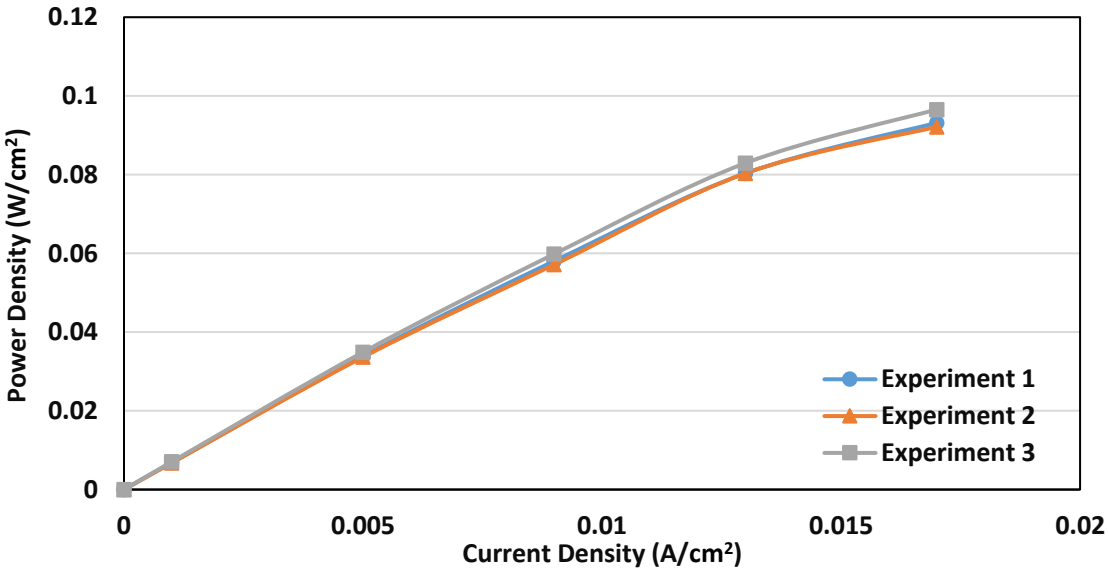

Figure 5.4 Power density vs current density at 20 °C humidifier temperature

In addition to this, energy efficiency vs current density graphs can be seen in Figure 5.5. Furthermore, the exergy efficiency vs current density graph is demonstrated in Figure 5.6. The highest energy efficiency is obtained as 11.3%. In addition to this, the highest exergy efficiency of the PEM fuel cell is calculated as 11.8% for 20 °C humidifier temperature. When the current density increases, enhancement in energy and exergy efficiencies are observed. The main reason of that, with an increase in current density, the generated power by the PEM fuel cell is increased and that enhances the efficiency of the fuel cell.

The exergy efficiency of the PEM fuel cell is calculated higher than the energy efficiency because of the exergy value of the hydrogen. It is lower than the lower heating value of the hydrogen. The obtained efficiencies at 20 °C humidifier temperature are lower than the efficiencies that are obtained at higher humidifier temperatures. The average energy efficiency of the fuel cell is 0.82% at 0.001 A/cm^2, 4.1% at 0.005 A/cm^2, 7% at 0.009 A/cm^2, 9.75% at 0.013 A/cm^2 and 11.3% at 0.017 A/cm^2. The average exergy efficiency is obtained as 0.84% at 0.001 A/cm^2, 4.17% at 0.005 A/cm^2, 7.12% at 0.009 A/cm^2, 9.91% at 0.013 A/cm^2 and 11.47% at 0.017 A/cm^2.

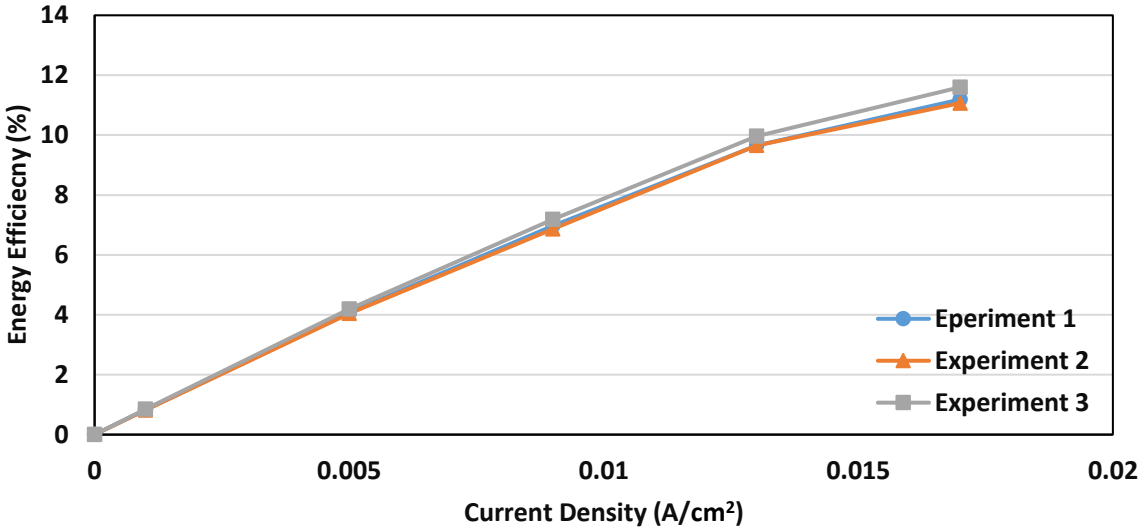

Figure 5.5 Energy efficiency vs current density at 20 °C humidifier temperature

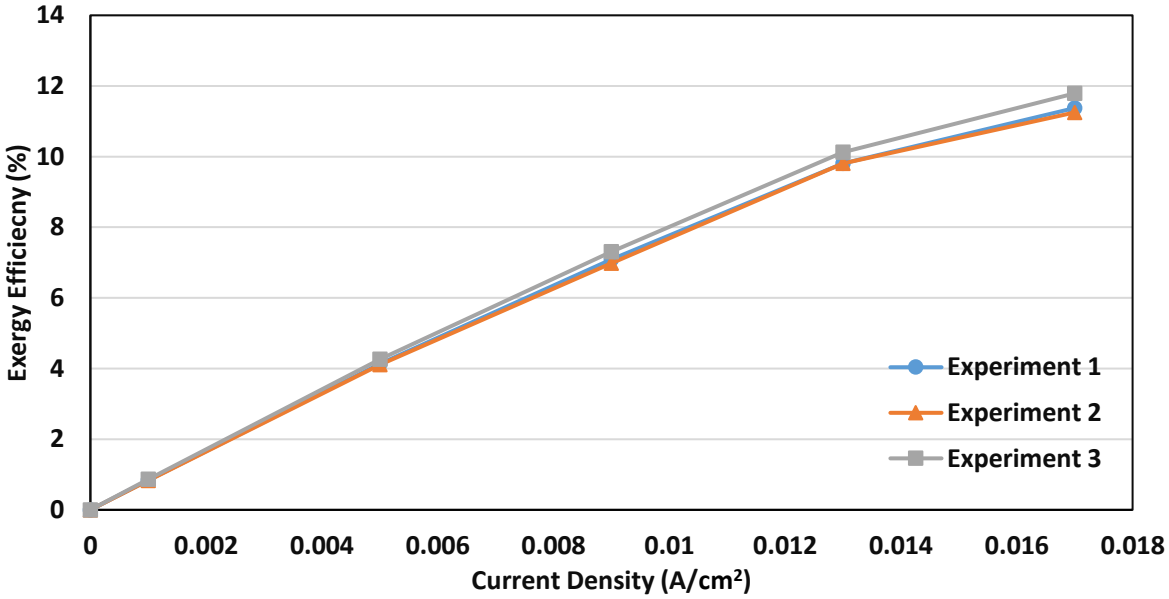

Figure 5.6 Exergy efficiency vs current density at 20 °C humidifier temperature

In Figures 5.7 and 5.8, voltage vs current density and power density vs current density graphs at 50 °C humidifier temperature operation are demonstrated. As seen in the polarization curves, the highest open circuit voltage is measured between 8.23 V and 8.53 V. The highest measured open circuit voltage, 8.53 V, is 4.53% greater than the highest open circuit voltage at 20 °C humidifier temperature operation. So, there is an increase in open circuit voltage with an increase in the temperature of the humidifier. In addition to this, the measured peak power density at 50 °C humidifier temperature operation is 0.097 W/cm^2 at 0.017 A/ cm^2. Furthermore, there is a 1.04% increase in measured greatest power density compared to the 20 °C temperature humidifier operation. The average voltage of the PEM fuel cell is obtained as 7.16 V at 0.001 A/cm^2, 7.09 V at 0.005 A/cm^2, 6.79 V at 0.009 A/cm^2, 6.54 V at 0.013 A/cm^2 and 5.56 V at 0.017 A/cm^2. The average power density is calculated as 0.0072 W/cm^2 at 0.001 A/cm^2, 0.035 W/cm^2 at 0.005 A/cm^2, 0.061 W/cm^2 at 0.009 A/cm^2, 0.085 W/cm^2 at 0.013 A/cm^2 and 0.094 W/cm^2 at 0.017 A/cm^2.

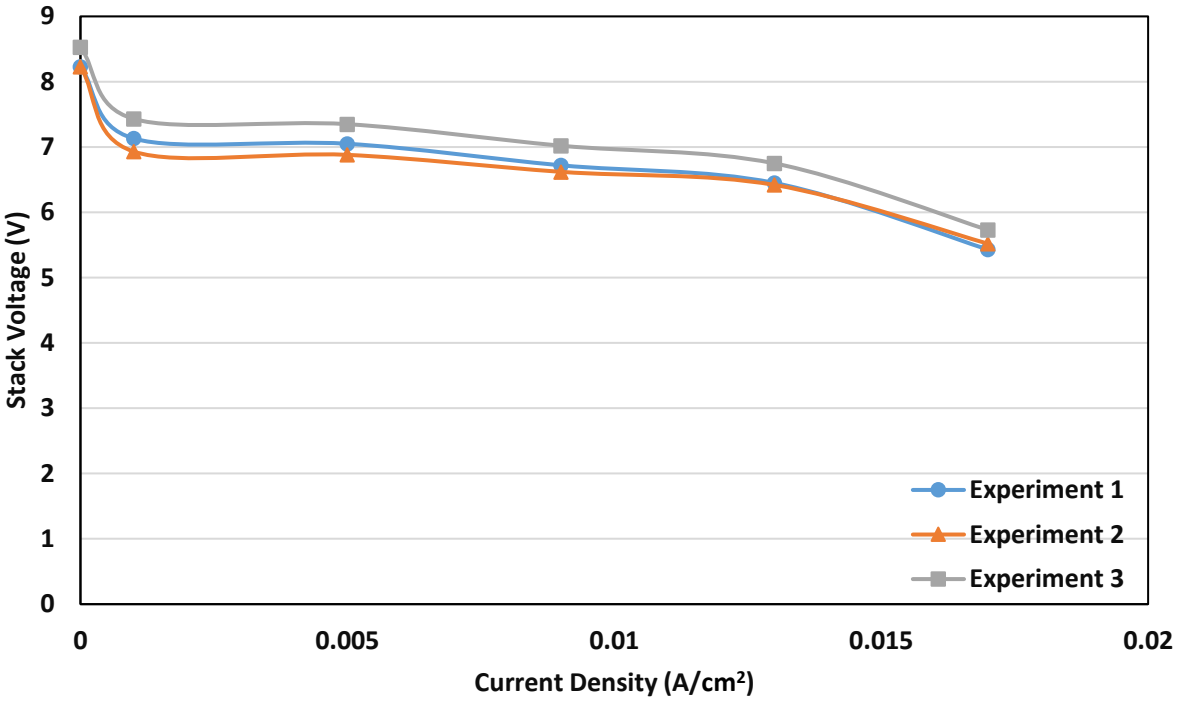

Figure 5.7 Stack voltage vs current density at 50 °C humidifier temperature

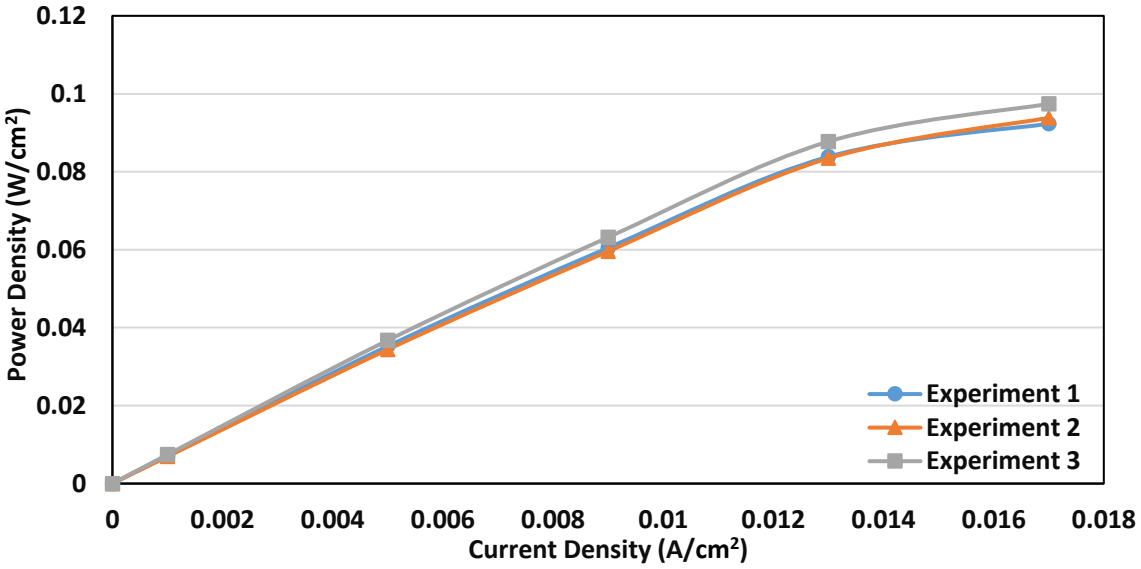

Figure 5.8 Power density vs current density at 50 °C humidifier temperature

In Figures 5.7 and 5.8, energy and exergy efficiencies of PEM fuel cells at different current densities and at 50 °C humidifier temperature operation are demonstrated. The highest energy and exergy efficiencies are obtained as 11.7% and 11.9%. There is an increase in energy efficiency and exergy efficiency at the 50 °C operating temperature compared to the 20 °C humidifier temperature. The average energy efficiency of the fuel cell is 0.86% at 0.001 A/cm^2, 4.26% at 0.005 A/cm^2, 7.33% at 0.009 A/cm^2, 10.21% at 0.013 A/cm^2 and 11.35% at 0.017 A/cm^2. The average exergy efficiency is obtained as 0.87% at 0.001 A/cm^2, 4.33% at 0.005 A/cm^2, 7.45% at 0.009 A/cm^2, 10.38% at 0.013 A/cm^2 and 11.54% at 0.017 A/cm^2.

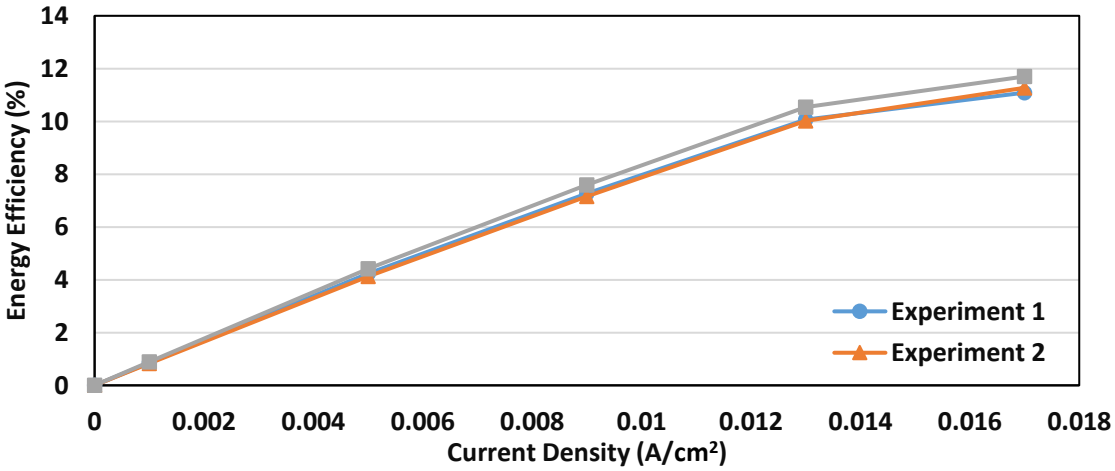

Figure 5.9 Energy efficiency vs current density at 50 °C humidifier temperature

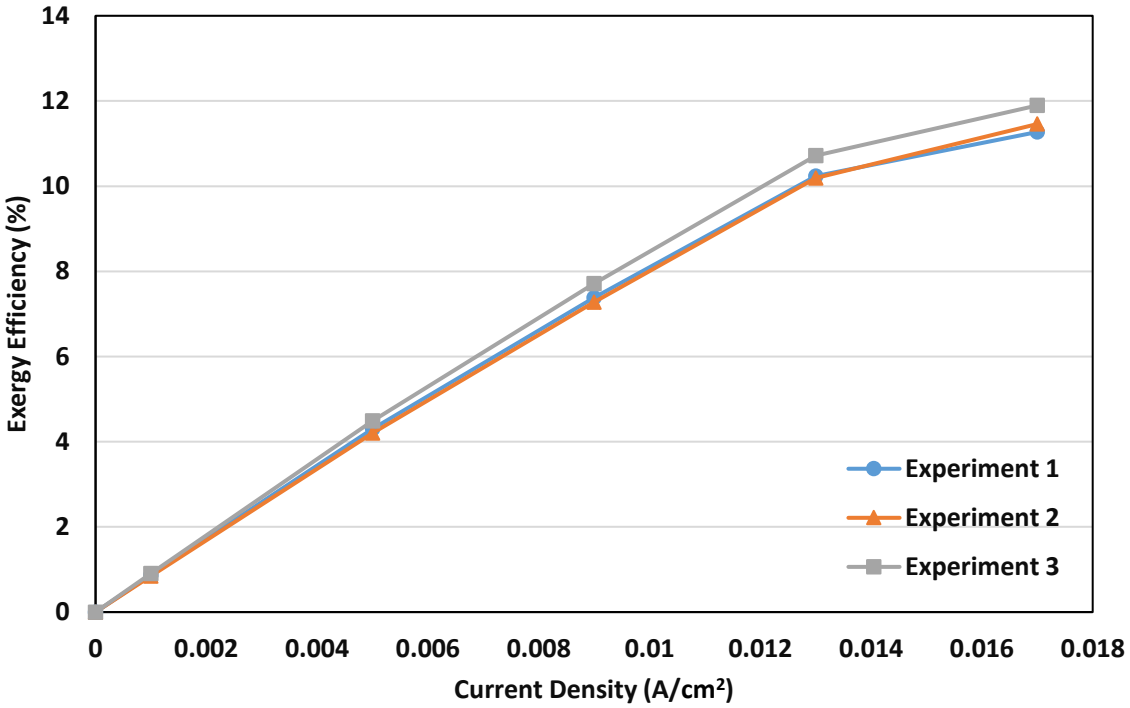

Figure 5.10 Exergy efficiency vs current density at 50 °C humidifier temperature

For 65°C humidifier temperature operation, the polarization curves and power density curves are demonstrated in Figures 5.11 and 5.12 respectively. The open circuit voltage is measured as 8.62 V which is higher than the open circuit voltage of 50°C humidifier temperature operation. In addition to this, the highest open circuit voltage is increased 4.25% compared to the 20 °C operation and 0.33% higher than the 50 °C operation. Furthermore, the highest power density in 65°C operation is higher than the 50 °C operation. At 65°C operation, peak power density is 0.102 W/cm^2 and that value is measured at 0.021 A/m^2 and 6.03 V. That value is 10% higher than the value at 50 °C operation. The average voltage of the fuel cell is obtained as 7.53 V at 0.001 A/cm^2, 7.39 V at 0.005 A/cm^2, 7.14 V at 0.009 A/cm^2, 6.78 V at 0.013 A/cm^2 and 5.82 V at 0.017 A/cm^2. The average power density is calculated as 0.0075 W/cm^2 at 0.001 A/cm^2, 0.037 W/cm^2 at 0.005 A/cm^2, 0.064 W/cm^2 at 0.009 A/cm^2, 0.088 W/cm^2 at 0.013 A/cm^2 and 0.099 W/cm^2 at 0.017 A/cm^2. In Figures 5.13 and 5.14, for 65 °C operation, energy and exergy efficiencies at different current densities are observed. The highest energy efficiency of the PEM fuel cell is calculated as 11.84%. Furthermore, highest exergy efficiency of the fuel cell is calculated as 12.09%. The average energy efficiency of the

fuel cell is 0.90% at 0.001 A/cm^2, 4.44% at 0.005 A/cm^2, 7.72% at 0.009 A/cm^2, 10.60% at 0.013 A/cm^2 and 11.89% at 0.017 A/cm^2.

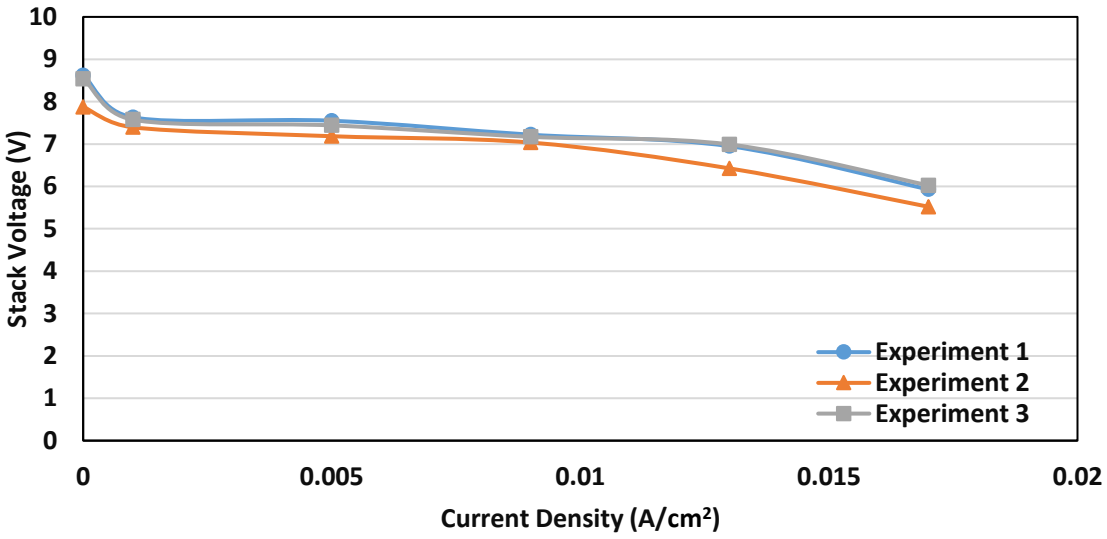

Figure 5.11 Stack voltage vs current density at 65 °C humidifier temperature

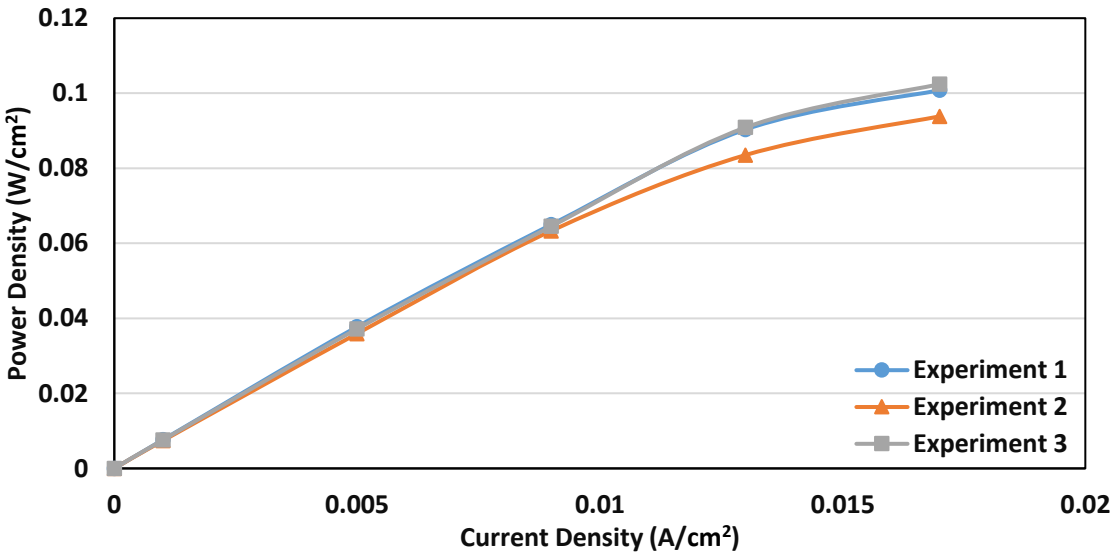

Figure 5.12 Power density vs current density at 65 °C humidifier temperature

The average exergy efficiency is obtained as 0.91% at 0.001 A/cm^2, 4.51% at 0.005 A/cm^2, 7.84% at 0.009 A/cm^2, 10.77% at 0.013 A/cm^2 and 12.09% at 0.017 A/cm^2. For 80°C humidifier temperature operation, the polarization curves and power density curves are demonstrated in Figures 5.15 and 5.16 respectively.

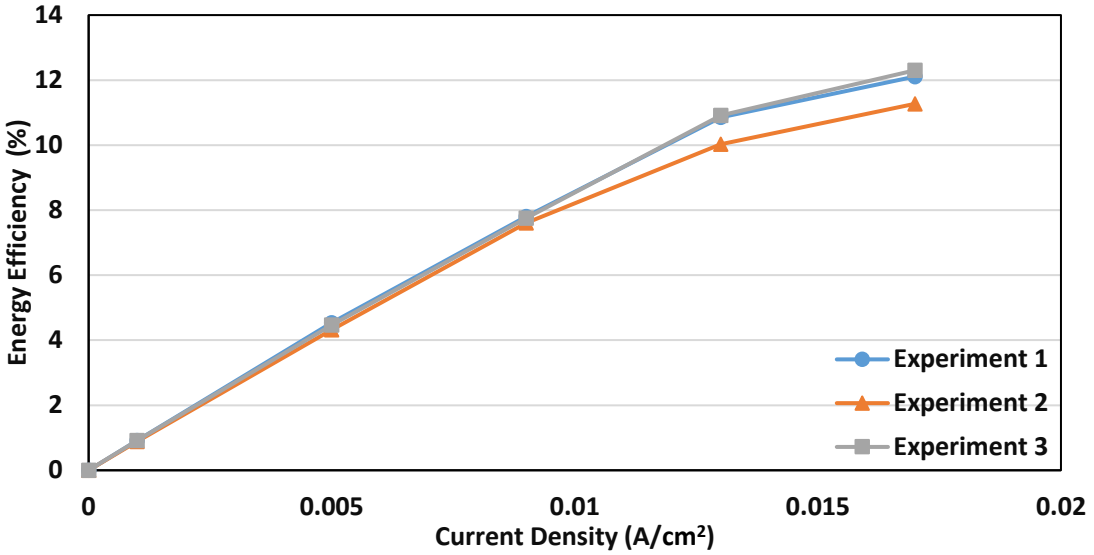

Figure 5.13 Energy efficiency vs current density at 65 °C humidifier temperature

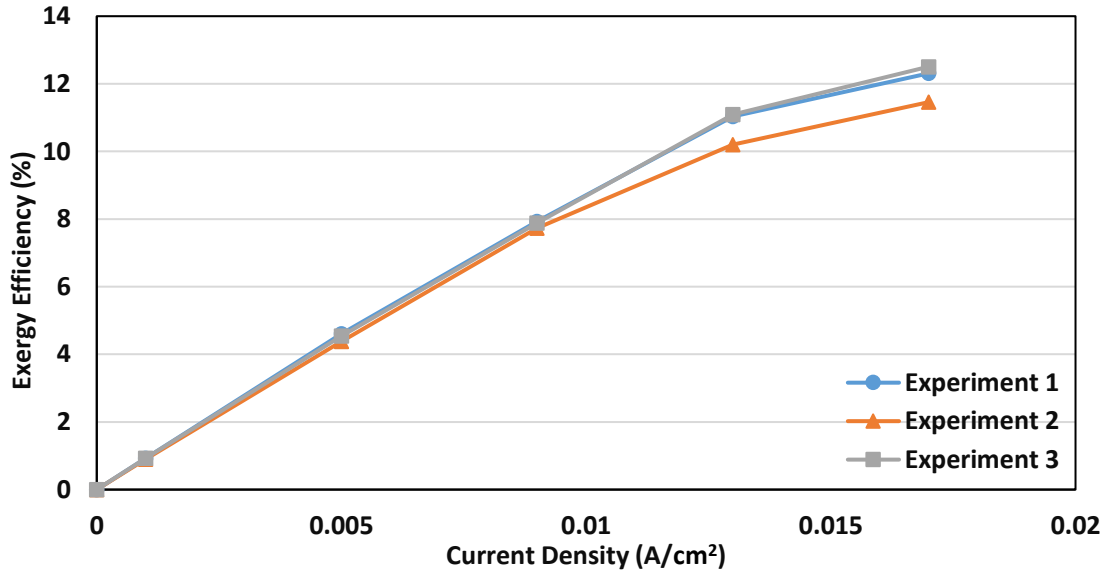

Figure 5.14 Exergy efficiency vs current density at 65 °C humidifier temperature

The open circuit voltage is measured as 8.79 V which is higher than the open circuit voltage of 50°C and 65°C humidifier temperature operation. In addition to this, open circuit voltage is increased 10% compared to the 20 °C operation and 5.52% higher than the 50 °C operation. Furthermore, the highest power density in 80°C operation is higher than the 50 °C operation. At 80°C operation, peak power density is 0.122 W/cm^2 and that value is measured at 0.021 A/m^2 and 5.83 V. The average voltage of the fuel cell is obtained as 7.92 V at 0.001 A/cm^2, 7.77 V at 0.005 A/cm^2, 7.56 V at 0.009 A/cm^2, 7.33 V

at 0.013 A/cm^2 and 6.32 V at 0.017 A/cm^2. The average power density is calculated as 0.0079 W/cm^2 at 0.001 A/cm^2, 0.039 W/cm^2 at 0.005 A/cm^2, 0.068 W/cm^2 at 0.009 A/cm^2, 0.095 W/cm^2 at 0.013 A/cm^2 and 0.107 W/cm^2 at 0.017 A/cm^2.

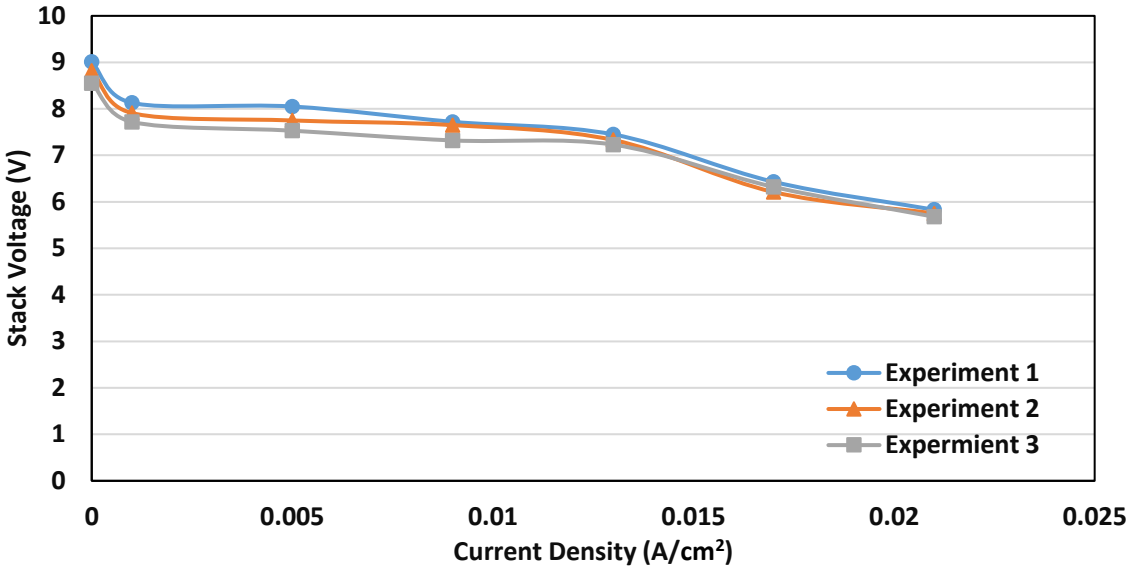

Figure 5.15 Stack voltage vs current density at 80 °C humidifier temperature

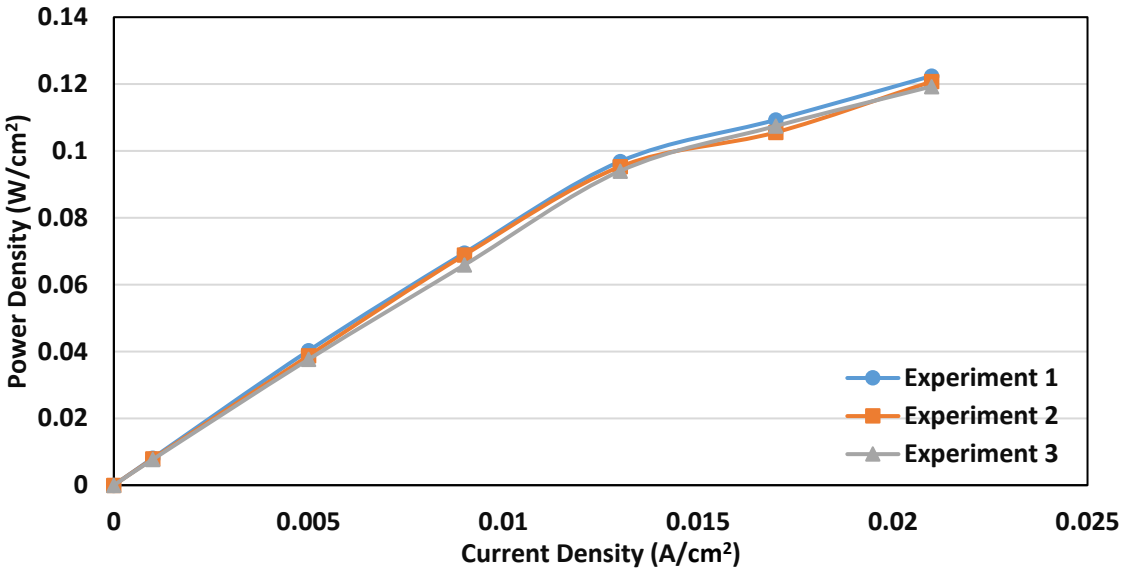

Figure 5.16 Power density vs current density at 80 °C humidifier temperature

In Figures 5.17 and 5.18, for 80 °C operation, energy and exergy efficiencies at different current densities are observed. The highest energy efficiency is calculated as 14.7% and exergy efficiency is calculated as 14.9%. The highest energy and exergy efficiencies are

obtained at 80 °C humidifier temperature. The average energy efficiency of the fuel cell is 0.95% at 0.001 A/cm^2, 4.67% at 0.005 A/cm^2, 8.17% at 0.009 A/cm^2, 11.45% at 0.013 A/cm^2 and 14.7% at 0.021 A/cm^2. The average exergy efficiency is obtained as 0.96% at 0.001 A/cm^2, 4.74% at 0.005 A/cm^2, 8.31% at 0.009 A/cm^2, 11.64% at 0.013 A/cm^2 and 14.9% at 0.021 A/cm^2.

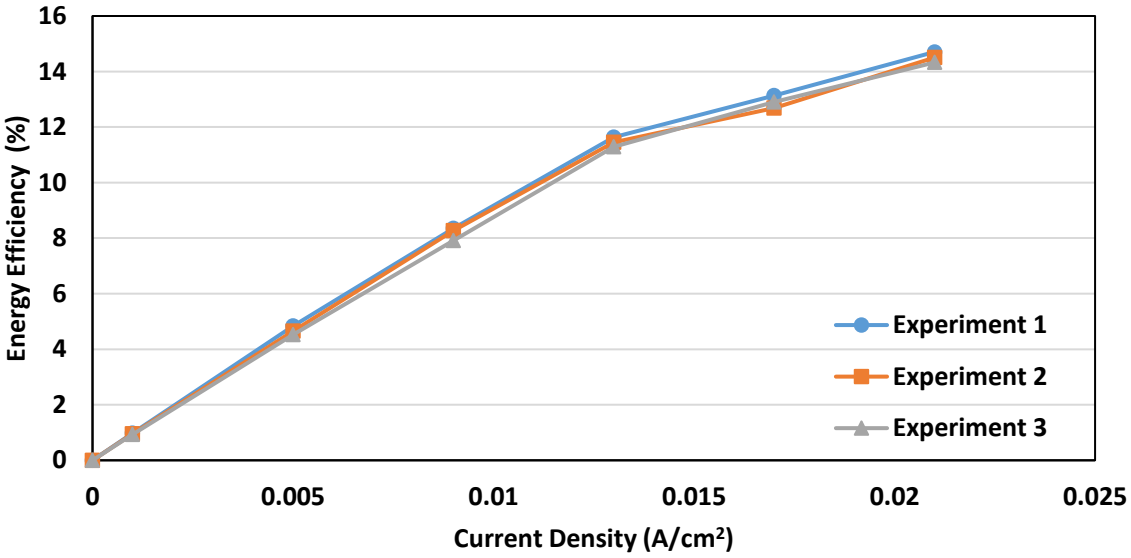

Figure 5.17 Energy efficiency vs current density at 80 °C humidifier temperature

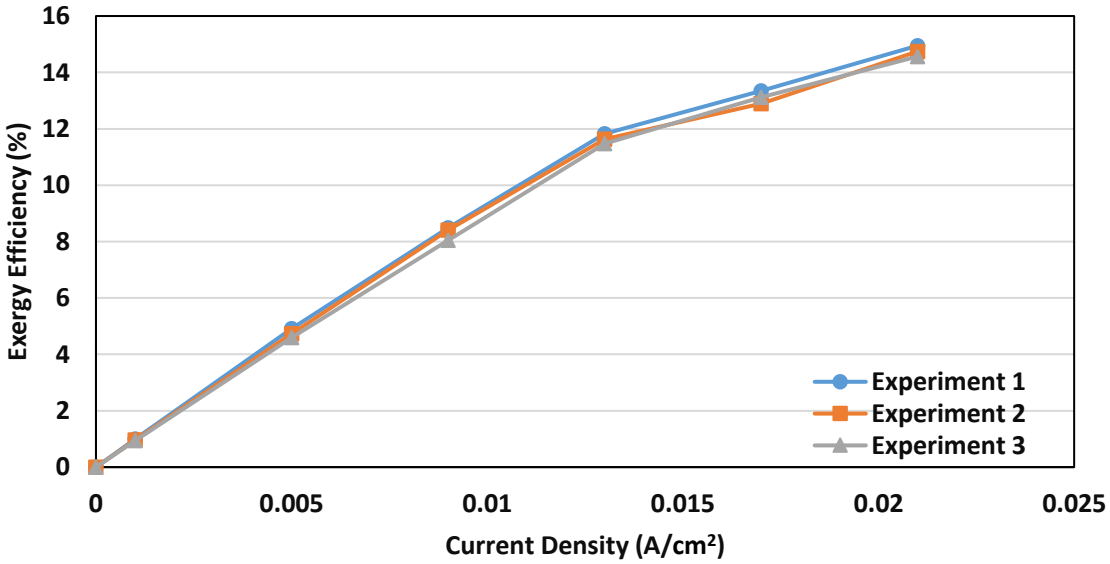

Figure 5.18 Exergy efficiency vs current density at 80 °C humidifier temperature

As seen in Figures 5.19 and 5.20, an increase in power density and voltage with temperature of the humidifier is observed. From uncertainty analysis, standard deviations are calculated as very low. The average highest voltage and peak power density are obtained as 8.79 V and 0.107 W/m^2, respectively at 80 °C. For 20 °C, the average highest voltage and power density are obtained as 7.99 V and 0.093 W/cm^2. Furthermore, for 50 °C humidifier temperature operation, the highest average voltage is obtained as 8.33 V and the greatest power density is 0.094 W/m^2. Finally, at 65 °C humidifier temperature, the highest voltage value is obtained as 8.34 V and the greatest power density is 0.099 W/m^2. The main reason for that rise in greatest power density with an operating temperature of the humidifier is the enhancement in the kinetics of the reaction. Furthermore, the required energy for the electrochemical reaction is decreased with an increase in temperature. Increase in current enhances the fuel consumption, and more electrons are produced because of the higher current operation. Initially, increase in current and decrease in voltage lead to increase in power density of the fuel cell and fuel cell reaches its maximum power density because voltage does not decrease significantly. However, if the current of the fuel cell is increased after it reached maximum power density, voltage decreases significantly and decrease in power density is observed. In this study, a decrease in power density couldn't be observed because of the limitations of the electric load device. The electric load device couldn't obtain data below 5.4 voltage operation. Because of that reason, the current density of the operation could not be increased more, and a decrease in power density was not observed. In Figures 5.21 and 5.22, average energy efficiency vs current density density and average exergy efficiency vs current density density of PEM fuel cell at different humidifier temperatures are demonstrated, respectively. An increase in energy and exergy efficiencies are observed with an increase in humidifier temperature. At 0.05 A/cm^2, average energy, and exergy efficiencies are calculated as 4.67% and 4.74% respectively for 80°C humidifier temperature. However, at 0.05 A/cm^2, average energy and exergy efficiencies are calculated as 4.10% and 4.17% respectively for 20°C humidifier temperature. Furthermore, at 0.17 A/cm^2, average energy and exergy efficiencies are calculated as 14.51% and 14.75% respectively for 80°C humidifier temperature.

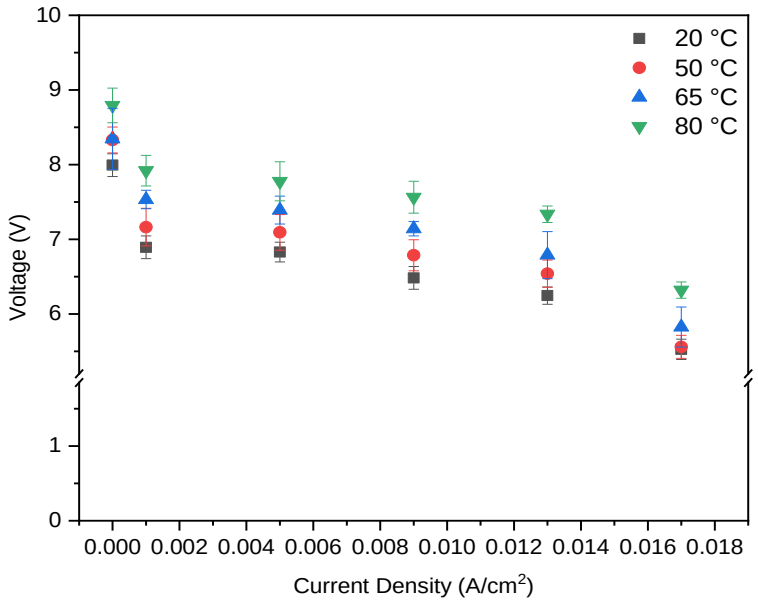

Figure 5.19 Voltage vs current density of PEM fuel cell at different humidifier temperatures

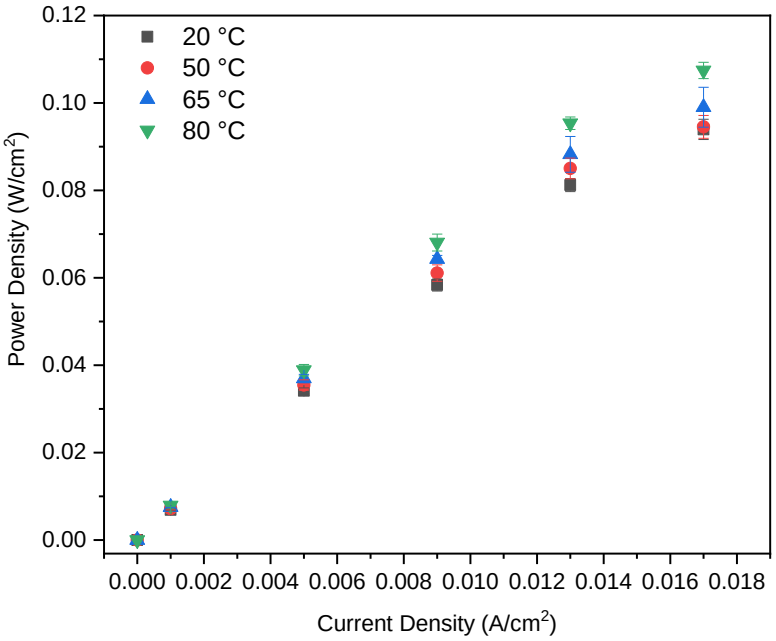

Figure 5.20 Power density vs current density of PEM fuel cell at different humidifier

However, at 0.17 A/cm^2, average energy and exergy efficiencies are calculated as 11.30% and 11.51% respectively for 20°C humidifier temperature. Energy efficiency vs current density (energy supplied to the humidifier included) and exergy efficiency vs current density (exergy supplied to the humidifier included) graphs have been given in Figures

5.23 and 5.24. When energy loss of the humidifier is included into efficiency calculations, the significant decrease in the efficiency of the system is observed. The main reason of that, much higher amount energy is utilized for heating water compared to the energy production capacity of the fuel cell system. Efficiency can be increased by designing more suitable condenser for the system. Insulation materials can be used for the condenser for decreasing the energy loss. Moreover, smaller condenser can be designed for providing less energy to water.

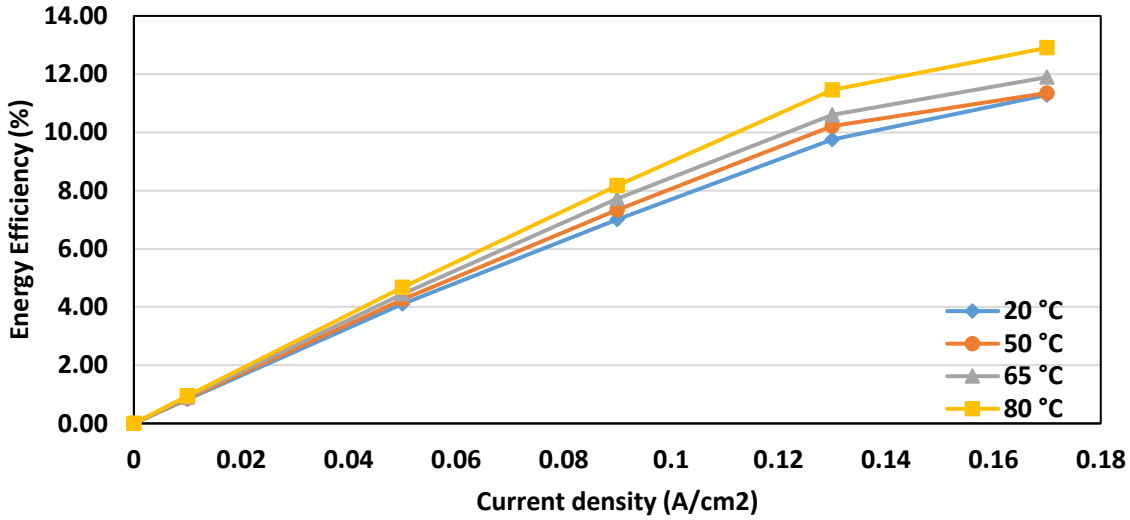

Figure 5.21 Average energy efficiency vs current density density of PEM fuel cell

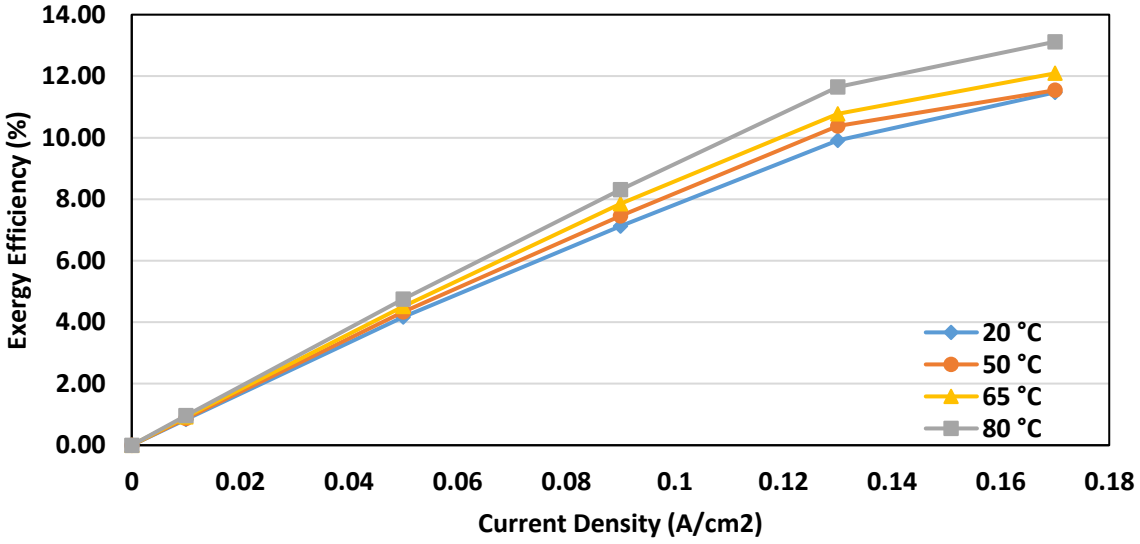

Figure 5.22 Average exergy efficiency vs current density of PEM fuel cell

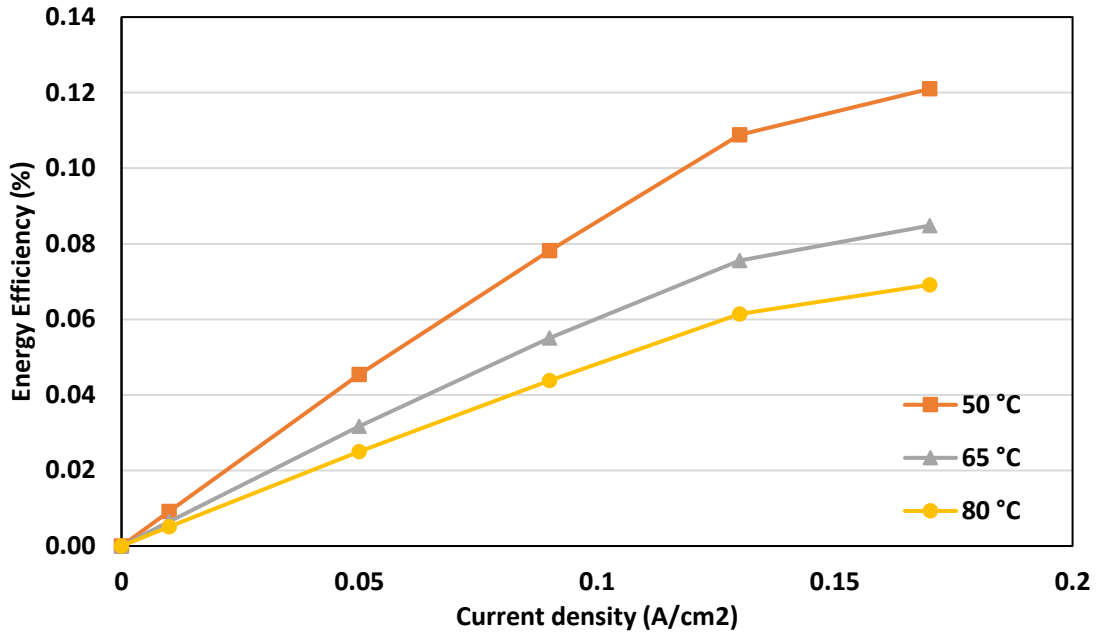

Figure 5.23 Energy efficiency vs current density (with energy consumption in humidifier)

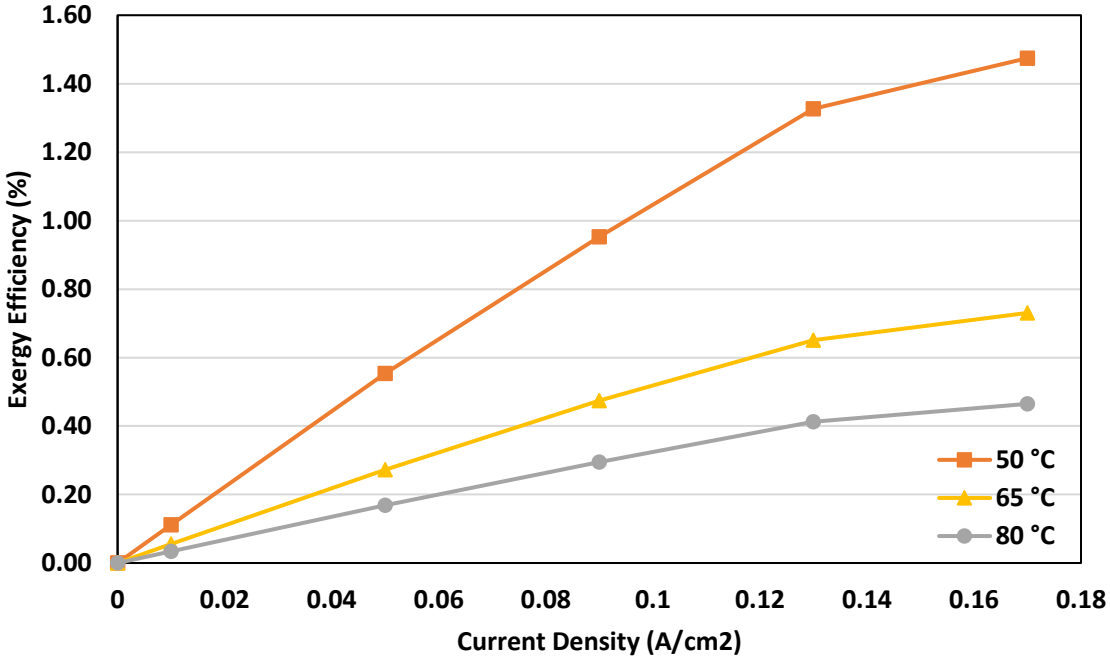

Figure 5.24 Exergy efficiency vs current density (with exergy consumption in humidifier)

5.3 Results of Case Studies

In Figure 5.25, scaled data of the electric load of California is demonstrated. For this case study, the effects of two different capacities of fuel cells have been observed. In Case-1 capacity of the fuel cell is 14 kWh, and in Case-2 capacity of fuel cell is 18 kWh.

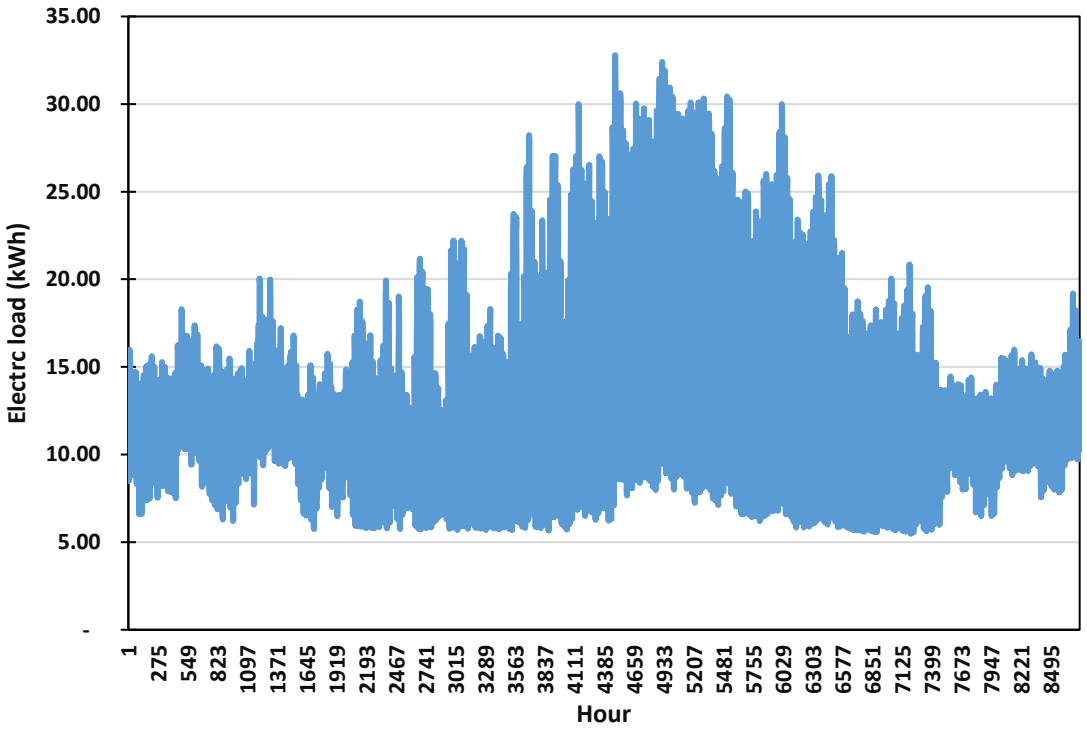

Figure 5.25 Electric load vs hours

5.3.1 Results for Case-1

In Figure 5.26, the battery charge-battery level vs hours graph is demonstrated. When the demand for electricity decreases, the battery is charged and the level of the battery increases. However, when the demand of electricity increases, the battery is discharged and the level of the battery decreases. So, it improves the control of the electric load very well. In addition to this, the response time of the fuel cell is very low compared to the battery systems. So, it provides improvements in control of electric load fluctuations. In Figure 5.26, initially, there is an increase in the level of the battery because of the low electric load. Then it reached its capacity. Then, there is a decrease in battery level because there is an increase in electric load. In Figure 5.27, Electric loads – Fuel cell energy for load vs Day graph is demonstrated. Energy production from hydrogen is constant; however, supplied energy to the electric load is not constant because when the electric load is lower than the fuel cell, part of the produced energy is directed to the battery. In Figure 5.28, the Hydrogen fuel cell for load – Battery charge vs Day graph is demonstrated.

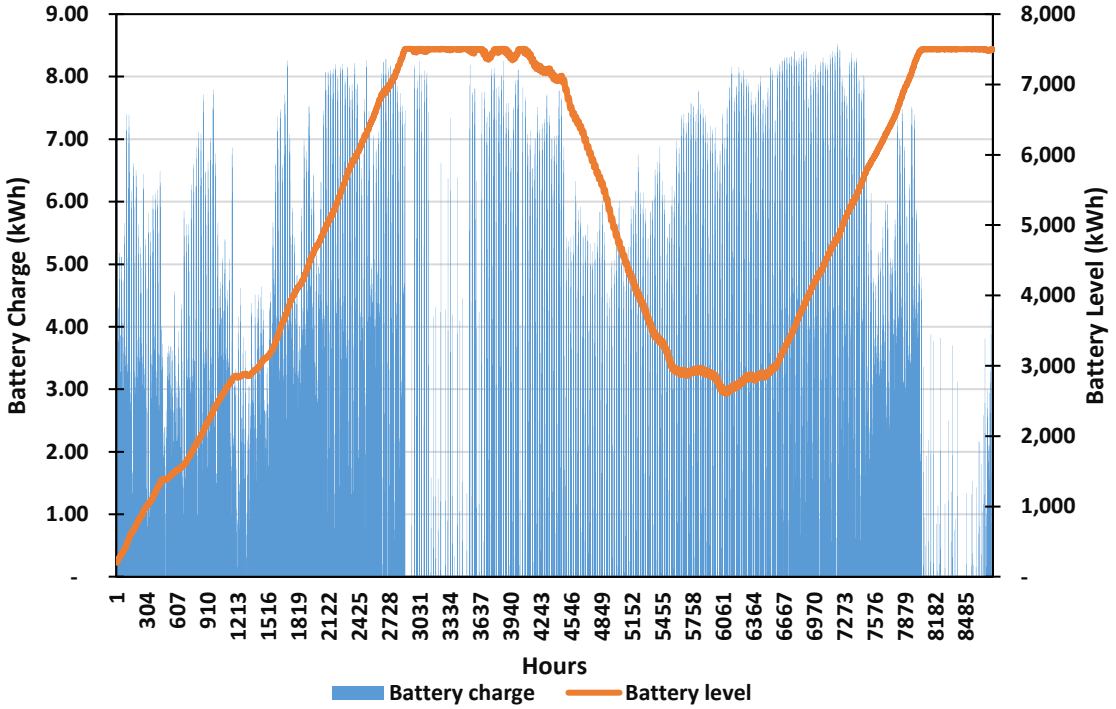

Figure 5.26 Battery charge – Battery level vs Hours (14 kWh fuel cell)

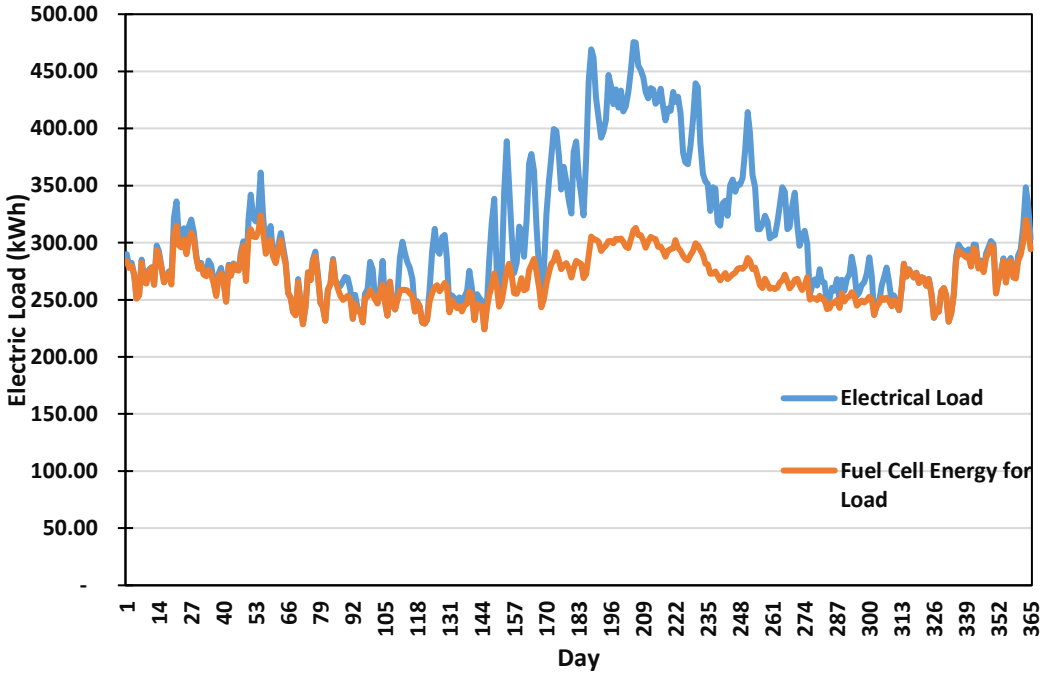

Figure 5.27 Electric loads – Fuel cell energy for load vs Day (14 kWh fuel cell)

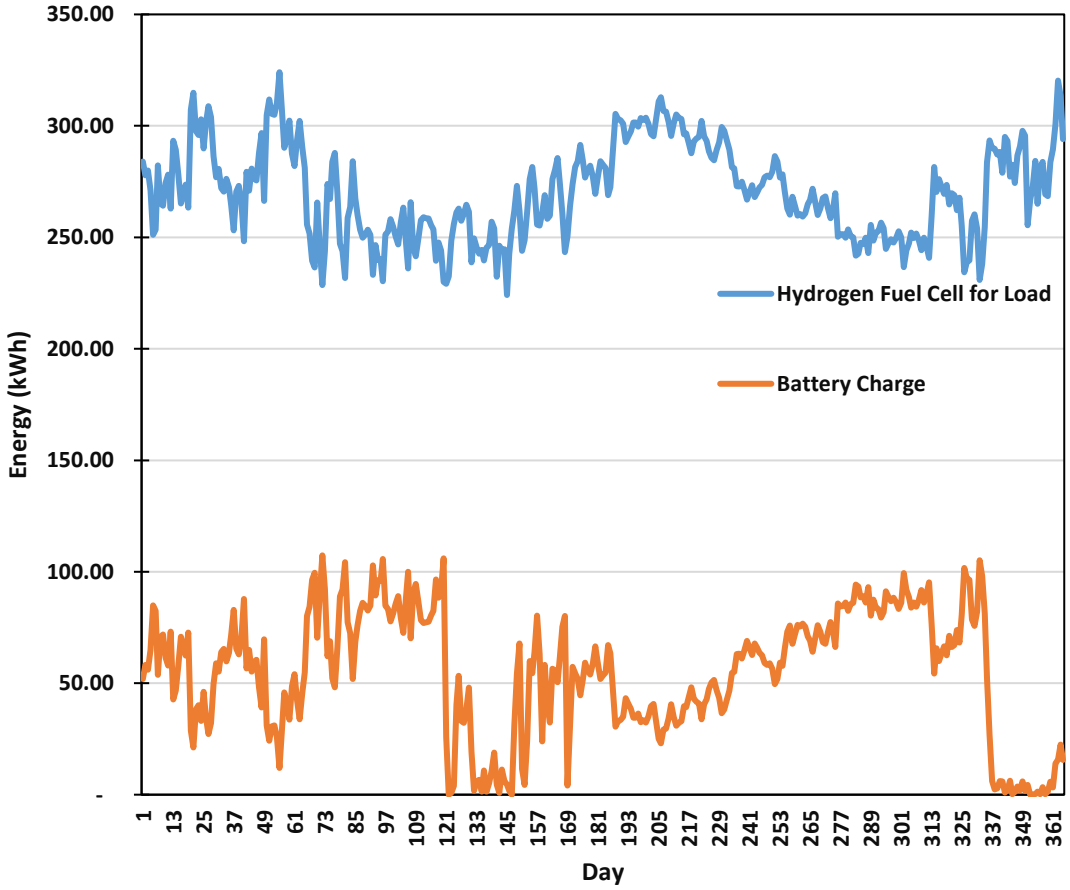

Figure 5.28 Hydrogen fuel cell for load – Battery charge vs Day (14 kWh fuel cell)

In Figures 5.29 and 5.30, energy efficiency vs day and exergy efficiency vs day graphs are demonstrated. Calculations for daily energy efficiencies and exergy efficiencies are calculated from equations 4.20, 4.21 and 4.22, 4.23, respectively. Because of the definitions of energy and exergy efficiencies, when the electric load is higher than the capacity of the fuel cell, energy efficiency is calculated higher compared to the days that the electric load is lower than the capacity of the fuel cell. Furthermore, in Figure 5.31, the Battery charge – Battery discharge vs Day graph is demonstrated. As seen in the Figure 5.31, when there is an increase in electric load, the battery charge decreases and the battery discharge increases. When the electric load decreases, battery charge increases and battery discharge decreases.

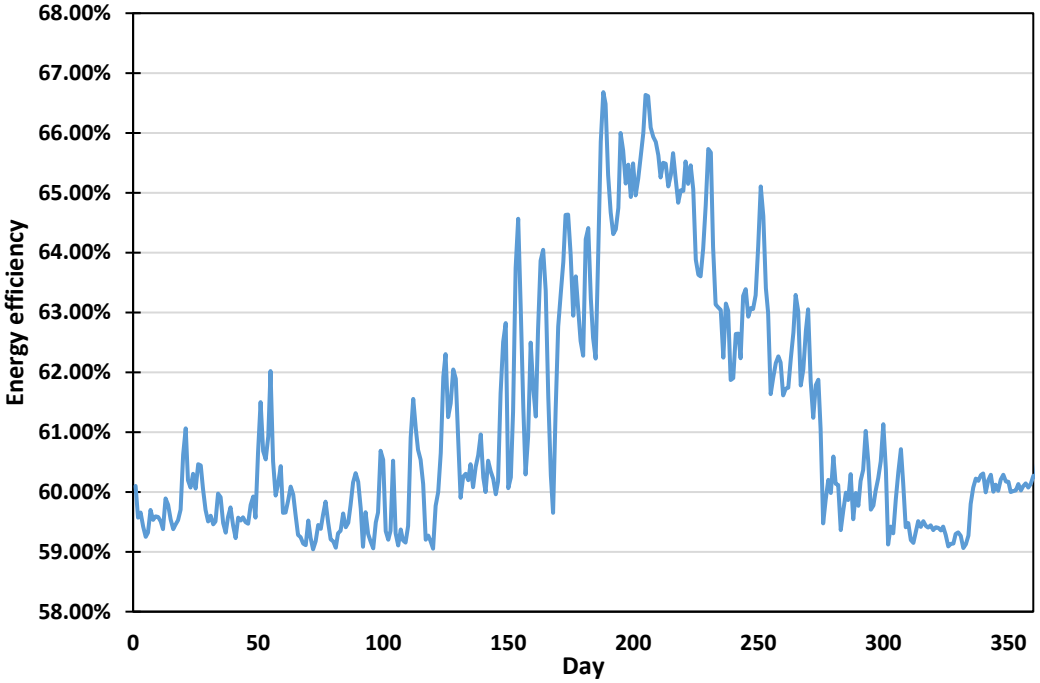

Figure 5.29 Energy efficiency vs Day (14 kWh fuel cell)

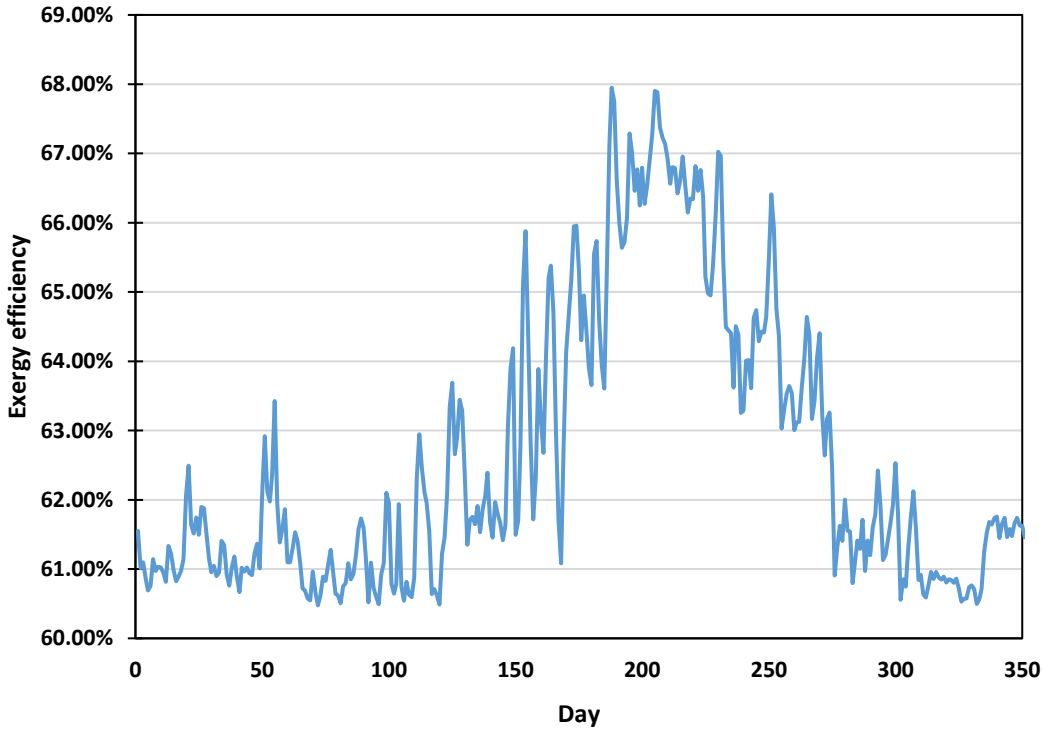

Figure 5.30 Exergy efficiency vs Day (14 kWh fuel cell)

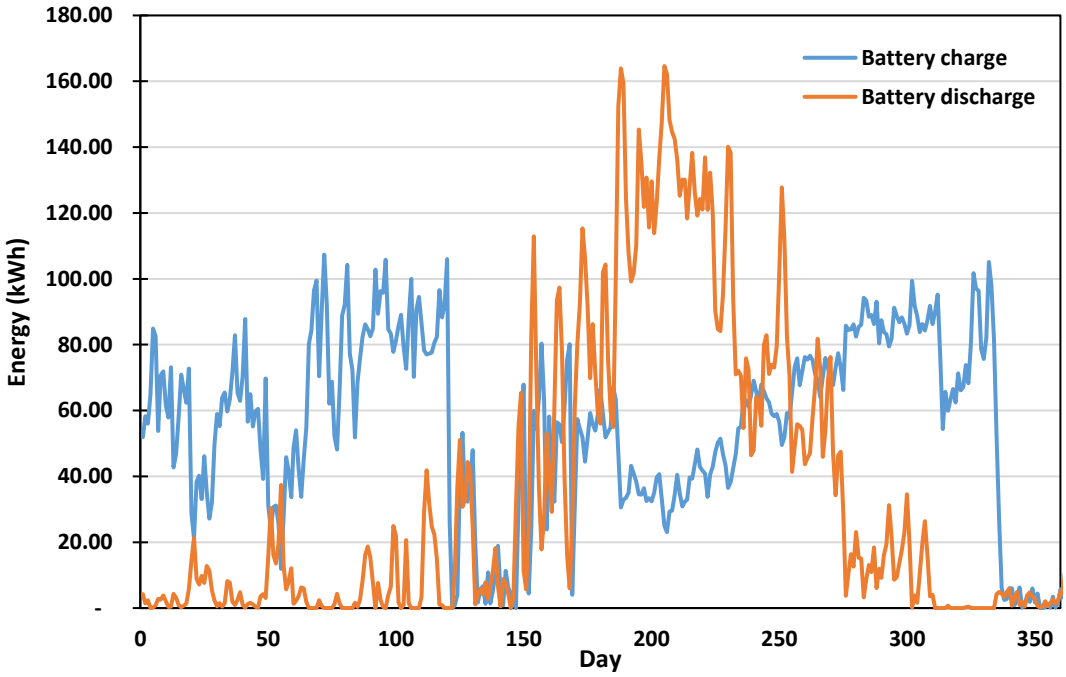

Figure 5.31 Battery charge – Battery discharge vs Day (14 kWh fuel cell)

5.3.2 Results for Case-2

In this section, a case study analysis for an 18 kWh capacity fuel cell is performed. In Figure 5.32, Electric loads – Fuel cell energy for load vs Day (18 kWh fuel cell) is demonstrated. Compared to the 14 kWh fuel cell capacity case, there is an increase in supplied electricity to the electrical load by the fuel cell. Because, compared to the 14 kWh case, in most days, the capacity of the fuel cell is enough for the electrical load. In Figure 5.33, the Hydrogen fuel cell for load – Battery charge vs Day graph is demonstrated. Battery charge for 18 kWh case is less than 14 kWh because most of the time, the capacity of the battery is full. That can also be observed in the Battery charge – Battery level vs Hours (18 kWh fuel cell) graph in Figure 5.34. In Figure 5.34, approximately after the 1000^{th} hour, there is no increase or decrease in battery level. The main reason of this situation is the high capacity of the fuel cell. Generally, the battery is not utilized because of the high capacity of the fuel cell. However, because of the full level of the battery, excess energy cannot be stored, and that causes a decrease in the efficiency of the system.

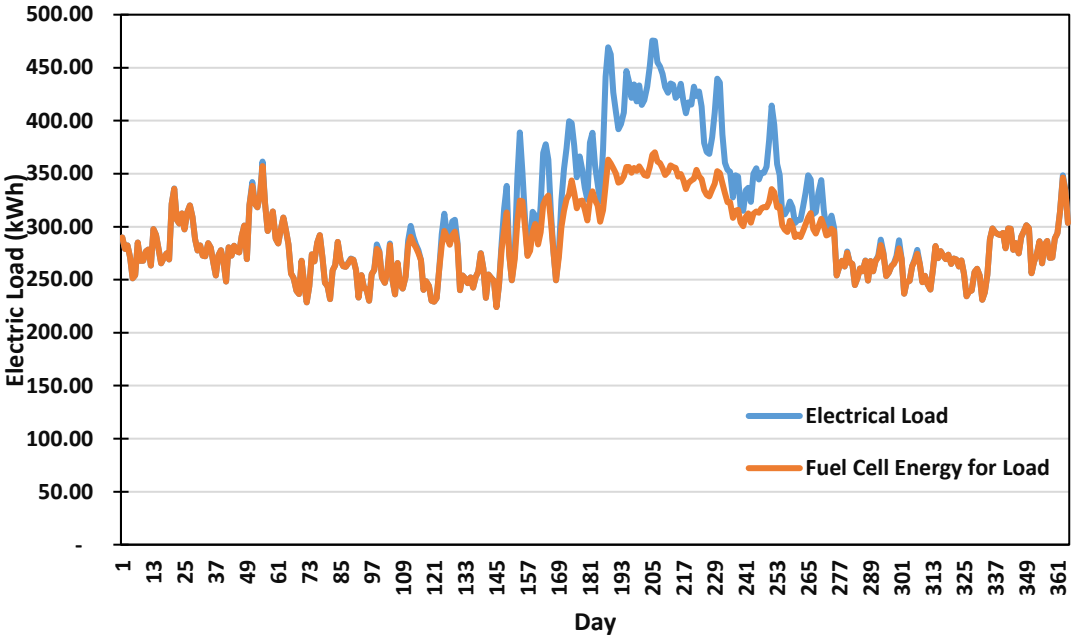

Figure 5.32 Electric load – Fuel cell energy for load vs Day (18 kWh fuel cell)

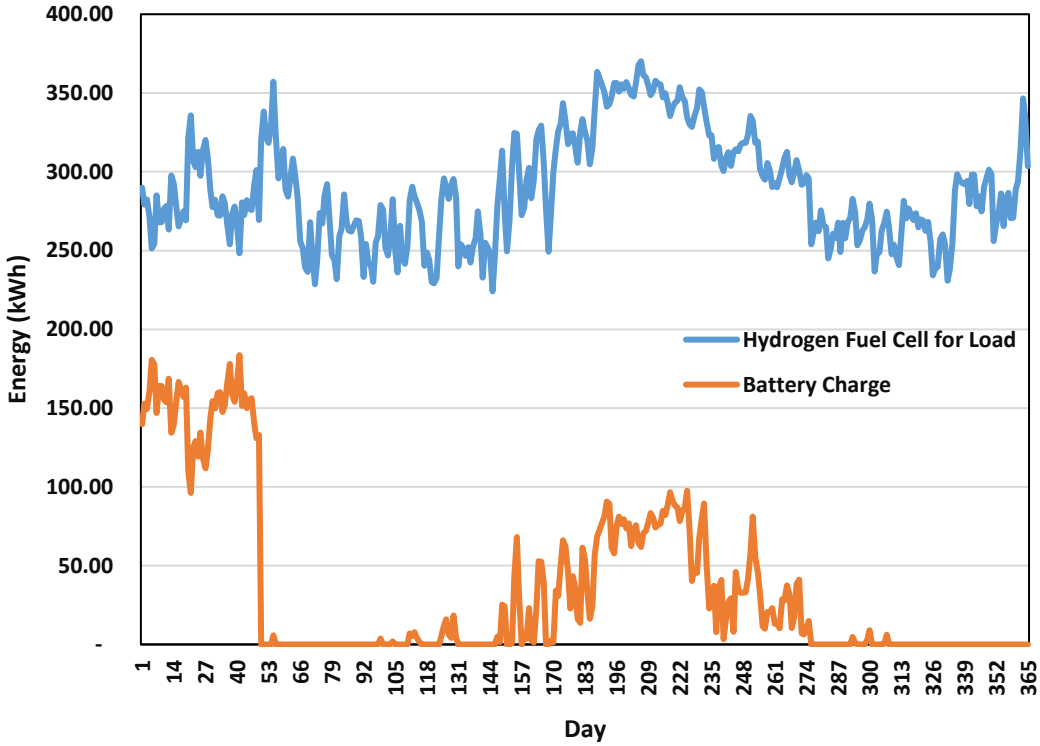

Figure 5.33 Hydrogen fuel cell for load – Battery charge vs Day (18 kWh fuel cell)

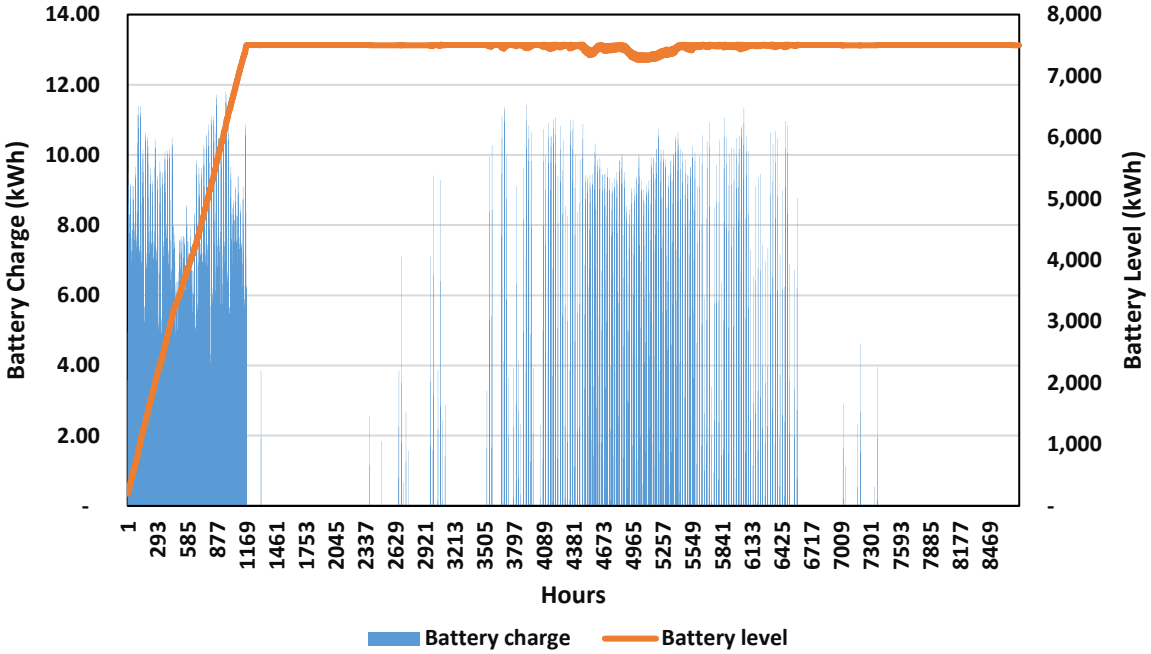

Figure 5.34 Battery charge – Battery level vs Hours (18 kWh fuel cell)

In Figures 5.35 and 5.36, energy and exergy efficiency graphs are demonstrated. In the 18 kWh fuel cell capacity case, there is an increase in energy and exergy efficiencies compared to the 14 kWh fuel cell capacity case. There are two main reasons for that. The first reason is that there is less charge and discharge, so less charging discharging losses are observed compared to the 14 kWh case. The second reason is that, because of the formula of the efficiency calculations demonstrated in equations 4.20, 4.21, 4.22 and 4.23, when the electrical load is lower than the capacity of the fuel cell, efficiencies are mostly calculated higher. In Figure 5.37, Battery charge – Battery discharge vs Day can be seen. There is a significant decrease in battery charge on days 50 and 100 because of the increase in electric load. There is an increase in battery charge and discharge between days 150 and 200. To conclude, this operation is done with a lower capacity fuel cell that consumes less hydrogen. In that case study, 14 kWh capacity fuel cell utilization is more efficient.

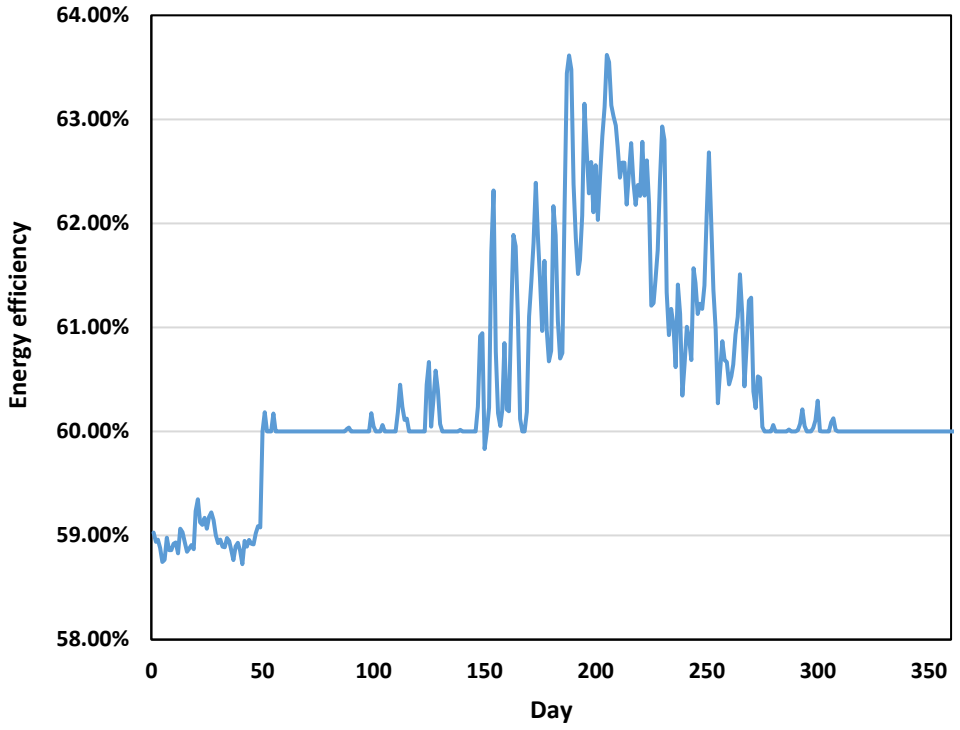

Figure 5.35 Energy efficiency vs Day (18 kWh fuel cell)

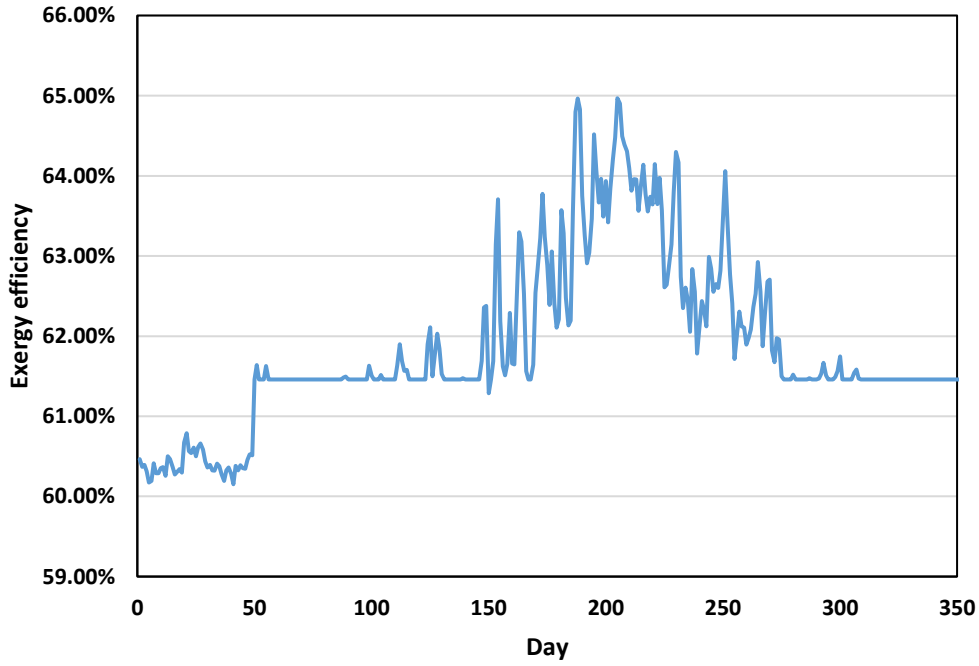

Figure 5.36 Exergy efficiency vs Day (18 kWh fuel cell)

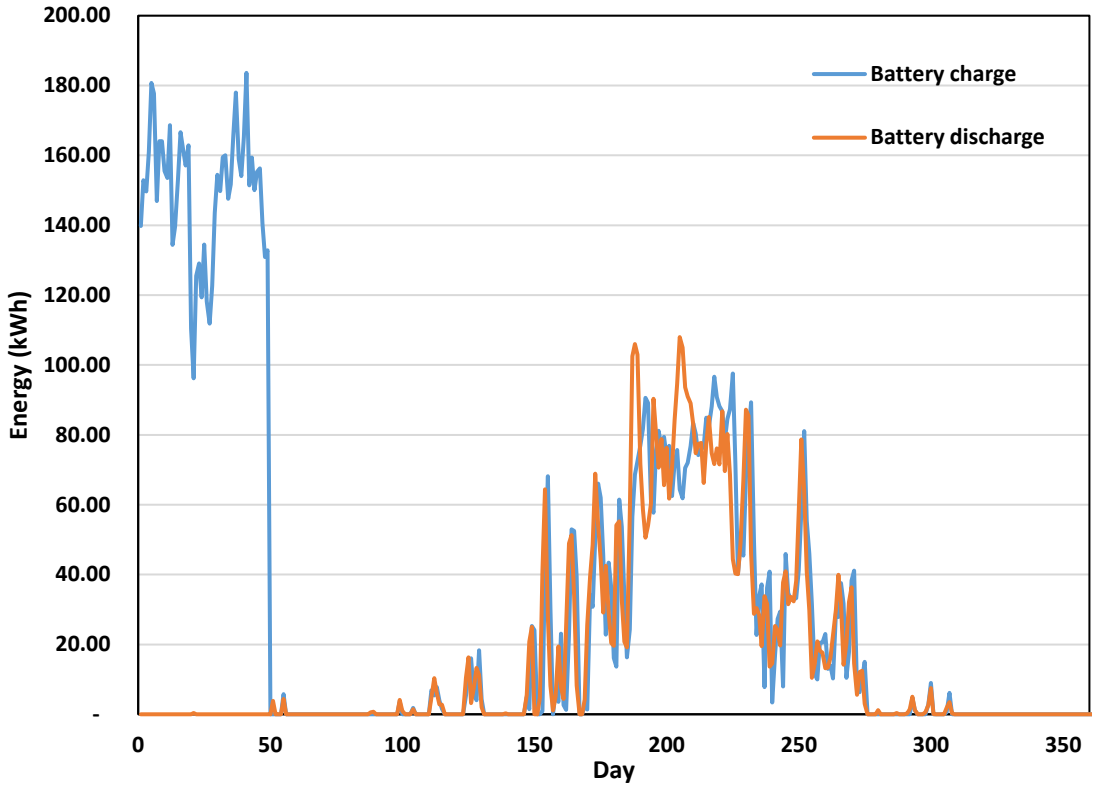

Figure 5.37 Battery charge – Battery discharge vs Day (18 kWh fuel cell)

5.4 Performance Comparison of Fuel Cell Performance with Literature Studies

In this section, the performance of the fuel cell is compared with studies in the literature. In Figure 5.38, the open circuit voltage of a single cell of the PEM fuel cells is compared. Data A and Data B are taken from a study performed by Zhang and Tang[110]. Data A and Data B are Nafion 112 and Nafion 117 respectively. Data C is taken from a study performed by Costamagna and Yang [111]. As seen in Figure 5.38, the highest open circuit voltage is observed in Zhang's study. The main reason for that can be operating conditions. The operation pressure of the PEM fuel cell is 100 Psi. In addition to this, the membrane of the utilized PEM fuel cell in the present study contains Pt as a catalyst. However, in Zhang's study, both Pt and Ru catalysts are utilized. Utilized catalysts are very significant parameters for the open circuit voltage of the cell. Moreover, in Zhang's study, catalyst loading is 1 mg/cm^2 and in the present study, catalyst loading is 0.5 mg/ cm^2. Higher catalyst loading provides higher open circuit voltage.

Furthermore, the thickness of the membrane is another important parameter for the open circuit voltage. An increase in the thickness of the proton exchange membrane leads to an increase in open circuit voltage [110]. The thickness of the utilized Nafion 117 membrane in Zhang's study is 175 micrometers, however, the thickness of utilized Nafion 212 in the present study is 50 micrometers. Moreover, in Data A, the Nafion 112 membrane which has 50 micrometers thickness is utilized. So, one of the reasons why the Nafion 117 membrane has the highest open circuit of voltage is the highest thickness of the membrane.

Table 5.2 Fuel cell properties of previous studies

	Type of Membrane	**Thickness of the Membrane (micrometer)**	**Catalyst Loading (mg/cm$^{2)}$**
Data A [89]	Nafion 112	50	1
Data B [89]	Nafion 117	175	1
Data C [111]	Nafion 115	125	0.5
Present Study	Nafion 212	50.8	0.5

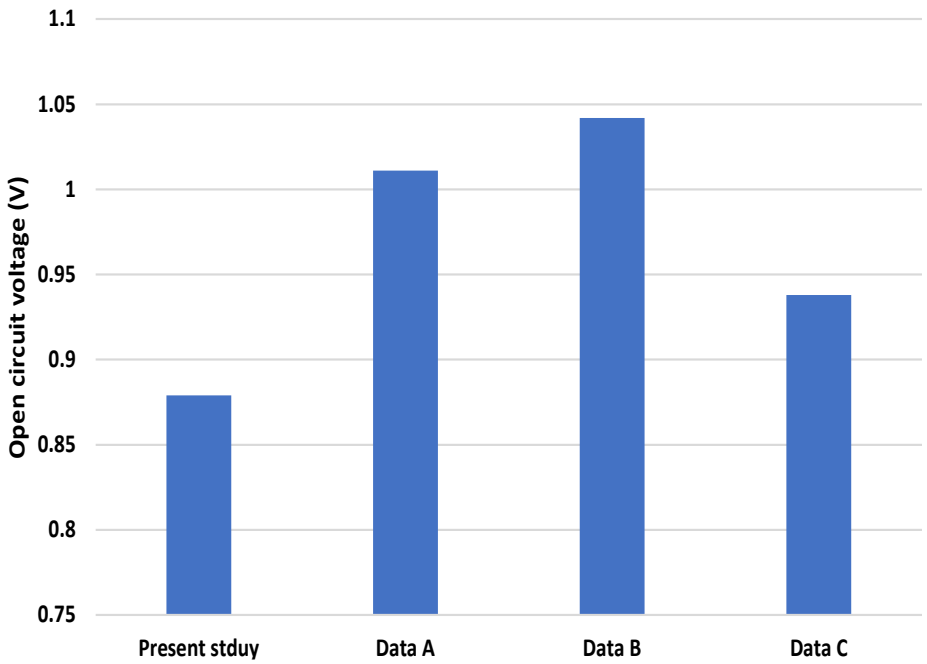

Figure 5.38 Open circuit voltage comparison of the present study and previous studies

In Costamagna's study, Data C, Nafion 115 is utilized. The thickness of the utilized Nafion 115 is 125 micrometers which is higher than the utilized Nafion 212 in the present study. In addition to that, in Costamagna's study, the operating temperature of the fuel cell is 120 °C; however, it is 25°C in the present study. Those are the main reasons why the open circuit voltage of Data C is higher than the open circuit voltage of the present study.

5.5 Fuel Cell and Battery Integrated System

In this section, the results of the fuel cell and battery integrated system are demonstrated and discussed. For experiments, battery charge and discharge losses are determined as 5%. During the experiments, the voltage of the boost converter is settled at 14.4 volts and the current is 0.02 A, so the produced power is 0.29 W. Experiments are performed at two different electric load currents, 0.01 A and 0.04 A. At a current of 0.01 A electric load, the average voltage equals 13 V, so consumed power by the electric load equals 0.13 W. In that case, approximately 0.16 W is directed to the battery pack.

For the 0.01 A electric load, the current-voltage vs time graph is demonstrated in Figure 5.39. In Figure 5.40, the current-voltage vs time graph is presented. In that case, the average voltage is calculated as 13.16 V. So, consumed power is equal to 0.53 W, and supplied power to the system equals 0.29 W. In that case, 0.24 W power is supplied from the battery pack to the electric load. In Figures 5.41 and 5.42, energy and exergy efficiencies of the experimental setup are demonstrated. Efficiency calculations are performed according to equations 4.20, 4.21, 4.22 and 4.23. For load current at 0.01 A, energy efficiency is calculated as 3.58% for and it is 6.18% for load current at 0.04 A. For the load current at 0.04 A, equation 4.20 is utilized and for 0.01 A load current, equation 4.21 is utilized. The exergy efficiency of the proposed system is calculated as 3.64% for the load current at 0.01 A and 6.28 % for the load current at 0.04 A. For the efficiency of 0.04 A load current, equation 4.22 is utilized and for 0.01 A load current, equation 4.23 is utilized. When energy supplied to the humidifier is included in efficiency calculations, the significant decrease in the efficiency of the system is observed as demonstrated in Figure 5.43.

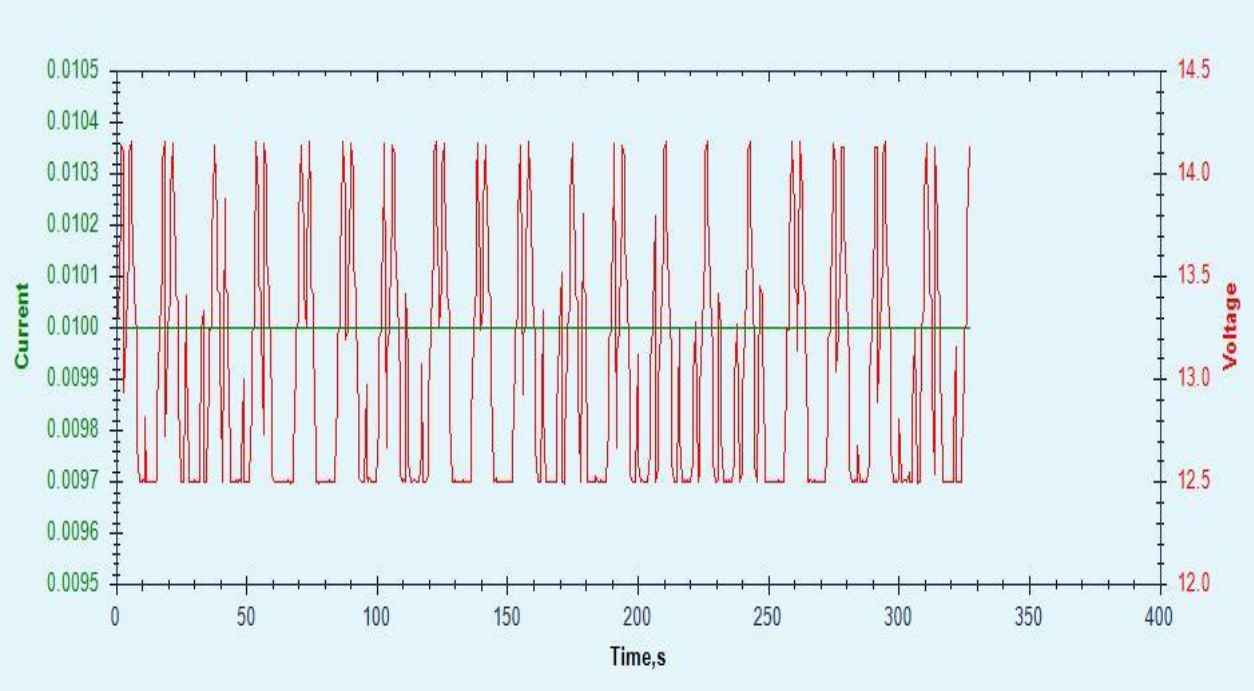

Figure 5.39 Current-voltage vs time graph for 0.04

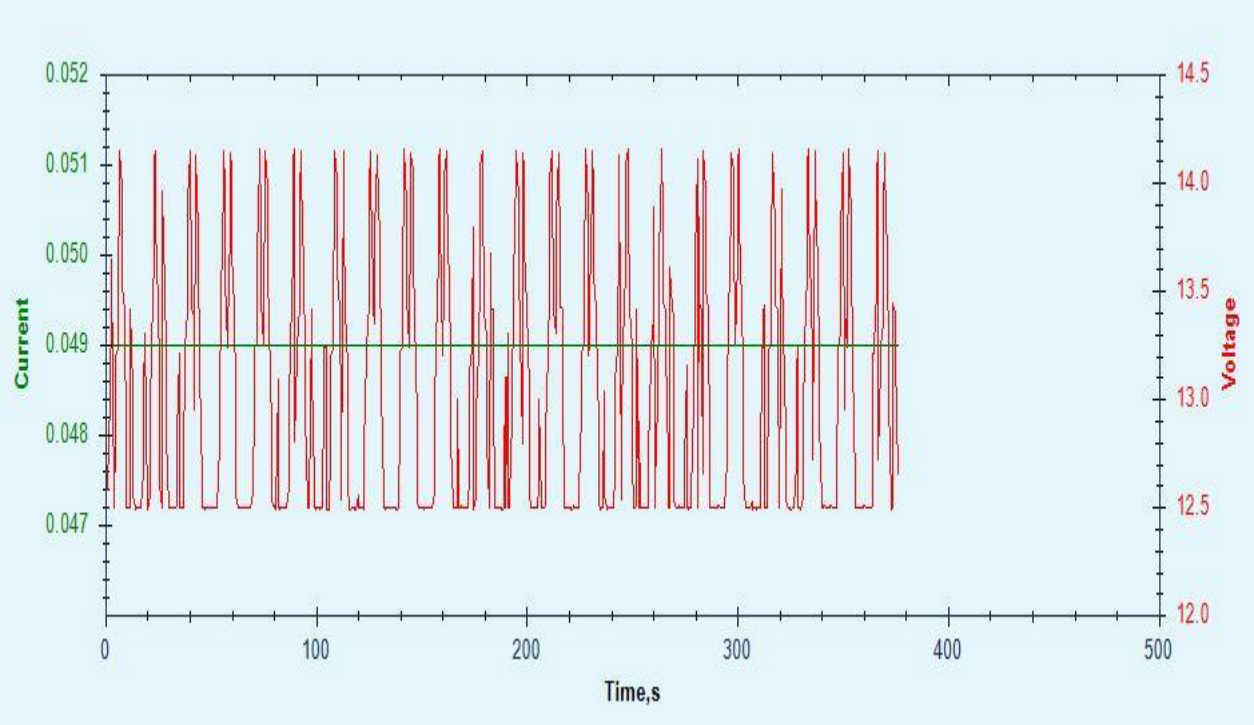

Figure 5.40 Current-voltage vs time graph for 0.04 A

Table 5.3 Fuel cell and battery integrated system values

Electric load (W)	Power Supplied by Fuel Cell (W)	Power Supplied to Battery (W)	Power Supplied by Battery (W)	Battery Charge losses (W)	Battery Discharge Losees (W)
0.13	0.29	0.16	0	0.008	0
0.53	0.29	0	0.24	0	0.012

Efficiency can be increased by designing a more suitable condenser for the system. Insulation materials can be used for the condenser to decrease the energy loss. Moreover, a smaller condenser can be designed to provide less energy to water.

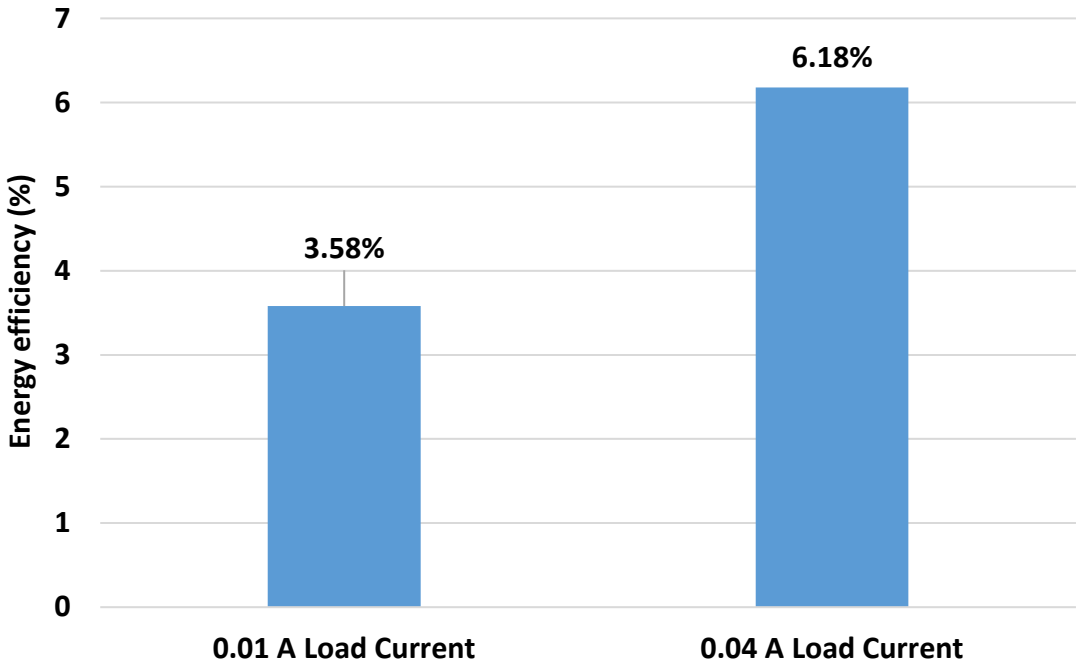

Figure 5.41 Energy efficiency for load current at 0.01 A and 0.04 A

In Figures 5.45 and 5.46, energy and exergy efficiencies with and without battery systems are demonstrated. In 0.01 A load current case, the capacity of the fuel cell is higher than the capacity of the electric load. Excess energy produced by the fuel cell is directed to the battery system, and that increases the efficiency of the system by decreasing energy loss. As seen in Figure 5.43, the energy efficiency of the system with a battery is 3.58% and the energy efficiency without a battery is 1.56%. Moreover, the exergy efficiency of the system with a battery is 3.64%, and without the battery, it is 1.56%.

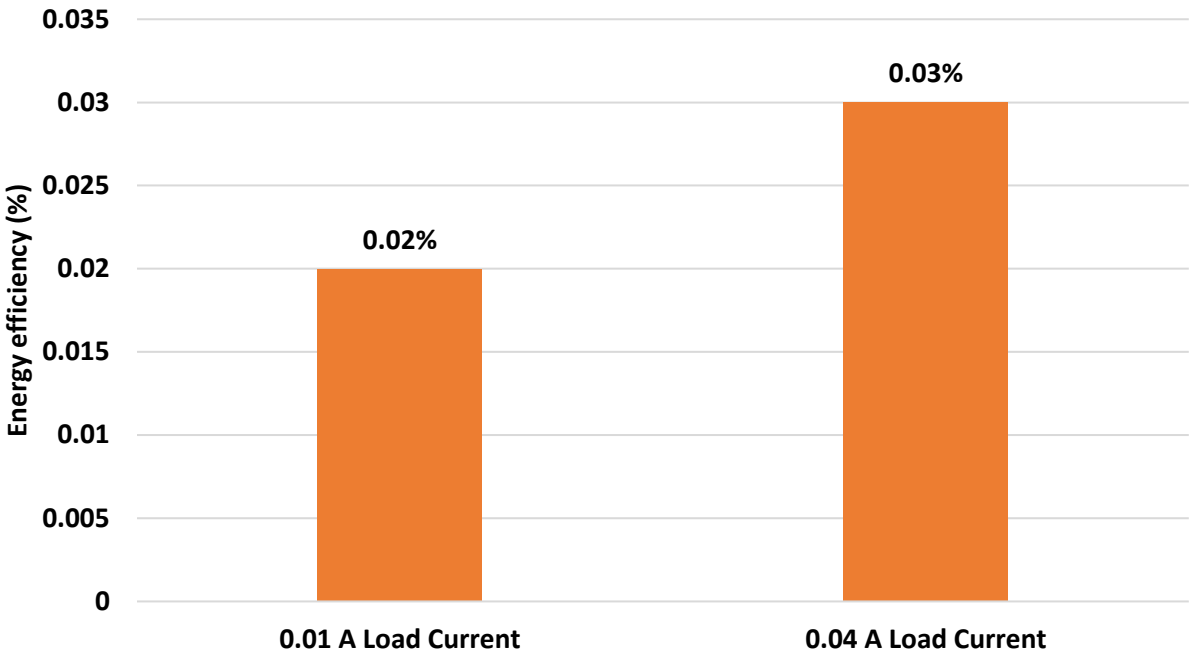

Figure 5.42 Energy efficiency for load current at 0.01 A and 0.04 A (with energy consumption in humidifier)

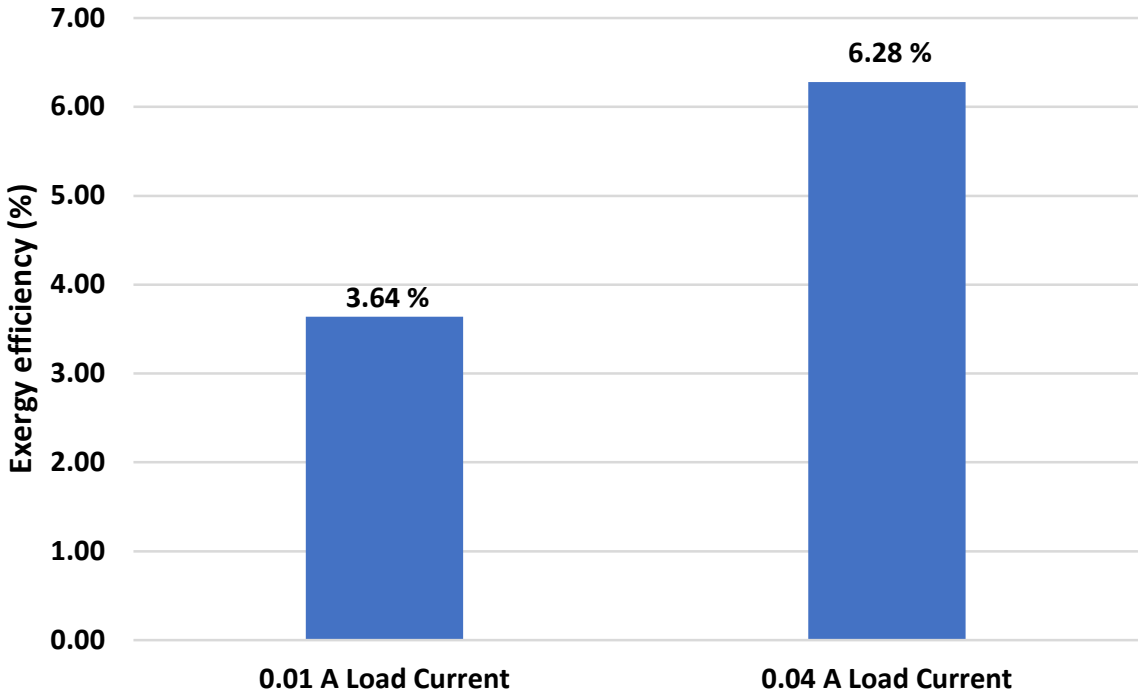

Figure 5.43 Exergy efficiency for load current at for 0.01 A and 0.04 A

The main reason of the increase in efficiency of the system is energy storage. Excess energy is storaed in battery system. Furthermore, in the 0.04 A electric load current case, the electric load is higher than the capacity of the fuel cell. By utilization of batteries, the demand increase in electric load can be controlled effectively.

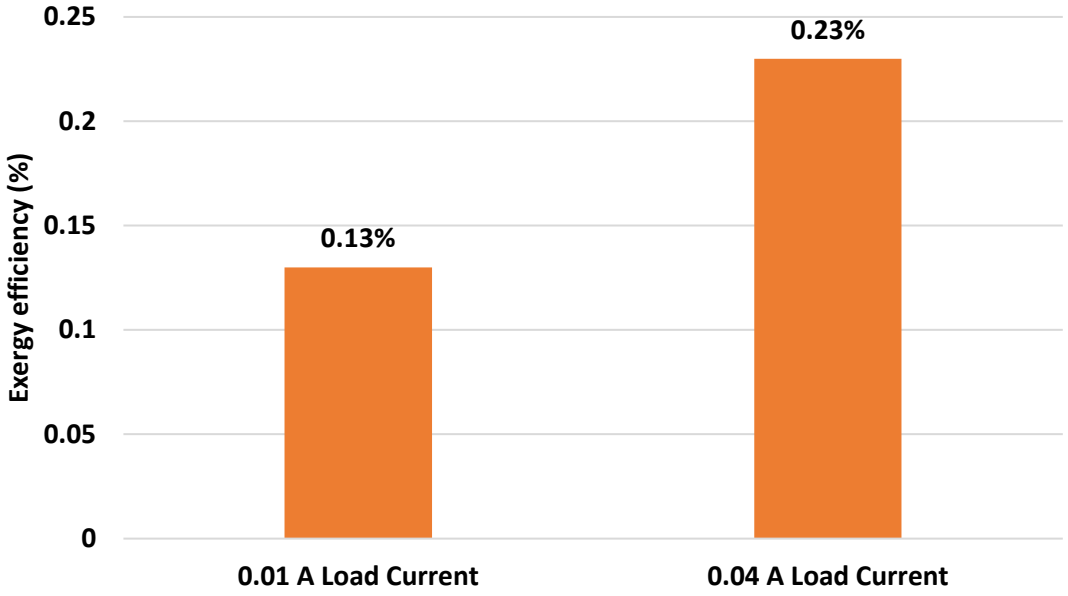

Figure 5.44 Exergy efficiency for load current at 0.01 A and 0.04 A (with exergy consumption in humidifier)

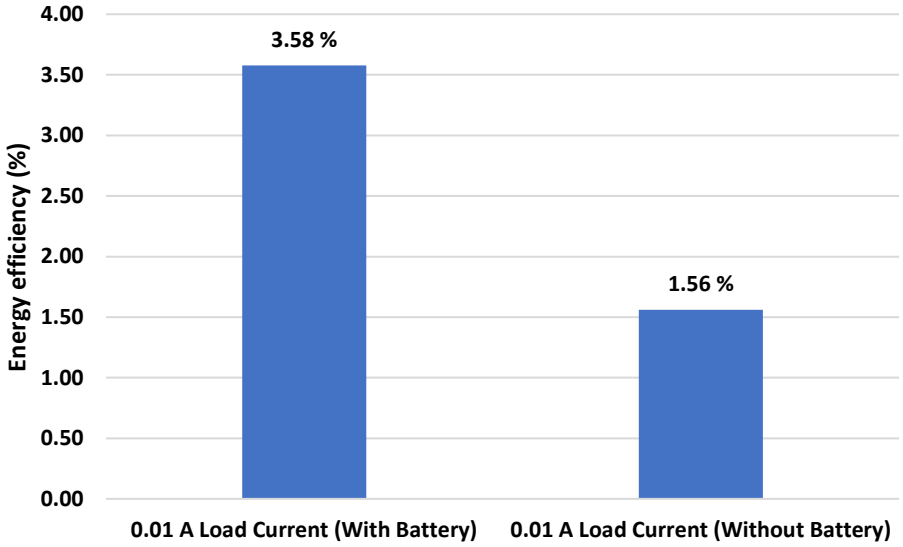

Figure 5.45 Energy efficiency with and without battery for load current at 0.01 A

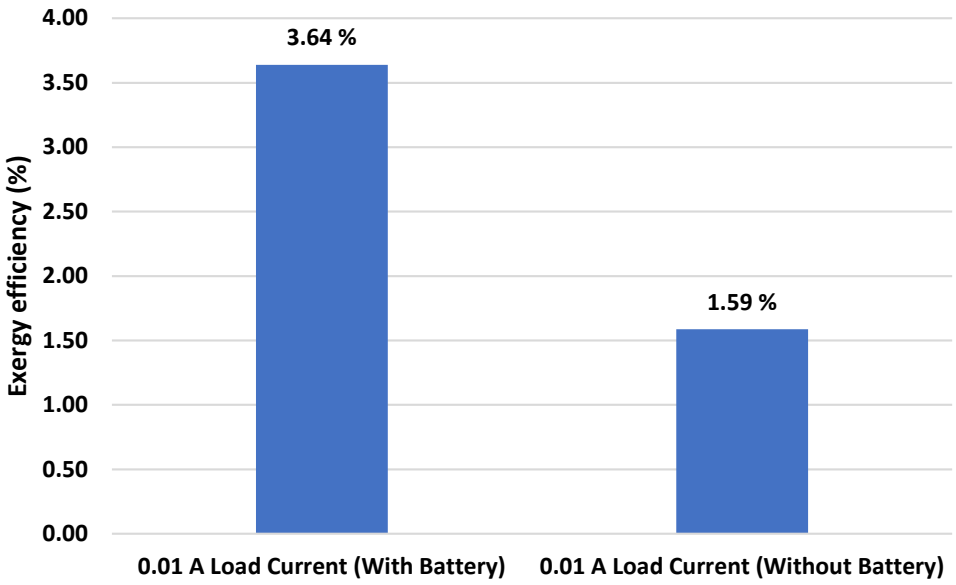

Figure 5.46 Exergy efficiency with and without battery for load current at 0.01 A

Chapter 6. Conclusions and Recommendations

In section 6.1, the conclusion of this study is discussed with the help of the primary results. Furthermore, in section 6.2, recommendations related to future works are demonstrated.

6.1 Conclusions

In this study, a PEM fuel cell and battery integrated system is developed, and its performance is investigated. The performance of the PEM fuel cell and battery integrated system is observed for 0.01 A electric load current and 0.04 electric load current. Energy and exergy efficiency calculations are performed for those cases. Furthermore, the effect of battery integration to fuel cell on energy and exergy efficiencies are investigated. With the integration of battery to fuel cell, energy and exergy efficiencies increase more than twice. In addition to this, the performance of the fuel cell for different humidifier temperatures is investigated. Performance of the PEM fuel cell is observed at 20 °C, 50 °C, 65 °C and 80 °C humidifier temperatures. Improvement in power density, open circuit voltage, energy efficiency and exergy efficiency are observed with the increase in temperature of the humidifier. In addition to this, a comparison of the experimental and theoretical polarization curves of the PEM fuel cell is performed. Furthermore, a comparison of the open circuit voltage of the PEM fuel cell with open circuit voltage values from the literature is performed. The open circuit voltage of the PEM fuel cell utilized in this study is lower than the open circuit voltages in the literature. The main reason of that is the amount of catalyst load and thickness of the utilized membrane. Moreover, a case study for the PEM fuel cell and battery integrated system is performed. Observations are done by utilization of daily energy-exergy analysis, battery charge-discharge, electrical load–fuel cell energy for load and hydrogen fuel cell for load–battery charge graphs.

For this study, quantitative results are demonstrated:

- For the 20 °C humidifier temperature, the average of the open circuit voltage of the PEM fuel cell is calculated as 7.99 V. Moreover, the highest power density is observed as 0.09 A/cm^2. The performance of the fuel cell is improved with a rise in humidifier temperature. At 80 °C humidifier temperature, open circuit voltage

is increased by 10 % compared to the 20 °C and 5.52% higher compared to the 50 °C humidifier temperature operation. Furthermore, peak power density is obtained at 80 °C humidifier operation. It is calculated as 0.122 W/cm^2 at 0.021 A/m^2 and 5.83 V. Furthermore, the highest energy efficiency is calculated as 14.7%, and the highest exergy efficiency is calculated as 14.9%.

- For the PEM fuel cell and battery integrated system, produced power is obtained as 0.29 W. Experiments are performed for two different electric loads, 0.13 W and 0.53 W. For a 0.13 W electric load, the power supplied to the battery is 0.16 W, and the battery charge loss is 0.008 W. For a 0.53 W electric load, the power supplied by the battery is 0.24 W, and the battery discharge loss is 0.012 W. For 0.13 W electric load, energy and exergy efficiencies are calculated as 3.58% and 3.64%. For 0.53 W electric load, energy and exergy efficiencies are calculated as 6.18% and 6.28%, respectively. Furthermore, for 0.13 W electric load, by integration of battery to fuel cell, increase in energy and exergy efficiencies are increased more than twice.
- When energy loss of the condenser is considered in energy efficiency and exergy efficiency calculations, a significant decrease in efficiency is observed. These efficiencies can be increased by utilization of insulation materials. Furthermore, better condenser design provide higher efficiencies.
- In the case study, 14 kWh and 18 kWh capacity fuel cell systems are utilized. Compared to the 14 kWh fuel cell capacity case, in the 18 kWh fuel cell capacity, there is an increase in supplied electricity to the electrical load by the fuel cell. In the 18 kWh case, after some point, there is no increase or decrease in battery level. The main reason for this situation is the high capacity of the fuel cell. Generally, the battery is not utilized because of the high capacity of the fuel cell. However, because of the full level of the battery, excess energy cannot be stored, and that causes a decrease in the efficiency of the system.

6.2 Recommendations

According to the results of the current study, the following recommendations are done for future research:

- For better performance tests, higher-capacity fuel cells and electric loads should be utilized.
- For the fuel cell and battery integrated system, a life cycle assessment can be performed.
- For the fuel Cell and battery integrated system, an exergoeconomic analysis can be performed.
- Different types of membranes (Nafion 112, Nafion 115, Nafion 117) and catalysts (Platinum-Ruthenium, Platinum-Iridium) can be utilized for PEM fuel cells.
- Different types of controllers can be utilized to increase the efficiency of the system.
- Different types of batteries (lead acid batteries, nickel-metal hydride batteries) can be utilized for observing the effect of the type of battery and increasing the overall efficiency of the system.

References

[1] Song C. Global challenges and strategies for control, conversion and utilization of CO2 for sustainable development involving energy, catalysis, adsorption and chemical processing. Catal Today 2006;115:2–32. https://doi.org/10.1016/j.cattod.2006.02.029.

[2] CO2 emissions - Our World in Data n.d. https://ourworldindata.org/co2-emissions (accessed May 16, 2023).

[3] Ritchie H, Roser M, Rosado P. CO_2 and Greenhouse Gas Emissions. Our World in Data 2020.

[4] Akerboom S, Botzen W, Buijze A, Michels A, van Rijswick M. Meeting goals of sustainability policy: CO2 emission reduction, cost-effectiveness and societal acceptance. An analysis of the proposal to phase-out coal in the Netherlands. Energy Policy, vol. 138, Elsevier Ltd; 2020. https://doi.org/10.1016/j.enpol.2019.111210.

[5] Ozturk M, Dincer I. An integrated system for clean hydrogen production from municipal solid wastes. Int J Hydrogen Energy 2021;46:6251–61. https://doi.org/10.1016/j.ijhydene.2020.11.145.

[6] Renewable Energy Jobs Reach 12 Million Globally n.d. https://www.irena.org/News/pressreleases/2021/Oct/Renewable-Energy-Jobs-Reach-12-Million-Globally (accessed June 4, 2023).

[7] Acar C, Dincer I. The potential role of hydrogen as a sustainable transportation fuel to combat global warming. Int J Hydrogen Energy 2020;45:3396–406. https://doi.org/10.1016/j.ijhydene.2018.10.149.

[8] Dincer I, Acar C. Review and evaluation of hydrogen production methods for better sustainability. Int J Hydrogen Energy 2014;40:11094–111. https://doi.org/10.1016/j.ijhydene.2014.12.035.

[9] Nikolaidis P, Poullikkas A. A comparative overview of hydrogen production processes. Renewable and Sustainable Energy Reviews 2017;67:597–611. https://doi.org/10.1016/j.rser.2016.09.044.

[10] Holladay JD, Hu J, King DL, Wang Y. An overview of hydrogen production technologies. Catal Today 2009;139:244–60. https://doi.org/10.1016/j.cattod.2008.08.039.

[11] Kothari R, Buddhi D, Sawhney RL. Comparison of environmental and economic aspects of various hydrogen production methods. Renewable and Sustainable Energy Reviews 2008;12:553–63. https://doi.org/10.1016/j.rser.2006.07.012.

[12] Bak T, Nowotny J, Rekas M, Sorrell CC. Photo-electrochemical properties of the TiO 2-Pt system in aqueous solutions. vol. 27. 2002.

[13] Iribarren D, Susmozas A, Petrakopoulou F, Dufour J. Environmental and exergetic evaluation of hydrogen production via lignocellulosic biomass gasification. J Clean Prod 2014;69:165–75. https://doi.org/10.1016/j.jclepro.2014.01.068.

[14] Wang Z, He T, Qin J, Wu J, Li J, Zi Z, et al. Gasification of biomass with oxygen-enriched air in a pilot scale two-stage gasifier. Fuel 2015;150:386–93. https://doi.org/10.1016/j.fuel.2015.02.056.

[15] Das D, Nejat T, Glu V. Hydrogen production by biological processes: a survey of literature. vol. 26. 2001.

[16] Hay JXW, Wu TY, Juan JC, Md. Jahim J. Biohydrogen production through photo fermentation or dark fermentation using waste as a substrate: Overview, economics, and future prospects of hydrogen usage. Biofuels, Bioproducts and Biorefining 2013;7:334–52. https://doi.org/10.1002/BBB.1403.

[17] Uddin MN, Nageshkar V V., Asmatulu R. Improving water-splitting efficiency of water electrolysis process via highly conductive nanomaterials at lower voltages. Energy Ecol Environ 2020;5:108–17. https://doi.org/10.1007/s40974-020-00147-5.

[18] Madadi Avargani V, Zendehboudi S, Cata Saady NM, Dusseault MB. A comprehensive review on hydrogen production and utilization in North America: Prospects and challenges. Energy Convers Manag 2022;269. https://doi.org/10.1016/j.enconman.2022.115927.

[19] Momirlan M, Veziroglu TN. The properties of hydrogen as fuel tomorrow in sustainable energy system for a cleaner planet. Int J Hydrogen Energy 2005;30:795–802. https://doi.org/10.1016/j.ijhydene.2004.10.011.

[20] Dutta S. A review on production, storage of hydrogen and its utilization as an energy resource. Journal of Industrial and Engineering Chemistry 2014;20:1148–56. https://doi.org/10.1016/J.JIEC.2013.07.037.

[21] Hydrogen Fuel Cells Market Size, Growth, Trends, Report 2022 to 2030 n.d. https://www.precedenceresearch.com/hydrogen-fuel-cells-market (accessed June 5, 2023).

[22] Couture G, Alaaeddine A, Boschet F, Ameduri B. Polymeric materials as anion-exchange membranes for alkaline fuel cells. Prog Polym Sci 2011;36:1521–57. https://doi.org/10.1016/j.progpolymsci.2011.04.004.

[23] Ibrahim H, Ilinca A, Perron J. Energy storage systems—Characteristics and comparisons. Renewable and Sustainable Energy Reviews 2008;12:1221–50. https://doi.org/10.1016/J.RSER.2007.01.023.

[24] Van Den Bossche P, Vergels F, Van Mierlo J, Matheys J, Van Autenboer W. SUBAT: An assessment of sustainable battery technology. J Power Sources 2006;162:913–9. https://doi.org/10.1016/j.jpowsour.2005.07.039.

[25] Alva G, Lin Y, Fang G. An overview of thermal energy storage systems. Energy 2018;144:341–78. https://doi.org/10.1016/J.ENERGY.2017.12.037.

[26] Ishaq H, Dincer I, Crawford C. A review on hydrogen production and utilization: Challenges and opportunities. Int J Hydrogen Energy 2022;47:26238–64. https://doi.org/10.1016/J.IJHYDENE.2021.11.149.

[27] Zhang J, Dong Y, Wang Y, Zhu Y, Duan Y. A novel route to synthesize hydrogen storage material ammonia borane via copper (II)-ammonia complex liquid phase oxidization. Int J Energy Res 2018;42:4395–401. https://doi.org/10.1002/ER.4181.

[28] Hosseini M, Dincer I, Naterer GF, Rosen MA. Thermodynamic analysis of filling compressed gaseous hydrogen storage tanks 2012. https://doi.org/10.1016/j.ijhydene.2011.12.047.

[29] Rivard E, Trudeau M, Zaghib K. Hydrogen Storage for Mobility: A Review. Materials 2019, Vol 12, Page 1973 2019;12:1973. https://doi.org/10.3390/MA12121973.

[30] Züttel A. Materials for hydrogen storage. Materials Today 2003;6:24–33. https://doi.org/10.1016/S1369-7021(03)00922-2.

[31] UBE Nylon Resin Used in High-Pressure Hydrogen Tank of Toyota Mirai Fuel Cell Sedan | UBE Corporation n.d. https://www.ube.co.jp/ube/en/news/2014/20141208_01.html (accessed June 28, 2023).

[32] Krasae-in S, Stang JH, Neksa P. Development of large-scale hydrogen liquefaction processes from 1898 to 2009. Int J Hydrogen Energy 2010;35:4524–33. https://doi.org/10.1016/J.IJHYDENE.2010.02.109.

[33] Colozza AJ. Hydrogen Storage for Aircraft Applications Overview 2002.

[34] Mehtab T, Yasin G, Arif M, Shakeel M, Korai RM, Nadeem M, et al. Metal-organic frameworks for energy storage devices: Batteries and supercapacitors. J Energy Storage 2019;21:632–46. https://doi.org/10.1016/J.EST.2018.12.025.

[35] Koizumi K, Nobusada K, Boero M. Hydrogen storage mechanism and diffusion in metal–organic frameworks. Physical Chemistry Chemical Physics 2019;21:7756–64. https://doi.org/10.1039/C8CP07467D.

[36] Proch S, Herrmannsdörfer J, Kempe R, Kern C, Jess A, Seyfarth L, et al. Pt@MOF-177: Synthesis, Room-Temperature Hydrogen Storage and Oxidation Catalysis. Chemistry – A European Journal 2008;14:8204–12. https://doi.org/10.1002/CHEM.200801043.

[37] Tarkowski R. Underground hydrogen storage: Characteristics and prospects. Renewable and Sustainable Energy Reviews 2019;105:86–94. https://doi.org/10.1016/J.RSER.2019.01.051.

[38] Zivar D, Kumar S, Foroozesh J. Underground hydrogen storage: A comprehensive review. Int J Hydrogen Energy 2021;46:23436–62. https://doi.org/10.1016/J.IJHYDENE.2020.08.138.

[39] Arregui G. Theoretical study of a power generation unit based on the hybridization of a fuel cell stack and ultra capacitors. 2007.

[40] Corcau JI, Dinca L, Grigorie TL, Tudosie AN. Fuzzy energy management for hybrid fuel cell/battery systems for more electric aircraft. AIP Conf Proc, vol. 1836, American Institute of Physics Inc.; 2017. https://doi.org/10.1063/1.4981996.

[41] International Symposium on Power Electronics, Electrical Drives, Automation and Motion : Pisa, Italy, June 14-16, 2010 : SPEEDAM 2010. n.d.

[42] Parts of a Fuel Cell | Department of Energy n.d. https://www.energy.gov/eere/fuelcells/parts-fuel-cell (accessed June 6, 2023).

[43] O'Hayre RP, Cha S-W, Colella WG, Prinz FB. Fuel cell fundamentals. n.d.

[44] Mehta V, Cooper JS. Review and analysis of PEM fuel cell design and manufacturing. n.d.

[45] Jin CK, Jung MG, Kang CG. Fabrication of Aluminum Bipolar Plates by Semi-solid Forging Process and Performance Test of TiN Coated Aluminum Bipolar Plates. Fuel Cells 2014;14:551–60. https://doi.org/10.1002/FUCE.201300137.

[46] Wang Y, Ruiz Diaz DF, Chen KS, Wang Z, Adroher XC. Materials, technological status, and fundamentals of PEM fuel cells – A review. Materials Today 2020;32:178–203. https://doi.org/10.1016/j.mattod.2019.06.005.

[47] Hermann A, Chaudhuri T, Spagnol P. Bipolar plates for PEM fuel cells: A review. Int J Hydrogen Energy 2005;30:1297–302. https://doi.org/10.1016/j.ijhydene.2005.04.016.

[48] Adloo A, Sadeghi M, Masoomi M, Pazhooh HN. High performance polymeric bipolar plate based on polypropylene/ graphite/graphene/nano-carbon black composites for PEM fuel cells 2016. https://doi.org/10.1016/j.renene.2016.07.062.

[49] Hentall PL, Lakeman JB, Mepsted GO, Adcock PL, Moore JM. New materials for polymer electrolyte membrane fuel cell current collectors. J Power Sources 1999;80:235–41.

[50] Haile SM. Fuel cell materials and components. Acta Mater 2003;51:5981–6000. https://doi.org/10.1016/j.actamat.2003.08.004.

[51] Peighambardoust SJ, Rowshanzamir S, Amjadi M. Review of the proton exchange membranes for fuel cell applications 2010. https://doi.org/10.1016/j.ijhydene.2010.05.017.

[52] Wu G. Current challenge and perspective of PGM-free cathode catalysts for PEM fuel cells. Frontiers in Energy 2017;11:286–98. https://doi.org/10.1007/S11708-017-0477-3/METRICS.

[53] Types of Fuel Cells | Department of Energy n.d. https://www.energy.gov/eere/fuelcells/types-fuel-cells (accessed May 22, 2023).

[54] Yan W-M, Chen C-Y, Mei S-C, Soong C-Y, Chen F. Effects of operating conditions on cell performance of PEM fuel cells with conventional or interdigitated flow field. J Power Sources 2006;162:1157–64. https://doi.org/10.1016/j.jpowsour.2006.07.044.

[55] Nguyen T V., White RE. A Water and Heat Management Model for Proton-Exchange-Membrane Fuel Cells. J Electrochem Soc 1993;140:2178–86. https://doi.org/10.1149/1.2220792/XML.

[56] Yan WM, Soong CY, Chen F, Chu HS. Effects of flow distributor geometry and diffusion layer porosity on reactant gas transport and performance of proton exchange membrane fuel cells. J Power Sources 2004;125:27–39. https://doi.org/10.1016/j.jpowsour.2003.07.017.

[57] Li P-W, Zhang T, Wang Q-M, Schaefer L, Chyu MK. The performance of PEM fuel cells fed with oxygen through the free-convection mode n.d.

[58] Liu H-C, Yan W-M, Soong C-Y, Chen F. Effects of baffle-blocked flow channel on reactant transport and cell performance of a proton exchange membrane fuel cell. J Power Sources 2005;142:125–33. https://doi.org/10.1016/j.jpowsour.2004.09.037.

[59] Mao X, Ying R, Yuan Y, Li F, Shen B. Simulation and analysis of hydrogen leakage and explosion behaviors in various compartments on a hydrogen fuel cell ship. Int J Hydrogen Energy 2021;46:6857–72. https://doi.org/10.1016/J.IJHYDENE.2020.11.158.

[60] Fang SY, Teoh LG, Huang RH, Hsueh KL, Yang KH, Chao WK, et al. Enhancement of proton exchange membrane fuel cell performance by titanium-

coated anode gas diffusion layer. Int J Hydrogen Energy 2014;39:21177–84. https://doi.org/10.1016/j.ijhydene.2014.10.055.

[61] Erce Şengül, Erdener H, Akay RG, Yücel H, Baç N, Eroğlu II. Effects of sulfonated polyether-etherketone (SPEEK) and composite membranes on the proton exchange membrane fuel cell (PEMFC) performance. Int J Hydrogen Energy 2009;34:4645–52. https://doi.org/10.1016/j.ijhydene.2008.08.066.

[62] Liu X, Guo H, Ye F, Ma CF. Flow dynamic characteristics in flow field of proton exchange membrane fuel cells. Int J Hydrogen Energy 2008;33:1040–51. https://doi.org/10.1016/j.ijhydene.2007.11.018.

[63] Williams M V., Kunz HR, Fenton JM. Operation of Nafion®-based PEM fuel cells with no external humidification: Influence of operating conditions and gas diffusion layers. J Power Sources 2004;135:122–34. https://doi.org/10.1016/j.jpowsour.2004.04.010.

[64] Wang L, Husar A, Zhou T, Liu H. A parametric study of PEM fuel cell performances. Int J Hydrogen Energy 2003;28:1263–72. https://doi.org/10.1016/S0360-3199(02)00284-7.

[65] Jiang R, Kunz HR, Fenton JM. Investigation of membrane property and fuel cell behavior with sulfonated poly(ether ether ketone) electrolyte: Temperature and relative humidity effects. J Power Sources 2005;150:120–8. https://doi.org/10.1016/j.jpowsour.2005.03.180.

[66] Ghaffar A, Lafi A. Cross Linked Sulphonated Poly(ether ether ketone) for the Development of Polymer Electrolyte Membrane Fuel Cell. 2009.

[67] Stambouli AB, Traversa E, Stambouli A. Solid oxide fuel cells (SOFCs): a review of an environmentally clean and efficient source of energy. vol. 6. 2002.

[68] Singhal SC. Solid oxide fuel cells for power generation. Wiley Interdiscip Rev Energy Environ 2014;3:179–94. https://doi.org/10.1002/wene.96.

[69] Stambouli AB, Traversa E, Stambouli A. Solid oxide fuel cells (SOFCs): a review of an environmentally clean and efficient source of energy. Renewable and Sustainable Energy Reviews 2002;6:433–55.

[70] Singh M, Zappa D, Comini E, Singh M. Solid oxide fuel cell: Decade of progress, future perspectives and challenges 2021. https://doi.org/10.1016/j.ijhydene.2021.06.020.

[71] Prakash BS, Kumar SS, Aruna ST. Properties and development of Ni/YSZ as an anode material in solid oxide fuel cell: A review 2014. https://doi.org/10.1016/j.rser.2014.04.043.

[72] Lee JG, Ho Park J, Shul YG. Tailoring gadolinium-doped ceria-based solid oxide fuel cells to achieve 2 W cm−2 at 550 °C 2014. https://doi.org/10.1038/ncomms5045.

[73] Adzfar Shabri H, Hafiz Dzarfan Othman M, Azuwa Mohamed M, Agustiono Kurniawan T, Munira Jamil S. Recent progress in metal-ceramic anode of solid oxide fuel cell for direct hydrocarbon fuel utilization: A review 2020. https://doi.org/10.1016/j.fuproc.2020.106626.

[74] Shen M, Zhang P. Progress and challenges of cathode contact layer for solid oxide fuel cell 2020. https://doi.org/10.1016/j.ijhydene.2020.09.147.

[75] Zakaria Z, Awang Mat Z, Abu Hassan SH, Boon Kar Y. A review of solid oxide fuel cell component fabrication methods toward lowering temperature. Int J Energy Res 2020;44:594–611. https://doi.org/10.1002/er.4907.

[76] Mahato N, Banerjee A, Gupta A, Omar S, Balani K. Progress in material selection for solid oxide fuel cell technology: A review. Prog Mater Sci 2015;72:141–337. https://doi.org/10.1016/j.pmatsci.2015.01.001.

[77] Wagner E, Kohnke HJ. Another Chance for Classic AFCs? Experimental Investigation of a Cost-Efficient Unitized Regenerative Alkaline Fuel Cell, Using Platinum-Free Gas Diffusion Electrodes. Fuel Cells 2020;20:718–29. https://doi.org/10.1002/fuce.202000083.

[78] Mclean GF, Niet T, Prince-Richard S, Djilali N. An assessment of alkaline fuel cell technology. Int J Hydrogen Energy 2002;27:507–26.

[79] Al-Saleh MA, Gultekin S, Al-Zakri AS, Khan AAA. 65’ 6hi. J Hydrogen Energy n.d.;21.

[80] Fuel cells - fundamentals and applications (Journal Article) | ETDEWEB n.d. https://www.osti.gov/etdeweb/biblio/20177347 (accessed June 13, 2023).

[81] Sammes N, Bove R, Stahl K. Phosphoric acid fuel cells: Fundamentals and applications. Curr Opin Solid State Mater Sci 2004;8:372–8. https://doi.org/10.1016/J.COSSMS.2005.01.001.

[82] Fuel Cell Systems Explained - Andrew L. Dicks, David A. J. Rand - Google Books n.d. https://books.google.ca/books?hl=en&lr=&id=CuhRDwAAQBAJ&oi=fnd&pg=PA13&ots=eKQBCBlZ4v&sig=9fNmcBRlOryc1sRRNzjaGr8oCJA&redir_esc=y#v=onepage&q&f=false (accessed June 14, 2023).

[83] Wakihara M. Recent developments in lithium ion batteries. Materials Science and Engineering: R: Reports 2001;33:109–34. https://doi.org/10.1016/S0927-796X(01)00030-4.

[84] Ritchie A, Howard W. Recent developments and likely advances in lithium-ion batteries. J Power Sources 2006;162:809–12. https://doi.org/10.1016/J.JPOWSOUR.2005.07.014.

[85] Franger S, Bourbon C, Le Cras F. Optimized Lithium Iron Phosphate for High-Rate Electrochemical Applications. J Electrochem Soc 2004;151:A1024. https://doi.org/10.1149/1.1758721/XML.

[86] Handwerker M, Wellnitz J, Marzbani H. Comparison of Hydrogen Powertrains with the Battery Powered Electric Vehicle and Investigation of Small-Scale Local Hydrogen Production Using Renewable Energy. Hydrogen 2021, Vol 2, Pages 76-100 2021;2:76–100. https://doi.org/10.3390/HYDROGEN2010005.

[87] Loskutov A, Kurkin A, Shalukho A, Lipuzhin I, Bedretdinov R. Investigation of PEM Fuel Cell Characteristics in Steady and Dynamic Operation Modes. Energies 2022, Vol 15, Page 6863 2022;15:6863. https://doi.org/10.3390/EN15196863.

[88] Farsi A, Rosen MA. PEM fuel cell-assisted lithium ion battery electric vehicle integrated with an air-based thermal management system. Int J Hydrogen Energy 2022;47:35810–24. https://doi.org/10.1016/J.IJHYDENE.2022.08.153.

[89] Choi CH, Yu S, Han IS, Kho BK, Kang DG, Lee HY, et al. Development and demonstration of PEM fuel-cell-battery hybrid system for propulsion of tourist boat. Int J Hydrogen Energy 2016;41:3591–9. https://doi.org/10.1016/J.IJHYDENE.2015.12.186.

[90] Folkesson A, Andersson C, Alvfors P, Alaküla M, Overgaard L. Real life testing of a Hybrid PEM Fuel Cell Bus. J Power Sources 2003;118:349–57. https://doi.org/10.1016/S0378-7753(03)00086-7.

[91] Premkumar K, Vishnupriya M, Thamizhselvan T, Sanjeevikumar P, Manikandan B V. PSO optimized PI controlled DC-DC buck converter-based proton-exchange membrane fuel cell emulator for testing of MPPT algorithm and battery charger controller. International Transactions on Electrical Energy Systems 2021;31:e12754. https://doi.org/10.1002/2050-7038.12754.

[92] Fuel Cell Store n.d. https://www.fuelcellstore.com/ (accessed August 26, 2023).

[93] Hydrogen Air MEA - 5 Layer n.d. https://www.fuelcellstore.com/fuel-cell-components/membrane-electrode-assembly/hydrogen-air-oxygen-fuel-cell-mea/hydrogen-air-mea (accessed August 25, 2023).

[94] Flex-Stak Open Bipolar Graphite Plate - 10 cm^2 n.d. https://www.fuelcellstore.com/flex-stack-bipolar-graphite-plate (accessed August 25, 2023).

[95] 3.2v 1500mAh Ba for Solar Power System Torch Scooter Laptop Audio Tool Ba Screwdriver Power Tool Shaver Electric Emergency Light,1pcs : Amazon.ca:

Electronics n.d. https://www.amazon.ca/1500mAh-Scooter-Screwdriver-Electric-Emergency/dp/B0BQ3TKQRP/ref=sr_1_4?crid=2PXFZA0DWAR7P&keywords=1500%2Bmah%2B3.2%2BV&qid=1692926198&sprefix=1500%2Bmah%2B3%2B2%2Bv%2Caps%2C402&sr=8-4&th=1

[96] PSM-ZK-4KX DC/DC Buck Boost Converter Module 0.5-30V 4A Adjustable Step Down/Up Voltage Regulator n.d. https://abra-electronics.com/voltage-regulator-modules/dc-dc-step-up-step-down-converters/psm-zk-4kx-dc-dc-buck-boost-converter-module-0.5-30v-4a-adjustable-step-down-up-voltage-regulator.html

[97] MPPT Solar Charge Controller with LCD Display,Multiple Load Control Modes : Amazon.ca: Patio, Lawn & Garden n.d. https://www.amazon.ca/Charge-Controller-Display-Multiple-Control/dp/B07L2V7YYC?th=1 (accessed August 26, 2023).

[98] KaiDeng Energy | MPPT SERIES | Solar Charge Controller Datasheet | ENF Charge Controller Directory n.d. https://www.enfsolar.com/pv/charge-controller-datasheet/3583 (accessed August 25, 2023).

[99] SkyRC BD250 Battery Discharger Analyzer - SkyRC n.d. https://www.skyrc.com/bd250 (accessed August 24, 2023).

[100] BD200 - SkyRC n.d. https://www.skyrc.com/Discontinued_Products/BD200 (accessed August 25, 2023).

[101] Low Pressure Drop Gas Mass Flow Meters | Omega Engineering n.d. https://www.omega.ca/en/flow-instruments/flow-meters/mass-flow-meters/p/FMA-LP1600A-Series (accessed June 18, 2023).

[102] Ren S, Liu J, Guo A, Zang W, Geng H, Tao X, et al. Mechanical properties and thermal conductivity of a temperature resistance hollow glass microspheres/borosilicate glass buoyance material. Materials Science and Engineering: A 2016;674:604–14. https://doi.org/10.1016/J.MSEA.2016.08.014.

[103] Spiegel C, York N, San C, Lisbon F, Madrid L, City M, et al. Designing and Building Fuel Cells 2007.

[104] ResStock - NREL n.d. https://resstock.nrel.gov/dataviewer/in-depth-load-chart/?datasetName=vizstock_resstock_amy2018_release_1_by_state&locationId=CA (accessed August 18, 2023).

[105] Izadian A, Girrens N, Khayyer P. Renewable energy policies: A brief review of the latest U.S. and E.U. policies. IEEE Industrial Electronics Magazine 2013;7:21–34. https://doi.org/10.1109/MIE.2013.2269701.

[106] Izadian A, Girrens N, Khayyer P. Renewable energy policies: A brief review of the latest U.S. and E.U. policies. IEEE Industrial Electronics Magazine 2013;7:21–34. https://doi.org/10.1109/MIE.2013.2269701.

[107] Kocha SS, Yang JD, Yi JS. Characterization of gas crossover and its implications in PEM fuel cells. AIChE Journal 2006;52:1916–25. https://doi.org/10.1002/AIC.10780.

[108] Revankar ST, Majumdar P. Fuel Cells : Principles, Design, and Analysis 2016. https://doi.org/10.1201/B15965.

[109] Sun H, Zhang G, Guo LJ, Dehua S, Liu H. Effects of humidification temperatures on local current characteristics in a PEM fuel cell. J Power Sources 2007;168:400–7. https://doi.org/10.1016/J.JPOWSOUR.2007.03.022.

[110] Zhang J, Tang Y, Song C, Zhang J, Wang H. PEM fuel cell open circuit voltage (OCV) in the temperature range of 23 °C to 120 °C. J Power Sources 2006;163:532–7. https://doi.org/10.1016/J.JPOWSOUR.2006.09.026.

[111] Costamagna P, Yang C, Bocarsly AB, Srinivasan S. Nafion® 115/zirconium phosphate composite membranes for operation of PEMFCs above 100 °C. Electrochim Acta 2002;47:1023–33. https://doi.org/10.1016/S0013-4686(01)00829-5.